RADIATIVE TRANSITIONS IN QUARKONIUM

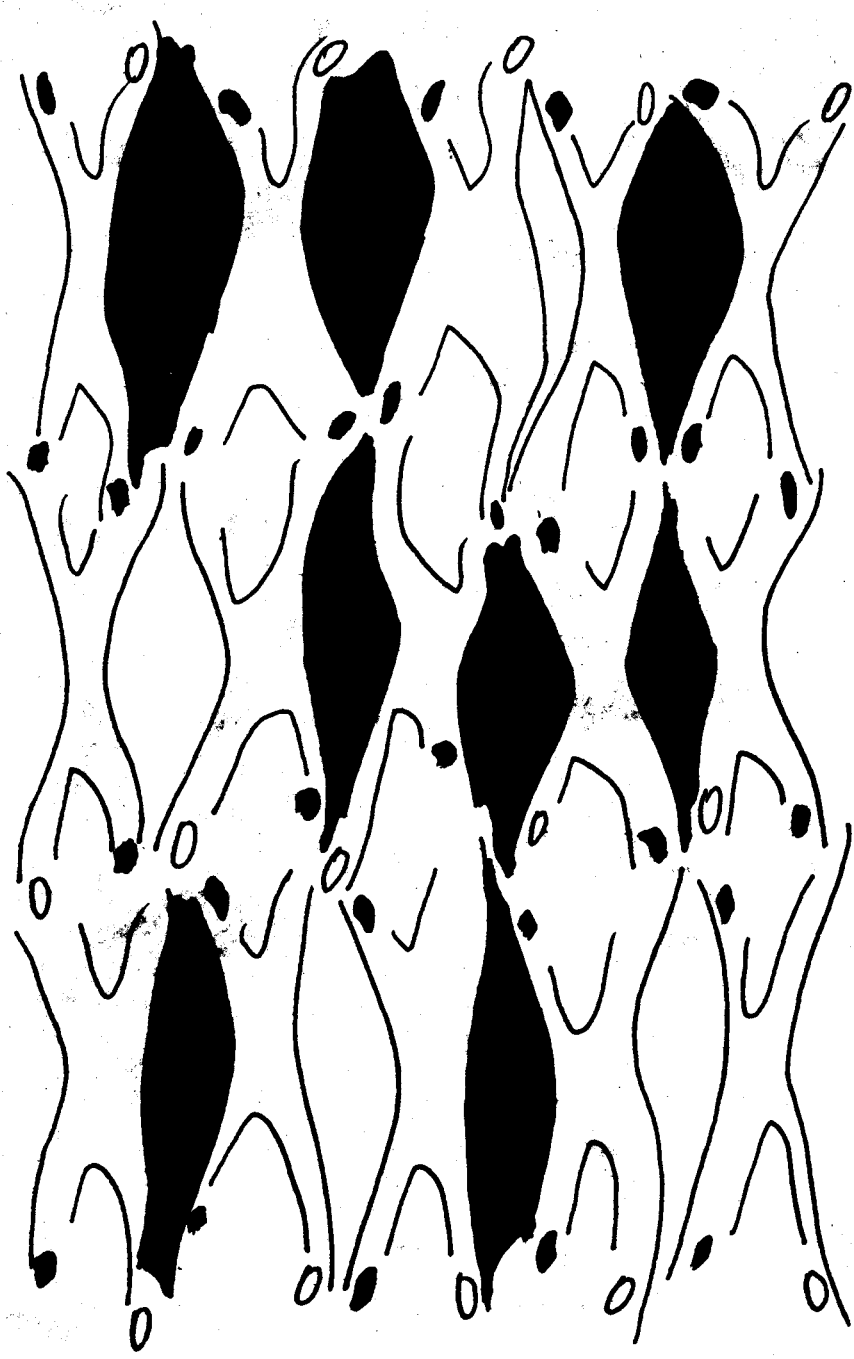

A.G.M. VERSCHUREN

RADIATIVE TRANSITIONS IN QUARKONIUM

Radiative transitions in quarkonium

Radiative transitions in quarkonium

Een wetenschappelijke proeve op het gebied van de natuurwetenschappen,
in het bijzonder de fysica.

Proefschrift

ter verkrijging van de graad van doctor
aan de Katholieke Universiteit te Nijmegen,
volgens besluit van het college van decanen
in het openbaar te verdedigen op
vrijdag 25 januari 1991
des namiddags te 1.30 uur precies

door

Antonius Gertrudes Marie Verschuren

geboren op 5 april 1964 te Eindhoven.

druk: FEBODRUK, Enschede
1991

Promotor:
Prof. dr. C. Dullemond

Co-Promotor:
Dr. E.J.H. van Beveren
(Universidade de Coimbra, Portugal)

CIP-GEGEVENS KONINKLIJKE BIBLIOTHEEK DEN HAAG

Verschuren, Antonius Gertrudes Marie

Radiative transitions in quarkonium /
Antonius Gertrudes Marie Verschuren. - [S.l. : s.n.]
(Enschede : FEBODRUK). – Ill.
Proefschrift Nijmegen. – Met lit. opg.
ISBN 90-9003801-9
SISO 538.3 UDC 539.166(043.3)
Trefw.: hoge energie fysica / potentiaal modellen.

This thesis contains a lot of charm and beauty but very little truth

Op deze plaats wil ik een aantal mensen bedanken zonder wiens hulp dit proefschrift er nu niet gelegen had, nooit gelegen had, of iets eerder gelegen had.

In de tweede kategorie valt Eef van Beveren, die mij erg veel geholpen heeft. Eef, bedankt, ook voor de leuke tijd in Portugal!

Uiteraard moet hier ook mijn promotor Kees Dullemond genoemd worden voor de tijd die hij aan mij besteed heeft.

In de eerste kategorie vallen alle medewerkers van de afdeling Theoretische Natuurkunde II. Ik denk dat iedereen wel een of andere bijdrage aan dit proefschrift heeft geleverd. Dus bedankt Tom Rijken voor je rol als lopende vraagbaak en het kritisch lezen van het manuskript, Johan de Swart voor de nuttige opmerkingen en daarnaast ook voor de grappen en pesterijtjes, William van de Heuvel en Paulus Maessen als mijn kamergenoten voor de—niet altijd even—nuttige diskussies, Rob Timmermans die alles van "echte" fysika weet, Caspar Terheggen en René Klomp voor de plotprogramma's en komputerzaken, Jean-Luc de Kok vooral vanwege zijn humoristische opmerkingen (en daden...), Vincent Stoks voor allerlei informatie over de procedures rond het promoveren en natuurlijk Wilma Vink voor van alles en nog wat.

Dan ben ik nog mijn dank verschuldigd aan mijn voorganger Kees Metzger, die waarschijnlijk in alle drie de kategorieën valt.

Hanneke, die zeker in de derde kategorie valt (en dat hoort ook zo), bedankt voor alles wat buiten de fysika ligt en voor het omslag ontwerp. Mijn ouders mogen hier niet ontbreken en ook hen bedank ik voor alle niet-fysische steun.

Verder bedank ik nog een aantal mensen van diverse pluimages: Jaap Broekman voor het kritisch bekijken van een gedeelte van dit proefschrift op al te opvallende fouten tegen de Engelse taal en ome Jan Verstralen voor de financiële bijstand om dit proefschrift en het bijbehorende feest mogelijk te maken. En tot slot alvast een woord van dank aan mijn paranimfen Manon en Jaap voor de morele ondersteuning tijdens mijn promotie.

Contents

List of Tables

List of Figures

Chapter 1

Introduction

1.1 Quarks and quarkonium

In 1964 quarks were "invented" by Gell-Mann and Zweig. These particles—in those days considered merely as mathematical entities—are now regarded as true elementary particles that are the building blocks of particles called *hadrons* which make up ordinary matter. The hadrons can be divided into two classes: the *baryons*, consisting of three quarks, and the *mesons*, consisting of a quark and an antiquark. The mesons are the subject of this thesis. If a meson is built up from a quark and its own antiquark, we speak of *quarkonium*.

The quarks occur in six different varieties, called *flavours*. The sixth flavour—the top quark—has not been discovered yet, but physicists have good reasons to believe it does exist. In present (LEP in Geneva, Switzerland) and future (LEP200 and SSC in Texas, USA) colliders the search for the missing quark continues. The belief that a sixth quark must exist emerges from a set of theories that contains our present knowledge of fundamental particles and their interactions, called the *Standard Model*.

A strange thing about these quarks, apart from their fractional charge ($+2/3e$, $-1/3e$), is their behaviour at very short distances from each other, where their interaction is very weak (*asymptotic freedom*), and at large distances, where the interaction is so strong that it is impossible to free a single quark from a hadron (*confinement*). The quarks are so to say glued together inside the hadrons.

Although confinement is still a bit mysterious, it has become clear that it has something to do with another property of quarks, *viz. colour*. Every flavour occurs in three colours: red, blue, and yellow. (Note that this is a mathematical property and not a "real" property: quarks are pointlike particles and hence cannot have real

colour, which is a macroscopic quantity.) If one has three colours (and three anti-colours) there are two ways to make "white", or colourless, particles: put together a red, a blue , and a yellow quark (a baryon), or a red (or a blue, or a yellow) quark and an antired (or antiblue, or antiyellow) antiquark (a meson). Under the assumption that we can observe only colourless particles, it is evident that we can't see free quarks.

The Standard Model prescribes that all fundamental forces act through the exchange of particles (so called *gauge bosons*) and in the case of hadrons these particles are the *gluons* and the force is called the *strong force*. The interaction of coloured quarks and coloured gluons is described by *Quantum Chromo Dynamics* (Fritzsch and Gell-Mann, 1972), or QCD in short ("chromo" means colour). This is a so called *gauge theory*, which is a very important kind of theory in modern physics and will be discussed in Section 1.2.

Despite the strong force the hadrons fall apart very quickly: their mean lifetime is about 10^{-23} secs. If we assume that they move with the speed of light ($3 \cdot 10^8$ m/s), then they travel during their life a distance of a few fermi (1 fm = 10^{-15} m), that is, a few times their own size.

Thus QCD is the theory of the strong interactions (see Section 1.3) and in principle all static and dynamic properties of hadrons could be calculated. In practice, however, most computations prove to be too difficult to perform due to the complexity of the theory. That's why we have to look for other methods to describe the hadrons. One approach is to discretize space-time and to do QCD calculations with the aid of fast powerful computers: *lattice QCD* (see Section 1.4). Another is to leave QCD for what it is and to follow a more empirical approach: what can we learn about the interquark interaction from the data? The latter method is a phenomenological one (see Section 1.5) and is the one followed in this thesis.

The Unitarized Meson model of the Nijmegen group tries to describe the properties of quarkonium (those consisting of light quarks as well as those with heavy quarks) in a consistent way. Our model is essentially non-relativistic and therefore heavy quarkonium, that is, charmonium and bottomonium, is particularly suited to be described by our model and that is where the emphasis lies in this thesis.

Recently, the model has been extended with a one-gluon-exchange potential in order to describe the P-wave levels next to the S-wave levels in quarkonium (see Chapter 3). This enables us to calculate the electric dipole radiative transitions. Some mesons can decay into another meson while radiating a photon; this process is called an *electromagnetic (or radiative) transition*. In Chapter 4 the theoretical background will be given for these processes and then applied to our (multi-channel)

model.

Our aim is to extract information from experimentally obtained data by comparing these data with the results from our model. A satisfactory agreement gives an indication of the correctness of the assumptions underlying the model. And this, in turn, will hint at the correct form of the interaction between (anti)quarks, which will bring us one step further in the—I think never ending—process of unravelling the secrets of nature.

But first a few words will be said about gauge theories and QCD.

1.2 Gauge theories

Since all known interactions can be described by so called *gauge theories*, I will discuss this subject shortly.

A gauge theory is characterized by the requirement of local symmetry with respect to a (non-abelian) Lie group G. A Lie group G is defined by the commutation relations of its generators T^a,

$$\left[T^a, T^b\right] = i f_{abc} T^c \ , \tag{1.1}$$

where f_{abc} is the structure constant tensor of the group and automatic summation over repeated indices is understood. The adjoint representation G is defined by

$$(T^a_G)_{bc} = \frac{1}{i} f_{abc} \ . \tag{1.2}$$

Furthermore let's introduce for objects X_a, $a = 1, \ldots, d(G)$ the matrix notation $X \equiv X_a T^a$. A gauge transformation now reads

$$U = \exp(-i\Lambda) \ , \ \Lambda \equiv \Lambda_a T^a \ , \tag{1.3}$$

with Λ real and hence U unitary. The vector $\psi \equiv \{\psi_i\}$ of fermions of the theory under consideration thus transforms according to

$$\psi \to \psi' = U\psi \ , \ \bar{\psi} \to \bar{\psi}' = \bar{\psi} U^{-1} \ . \tag{1.4}$$

Let us start with the Lagrangian of free Dirac spinors,

$$\mathcal{L} = \bar{\psi}(i\partial\!\!\!/ - m)\psi \ . \tag{1.5}$$

This Lagrangian is obviously invariant under *global* symmetry transformations, $\partial_\mu \Lambda = 0$, if the fermion mass matrix $m \equiv \{m_{ik}\}$ satisfies $U^{-1} m U = m$, *i.e.*, if it

commutes with all generators T^a of the gauge group, $[T^a, m] = 0\ \forall_a$. Consequently, the mass matrix has to be proportional to the unit matrix in every irreducible representation R_σ. (For a unitary representation R we can make a decomposition $R = \oplus_\sigma R_\sigma$, with R_σ an irreducible unitary representation.) In contrast to that, the kinetic term $i\bar{\psi}\partial\!\!\!/\psi$ is not invariant under *local* symmetry transformations, $\Lambda = \Lambda(x)$, since in this case the derivation of the fermion field generates an additional term,

$$\partial_\mu \psi \to \partial_\mu \psi' = U \partial_\mu \psi + (\partial_\mu U)\psi \ . \tag{1.6}$$

Nevertheless, the requirement of local gauge symmetry may be fulfilled by introducing *vector gauge fields* $V_\mu \equiv V_\mu^a T^a$ with the transformation behaviour

$$V_\mu \to V_\mu' = U(V_\mu + \frac{i}{g}\partial_\mu)U^{-1} \ , \tag{1.7}$$

where g denotes the *gauge coupling constant*. Furthermore, every partial derivative ∂_μ has to be replaced by the *(gauge) covariant derivative*

$$D_\mu = \partial_\mu - igV_\mu \ . \tag{1.8}$$

In particular, this covariant derivative reads

$$D_\mu^{ab} = \partial_\mu \delta_{ab} - g f_{abc} V_\mu^c \tag{1.9}$$

for the adjoint representation (1.2), and

$$D_\mu X = \partial_\mu X - ig\,[V_\mu, X] \tag{1.10}$$

when applied to the matrices defined above. The transformation behaviour of the covariant derivative $D_\mu \psi$ is then identical to the transformation behaviour of the fields themselves,

$$D_\mu \psi \to (D_\mu \psi)' = U D_\mu \psi \ . \tag{1.11}$$

This can easily be checked with the help of the relation

$$(\partial_\mu U^{-1})U + U^{-1}\partial_\mu U = 0 \tag{1.12}$$

resulting from $U^{-1}U = 1$. The above transformation behaviour of the covariant derivative ensures the local gauge invariance of the Lagrangian

$$\mathcal{L}_F = \bar{\psi}(iD\!\!\!/ - m)\psi \ . \tag{1.13}$$

In order to be able to regard the vector fields as genuine dynamical degrees of freedom of the theory, a corresponding kinetic term has to be present in the Lagrangian. The kinetic term for vector fields is

$$\mathcal{L}_V = -\frac{1}{4} F^a_{\mu\nu} F^{\mu\nu}_a \tag{1.14}$$

with the field strength tensor

$$F_{\mu\nu} \equiv F^a_{\mu\nu} T^a = \partial_\mu V_\nu - \partial_\nu V_\mu - ig\,[V_\mu, V_\nu] \tag{1.15}$$

or

$$F^a_{\mu\nu} = \partial_\mu V^a_\nu - \partial_\nu V^a_\mu + g f_{abc} V^b_\mu V^c_\nu \,. \tag{1.16}$$

The homogeneous transformation behaviour of the field strength, resulting from (1.7),

$$F_{\mu\nu} \to F'_{\mu\nu} = U F_{\mu\nu} U^{-1} \,, \tag{1.17}$$

guarantees the gauge invariance of the kinetic term $\mathcal{L}_V$ of the vector bosons. The covariant derivative D_μ and the field strength tensor $F_{\mu\nu}$ are connected via the relation

$$[D_\mu, D_\nu] = -igF_{\mu\nu} \,. \tag{1.18}$$

A mass term for the vector bosons

$$\mathcal{L}_M = \frac{1}{2} M^2_{ab} V^a_\mu V^b_\nu \tag{1.19}$$

is forbidden by the requirement of gauge invariance. The gauge fields V^a_μ are therefore (apparently) massless.

In summary, the most general gauge invariant Lagrangian for Dirac spinors, but without scalar bosons, reads

$$\begin{aligned} \mathcal{L} &= \mathcal{L}_V + \mathcal{L}_F \\ &= -\frac{1}{4} F^a_{\mu\nu} F^{\mu\nu}_a + \bar{\psi}(i\not{D} - m)\psi \\ &= -\frac{1}{4} F^a_{\mu\nu} F^{\mu\nu}_a + \bar{\psi}(i\not{\partial} + g\not{V}_a T^a - m)\psi \,. \end{aligned} \tag{1.20}$$

The requirement of local gauge invariance implies the existence of (apparently) massless gauge bosons. The number of these gauge bosons is equal to the order of the gauge group G, that is, equal to the number of independent generators or parameters of the group. Replacing all partial derivatives ∂_μ by the corresponding covariant derivatives D_μ, the global invariance of a Lagrangian $\mathcal{L}(\psi, \partial_\mu \psi)$ becomes the local invariance of $\mathcal{L}(\psi, D_\mu \psi)$.

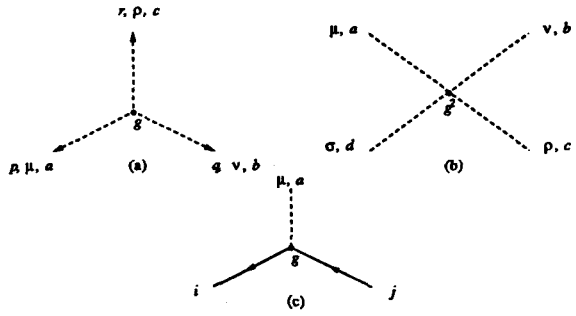

Figure 1.1: Vertices in a general (non-abelian) gauge theory: (a) three–vector-boson vertex, (b) four–vector-boson vertex, (c) vector-boson–fermion vertex.

In contrast to abelian gauge theories the kinetic term of the vector bosons, $\mathcal{L}_V$, describes in the case of non-abelian gauge theories not only free gauge fields but also self-interactions of the vector bosons. The form of these self-couplings is unambiguously prescribed by gauge invariance:

$$\begin{aligned}\mathcal{L}_V &= -\frac{1}{4}F^a_{\mu\nu}F^{\mu\nu}_a \\ &= -\frac{1}{4}(\partial_\mu V^a_\nu - \partial_\nu V^a_\mu)(\partial^\mu V^\nu_a - \partial^\nu V^\mu_a) - g f_{abc} V^\mu_a V^\nu_b \partial_\mu V^c_\nu \\ &\quad -\frac{1}{4}g^2 f_{abc} f_{ade} V^b_\mu V^c_\nu V^\mu_d V^\nu_e \ . \end{aligned} \tag{1.21}$$

Accordingly, there are three types of vertices in the theory, namely the three–vector-boson vertex (given by the second term of (1.21), the four–vector-boson vertex (given by the third term), and the vector-boson–fermion vertex (given by the second term of (1.20)) depicted in Fig. 1.1. Abelian gauge theories are contained in the above discussion as the special case $f_{abc} = 0\ \forall_{a,b,c}$. Of course, here are no self-couplings of the vector bosons present.

In the course of quantization of gauge theories one encounters a further difficulty. The definition of the vector-boson propagator requires the free equation of motion of the vector bosons to be invertible. However, as a consequence of gauge invariance, the differential operator following from (1.14), $g_{\mu\nu}\Box - \partial_\mu\partial_\nu$, is singular. This problem may be circumvented by restricting oneself to a certain gauge. This *gauge fixing*, in turn, may be realized by adding to the Lagrangian a "gauge fixing" term $\mathcal{L}_{GF}$ which is reminiscent of the chosen gauge condition. A popular gauge—and, in fact, the most convenient one for performing high-energy investigations—is the so called

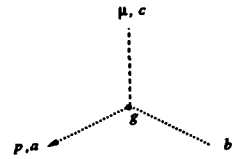

Figure 1.2: Vector-boson–ghost vertex in a general (non-abelian) gauge theory.

R_ξ *gauge*, which leads to the gauge-fixing term

$$\mathcal{L}_{GF} = -\frac{\xi}{2}(\partial_\mu V_a^\mu)^2 \,, \tag{1.22}$$

where the gauge parameter ξ (also denoted by λ^{-1}) is left arbitrary. However, any addition of a term like this to a Lagrangian represents a modification of the original theory. In order to maintain the unitarity of the S-matrix a further modification of the theory is necessary. This further modification may be achieved by adding a term to the Lagrangian—at the price of introducing so called *ghost fields*. These Faddeev-Popov ghosts, ζ_a, $\bar{\zeta}_a$, are anticommuting scalar fields in the adjoint representation of the gauge group which, however, only show up as internal lines. To each independent gauge symmetry, i.e., to each gauge boson V_μ^a, are associated two of these ghosts, ζ_a and $\bar{\zeta}_a$. The corresponding ghost Lagrangian $\mathcal{L}_G$ is in general not hermitian and depends on the chosen gauge condition. For the R_ξ gauge it reads

$$\begin{aligned} \mathcal{L}_G &= (\partial_\mu \bar{\zeta}) D^\mu \zeta \\ &= (\partial_\mu \bar{\zeta}_a)\partial^\mu \zeta_a - g f_{abc}(\partial_\mu \bar{\zeta}_a)\zeta_b V_c^\mu \,, \end{aligned} \tag{1.23}$$

yielding the vector-boson–ghost vertex in Fig. 1.2. Notice that because of the non-hermitian character of the ghost term the ghost lines have to be oriented.

In an abelian gauge theory (with linear gauge condition) the ghosts decouple due to $D_{ab}^\mu = \partial^\mu \delta_{ab}$ for $f_{abc} = 0$. Hence, abelian gauge theories are free of ghosts or, more precisely, may be formulated without introduction of ghosts.

Now let us apply the concept of gauge invariance to the strong interactions.

1.3 Quantum chromodynamics (QCD)

Quantum chromodynamics is the theory of the strong interactions, that is, the interactions between (anti)quarks. The name QCD is derived from QED. The electric charge from QED has been replaced by the colour charge of QCD ("chromo" means colour). The gauge group is $SU(3)_C$, where C stands for colour. It is an unbroken,

non-abelian symmetry group. The eight generators give rise to eight massless vector bosons G^a_μ (a=1,...,8), so called *gluons*, in the adjoint representation $\underline{8}$ of $SU(3)$. These gluons carry the forces between at least six *quarks* (the fermions of the theory), transforming as the fundamental three dimensional representation $\underline{3}$ of $SU(3)$. The fundamental generators are

$$T^a_{\text{fund}} = \frac{\lambda^a}{2} \; (a = 1, \ldots, 8) \tag{1.24}$$

with λ^a the Gell-Mann matrices. The Lagrangian becomes

$$\mathcal{L} = -\frac{1}{4} F_{\mu\nu} F^{\mu\nu} + \sum_{f=1}^{n_f} \bar{q}_f (i\not{D} - m_f) q_f - \frac{\xi}{2} (\partial^\mu G^a_\mu)^2 + (\partial_\mu \bar{\zeta}) D^\mu \zeta \; , \tag{1.25}$$

with

$$F^a_{\mu\nu} = \partial_\mu G^a_\nu - \partial_\nu G^a_\mu + g_s f_{abc} G^b_\mu G^c_\nu \tag{1.26}$$

$$D_\mu = \partial_\mu - i g_s G^a_\mu \frac{\lambda^a}{2} \; . \tag{1.27}$$

The parameters of the theory are the strong coupling constant, g_s, and the (bare) quark masses, m_f. In a renormalization procedure the bare coupling g_s becomes an *effective (running) coupling constant* (see for example [Luc89])

$$\alpha_s(Q^2) = \frac{12\pi}{(33 - 2n_f) \ln Q^2/\Lambda^2} \; , \tag{1.28}$$

where $\alpha_s = g_s^2/4\pi$, n_f is the number of (effective) quark flavours and Q is the momentum exchanged between the (anti)quarks. Λ is an invariant scale parameter that comes into the expression for α_s as an integration constant. From the expression (1.28) we note that $\alpha_s(Q^2) \to 0$ for $Q^2 \to \infty$ (as long as $n_f \leq 16 < \frac{33}{2}$). This means that QCD becomes a free theory (no interactions) in the high-energy limit. This fact is expressed by saying that QCD is *asymptotically free.*

To the massless gluons should correspond a long-range interaction associated with colour (*cf.* the photon and the electromagnetic force). But this force is not observed, so there must be more than sketched above. Two possible explanations are:

- there exists a kind of spontaneous symmetry breaking, like in the electroweak case, which will give a mass to the gluons and limit the range of the interaction, or

- only colour singlets are observable, because singlet colour states don't exert a force on one another (except possibly a Van der Waals force)—*cf.* two electrically neutral particles are not subject to the electromagnetic force.

Current prejudices favour the second opinion, known as *colour confinement*, which is believed to be a consequence of the $SU(3)_C$ gauge theory. Experimentally, single quarks or gluons are not observed. The precise mechanism responsible for confinement, however, is not yet understood.

Is it now possible to calculate diagrams (as part of a perturbation series) for processes governed by QCD, like in QED? Unfortunately, the answer is no. In QED the series expansion parameter $\alpha(Q^2)$ starts at $\alpha(0) = 1/137$. (Also in QED the coupling constant is running, although very slowly.) This is a small number, so the series will converge rapidly. In QCD, however, $\alpha_s(0)$ is infinite, so a perturbation approach is doomed to fail. But as we saw in the expression for $\alpha_s(Q^2)$, Q^2 is scaled by the scale parameter Λ. Hence if $Q^2 \gg \Lambda^2$ a perturbation approach will make sense. Experimentally Λ lies in the range from 100-500 MeV. (Λ depends on the number of active flavours).

Until now only QCD calculations have been performed for processes with $Q^2 \gg \Lambda^2$. In order to learn more about confinement we will have to look for other methods, because of the non-perturbative character of confinement. But we hope that some day we will be able to use QCD for classic problems in hadron physics, such as the force between two protons, or the binding energy of the deuteron, etc., which is impossible now due to the complicated many-body systems involved. Compare this situation to the one in physical chemistry: there quantum mechanics has been applied successfully for the calculations on large molecules.

But what cán we do at the moment? Roughly speaking there are two different approaches:

- investigate non-perturbative methods: *lattice QCD*, or *flux-tube* and *string models*, or *bag models*.

- use perturbative methods for $Q^2 \gg \Lambda^2$: *potential models*.

Of the former three approaches lattice QCD is closest to the fundamental theory (QCD). In this theory space-time and fields are discretized on a so called lattice. Because in this theory the approximations are being made in the calculations and not (so much) in the theory, I will pay more attention to lattice QCD in the next section. Moreover, I think lattice QCD might be the only serious competitor for the phenomenological models. Flux-tube and string models—like QCD—have not been

used to a great extent to calculate the static properties of quarkonia, so I will not discuss these models here. Bag models have had a number of successes, mainly with calculations of the properties of light ground-state mesons. It has not been useful in calculating properties of heavy quarkonia, so I will leave it out too.

The second approach will be followed in this thesis, but first I shall pay some attention to lattice QCD.

1.4 Lattice QCD

At very high energies a perturbation approach to quantum chromodynamics will fail due to the large coupling constant, α_s. Therefore one has to turn to non-perturbative methods for calculations at these energy scales. Moreover, with these methods solutions to puzzles like proton stability and CP violation might be found. Indeed, a fundamental theory—which QCD is believed to be—should answer such questions. Whether the above mentioned non-perturbative methods make it possible to do investigations on this fundamental theory, or make approximations necessary such that the theory turns into an effective theory remains a question. Effective theories differ from fundamental theories in that they provide a valid phenomenology up to some finite momentum cut-off. For momenta much smaller than the cut-off, they appear very much like fundamental theories, but close to the cut-off the need for an underlying fundamental theory becomes apparent.

Non-perturbative quantum field theory is an extension of statistical mechanics to four dimensions, using the Feynman path integral. Space-time and fields are discretized on a finite *lattice* to make the theory accessible for computer applications. By discretization some important symmetries are broken; which of them are restored in the zero-lattice-spacing or *continuum limit* is a question of fundamental importance. Continuum physics is found at *critical points* of the lattice theory corresponding to second order phase transitions. It can be shown that any gauge theory exhibits confinement on a finite lattice. In the continuum limit QED undergoes a phase transition to a non-confining mode, but it is unclear if this also holds for QCD.

In taking the continuum limit it is not necessary to take the lattice spacing, a, to zero, but it suffices to take it small enough such that predictions do not depend significantly on it. This is called *scaling* with which an important parameter is associated that determines the quality of the computer solution. This computer solution must be validated against experimental or analytical results before any explanation or prediction can be made. The work on quantum field theory has not

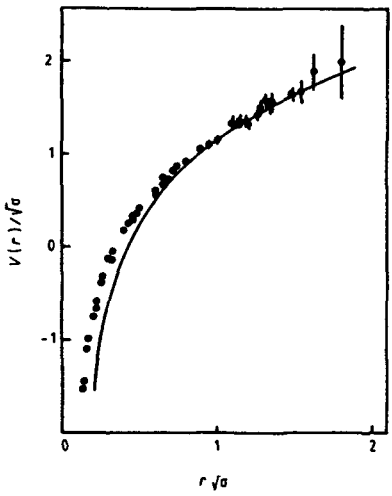

Figure 1.3: Comparison of the computed potential with the phenomenological Cornell potential for charmonium, normalized to agree at $r\sqrt{\sigma} = 1$.

yet passed the validation stage. In this sense lattice QCD (still) is an effective theory with a cut-off in the form of a lower bound on the lattice spacing.

In the calculations *Monte Carlo* methods are used to generate a sample of lattice field configurations. Then expectation values of products of fields are approximated by averages over this finite sample. The motivation for the computer simulation of a quantum field theory is that it provides a controlled approximation to the non-perturbative solution. It is necessary, therefore, to identify and analyze the sources of systematic error, coming from the algorithms used. Apart from the systematic errors there are of course statistical errors. These are proportional to $1/\sqrt{\sharp\text{configurations}}$ and the current number of configurations is up to a few hundred. Another source of error is scaling violation: due to computer hardware limitations the lattice volume is too small. As a consequence, in many current simulations the particles involved are squeezed into a box smaller than their size.

The current state-of-the-art [Ken89] is summarized below for the two main approaches in lattice QCD: the *quenched approximation*, where the quarks are taken to be very massive and hence there is no dynamics, and *fully interacting QCD*, where dynamical effects are responsible for (part of) the masses of the interacting fermions.

Quenched QCD:

- This approximation is the oldest approach and the numerical results are best established.

- The static quark-antiquark potential agrees with the phenomenological Cornell potential [Eic80],

$$V(r) = -\frac{4\alpha_s}{3r} + \sigma r \ ,$$

for long distances but not at short distances (see Figure 1.3 where the potential is plotted for charmonium). In a very recent paper [Din90] a new lattice simulation (of 1300 CPU hours(!) on a new fast computer) yielded a result for the potential for charmonium comparable to the result of the Cornell group, whereas previous calculations [For86, Din88] gave different results:

	[Din88, For86]	[Din90]	[Eic80]
κ	0.25–0.35	0.58	0.52
σ (GeV^2)	0.20	0.15	0.18

Here $\kappa \equiv \frac{4}{3}\alpha_s$.

- There exists a transition to a non-confining mode at a critical temperature, $T_c \simeq 250$ MeV. The order of the transition is not yet established, so it is unclear whether this non-confining mode is an artifact due to the method used (lattice too small) or a real feature of the theory.

- Hadron masses can be calculated only as ratios. Usually the results are depicted in a so called Edinburgh plot (Figure 1.4). The quantitative agreement with experiment is poor.

Fully interacting QCD:

- It is developed over the last three years. In general the couplings are too large and the lattice too small for scaling to be demonstrable.

- There is not much difference with the quenched approximation for the quark-antiquark potential.

- The situation for the hadron masses is depicted in Figure 1.5; it is in a similar state as the quenched hadron masses five years ago.

It should be noted that the computer solution of quantum field theories is barely ten years old. Due to the rapid advances in computer performance, the development

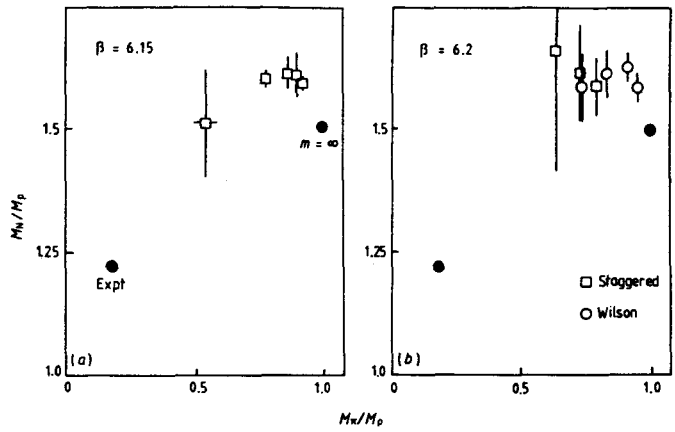

Figure 1.4: Edinburgh plot for the nucleon mass versus the pion mass in units of the ρ meson mass: (a) Edinburgh data [Bow88], (b) Los Alamos data [Gup87]. The legend of the data points refers to different approximation methods (staggered *vs.* Wilson fermions) and the quantity β contains information about the scaling.

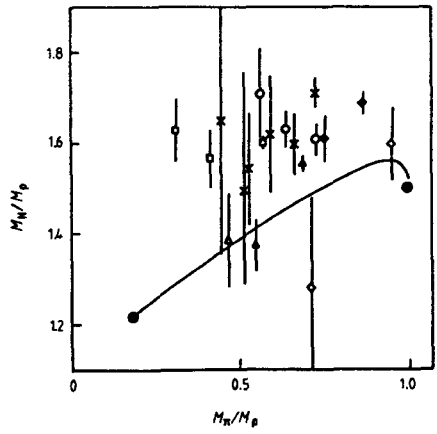

Figure 1.5: Compilation of hadron mass data for fully interacting QCD.

of algorithms and programming tools, and our better understanding of quantum field theory, the prospects for the next ten years look good. There is hope that convincing solutions to many fundamental questions about the Standard Model—and about quantum chromodynamics in particular—might be obtained. Even then, however, the practical significance of lattice QCD remains questionable.

But, at the moment, lattice QCD is not very powerful in the prediction of properties of quarkonia. If we want to describe these properties (masses, widths, etc.) we have to try our luck with other approaches. The approach with the most descriptive and predictive power is the one with potential models and these are the subject of the next section.

1.5 Phenomenology

As we saw in the previous sections, gauge theories prove to be successful in the description of the interactions between (fundamental) particles. If we want to study particles that are bound states of (anti)quarks the appropriate framework is the Bethe-Salpeter formalism. The Bethe-Salpeter equation, however, cannot be solved in general but only in ladder approximation. The interaction kernel entering in this equation is not derivable from QCD, but some approximations can be made in order to use this formalism. Even then it is hard to obtain information from this approach.

An approach that has proven to be successful for the calculations of the properties of bound states is the non-relativistic Schrödinger equation. This is a so called *phenomenological* approach. According to the Webster dictionary phenomenology means "the description of the formal structure of phenomena in abstraction from interpretation or evaluation especially as a foundation for the sciences." That is, the attempt to discover regularities from the experimental data and to mould these regularities into a model, which cannot only describe the data but also predict new phenomena.

Phenomenology can help us testing some predictions QCD makes:

- is the interquark interaction independent of quark species?
- does the interaction approach a Coulomb-like form near the origin?

In the remainder of this chapter I will investigate these issues. I will start with the central point of the Schrödinger equation: the potential.

1.5.1 Potentials

The potential that enters into the Schrödinger equation describes the interaction of the particles constituting the bound state. How can this potential be obtained? One way is to make a more or less ad hoc assumption and see how good it fits the data; another is to try and extract information about the potential from QCD. An example of this method is to consider the scattering of the constituents and derive the *perturbatively* accessible part of the potential by taking the Fourier transform of the scattering amplitude T_{fi}:

$$V(\boldsymbol{r}) = -(2\pi)^3 \int d^3k e^{-i\boldsymbol{k}\cdot\boldsymbol{r}} T_{fi}^{\mathrm{NR}}(k) \,, \tag{1.29}$$

where T_{fi}^{NR} is the non-relativistic limit of T_{fi} defined in terms of the S-matrix element S_{fi} by

$$S_{fi} = \delta_{fi} + i(2\pi)^4 \delta^{(4)}(P_f - P_i) \cdot T_{fi} \tag{1.30}$$

in lowest order of perturbation theory.

When we follow this recipe in case of one-gluon-exchange (one-gluon-exchange is the lowest-order diagram in quark-antiquark scattering) between a quark and an antiquark in a meson, we obtain a Coulomb-like potential (see [Luc89])

$$V(r) = -\frac{4}{3}\frac{\alpha_s}{r} \qquad , \alpha_s \equiv \frac{g_s^2}{4\pi} \,. \tag{1.31}$$

The potential obtained in this way is called a *QCD-motivated* potential, because it was derived from lowest-order perturbative QCD. As we saw from Figure 1.3, where the potential from lattice QCD was plotted, the combination of a Coulomb-like and a linear potential is also derived from QCD and hence called QCD motivated.

There are two other classes of potentials, *viz. partly* and *purely phenomenological.* In the former category are potentials that consist of a Coulomb part and a non-linear confining part, in the latter the potential can be arbitrary. Later on I will discuss some potentials from these three categories, but first I will look at power-law potentials in general.

An attractive feature of the Schrödinger equation is the fact that it is easy to investigate the scaling properties of a given potential. By *scaling* is meant the (in)dependence of energy levels, wave functions, etc. upon mass and coupling strength. Scaling is particularly easy to demonstrate for *power-law potentials*

$$V(r) = \lambda r^{\nu} \qquad (-2 < \nu < \infty) \,. \tag{1.32}$$

Some interesting results, taken from [Qui79], are listed below.

- The level spacings scale according to

$$\Delta E \propto (2\mu)^{-\nu/(2+\nu)}|\lambda|^{2/(2+\nu)} . \tag{1.33}$$

- The probability density at the origin scales as

$$|\Psi(0)|^2 \propto (\mu|\lambda|)^{3/(2+\nu)} , \tag{1.34}$$

- and the electric and magnetic dipole widths as

$$\Gamma(E1) \propto \mu^{-(2+3\nu)/(2+\nu)}|\lambda|^{4/(2+\nu)} \tag{1.35}$$
$$\Gamma(M1) \propto \mu^{-(4+5\nu)/(2+\nu)}|\lambda|^{6/(2+\nu)} \tag{1.36}$$

  respectively.

The leptonic decay width [Roy67] is related to (1.34) by

$$\begin{aligned}\Gamma(V \to l^+l^-) &= 16\pi\alpha^2 e_Q^2 |\Psi(0)|^2/M_V^2 \\ &\propto e_Q^2 \mu^{-(1+2\nu)/(2+\nu)}|\lambda|^{3/(2+\nu)} \ (\nu \geq -1)\end{aligned} \tag{1.37}$$

if we assume $M_V \simeq 2 \cdot 2\mu$, that is, we neglect the binding energy.

Of interest is, also, the logarithmic potential

$$V(r) = C\ln(r/r_0) , \tag{1.38}$$

which behaves in some respects as the $\nu \to 0$, $\lambda \to \infty$, $\lambda\nu \to C$ limit of (1.32). For the logarithmic potential, the level spacings are independent of the reduced mass, which is an important property because the level spacings in quarkonium seem to be independent of μ as we will see later.

If we assume that for the harmonic-oscillator potential the coupling λ is proportional to the reduced mass ($V_{\rm HO} = \frac{1}{2}\mu\omega^2 r^2$), the level spacings prove to be mass independent too. Moreover, they are constant: $\Delta E \propto \omega$. In Table 1.1 the scaling properties for various potentials are tabulated. From this table we see that the scaling properties of the logarithmic and harmonic-oscillator potential are identical. This is an important property of the harmonic oscillator.

Now that we know the scaling properties of several potentials, let us turn to the experimental situation: is it possible to deduce a value for ν from the data? In Table 1.2 the first three triplet-S states for charmonium and bottomonium with

Potentials	ν	ΔE	$\Gamma(E1)$	$\Gamma(M1)$	$\Gamma(V \to l^+l^-)$
Coulomb	-1	μ	μ	μ	μ
Logarithmic	0	μ^0	μ^{-1}	μ^{-2}	$\mu^{-1/2}$
Linear	1	$\mu^{-1/3}$	$\mu^{-5/3}$	μ^{-3}	μ^{-1}
Harmonic oscillator[a]	2	μ^0	μ^{-1}	μ^{-2}	$\mu^{-1/2}$
Square well	∞	μ^{-1}	μ^{-3}	μ^{-5}	μ^{-2}

[a] Assumed is $\lambda \propto \mu$.

Table 1.1: Scaling properties of some physical quantities in various power-law potentials.

their masses and leptonic widths are listed. These give

$$\begin{aligned}
\frac{E_3(\psi) - E_2(\psi)}{E_2(\psi) - E_1(\psi)} &= 0.60 \pm 0.02 \ , \\
\frac{E_3(\Upsilon) - E_2(\Upsilon)}{E_2(\Upsilon) - E_1(\Upsilon)} &= 0.590 \pm 0.002 \ , \text{ and} \\
\frac{E_2(\Upsilon) - E_1(\Upsilon)}{E_2(\psi) - E_1(\psi)} &= 0.956 \pm 0.001 \ .
\end{aligned}$$

These results indicate that the scaling almost goes like μ^0 and with $m_b/m_c \simeq 3$ (it is 2.98 in our Unitarized Meson model, see Chapter 3) and equation (1.33) we find[1]

$$\nu = 0.085 \pm 0.002 \ , \tag{1.39}$$

that is, the effective power is close to zero.

What can be deduced from the leptonic widths? Table 1.2 in combination with equation (1.37) yields

$$\begin{aligned}
1S \quad \nu &= -0.6 \pm 0.2 \\
2S \quad \nu &= -0.6 \pm 0.1 \\
3S \quad \nu &= -0.9 \pm 0.1 \ .
\end{aligned} \tag{1.40}$$

The fact that these values are not at all in agreement with the value for ν from the level spacings is no cause for concern. Indeed, the powers deduced from the leptonic widths give information about the effective power near the origin (because

[1] For $m_b/m_c = 3.5$, $\nu = 0.075$ and for $m_b/m_c = 4$, $\nu = 0.067$, so probably $\nu = 0.08 \pm 0.01$ is more correct a statement.

	mass (MeV)	$\Gamma_{e^+e^-}$ (keV)		mass (MeV)	$\Gamma_{e^+e^-}$ (keV)
J/ψ	3096.9 ± 0.1	4.72 ± 0.35	Υ	9460.3 ± 0.2	1.34 ± 0.05
ψ'	3686.0 ± 0.1	2.15 ± 0.21	Υ'	10023.3 ± 0.3	0.60 ± 0.04
ψ''	4040 ± 10	0.75 ± 0.15	Υ''	10355.3 ± 0.5	0.44 ± 0.03

Table 1.2: Masses and leptonic widths of the first three $^3S_1$-states in charmonium and bottomonium. Data are taken from [PDG88].

of the occurrence of the wave function in the origin in the formula for the leptonic width) and we expect this power to be negative because of the singular Coulomb interaction in that region. The power deduced from the level spacings gives more information on the form of the potential at intermediate distances. Note that it does not necessarily give information about the precise form of the confining part of the potential, which governs at large distances.

From the scaling properties of power-law potentials and the experimental data we can conclude that near the origin the effective potential is singular and attractive and at intermediate distances it is logarithmic or a harmonic oscillator (as both have the same scaling properties). The latter conclusion seems to contradict the QCD prediction of a linear confining term. This result was deduced, however, from the data of charmonium and bottomonium. These states lie in a limited interval (0.2–1.0 fm) and other quarkonium systems—such as toponium for smaller distances and the light mesons for larger distances—may give other information. A problem with the light mesons is the fact that a non-relativistic description is no longer valid. Toponium, on the other hand, has not been discovered yet.

Besides, there is a wide variety of potential models that is able to describe the charmonium and bottomonium spectra fairly well. This has to do with the fact that the potentials of these models are almost equal in the $c\bar{c}$ and $b\bar{b}$ region 0.2–1.0 fm (see Figure 1.6).

Below several potentials are listed:

- Potentials of the type

$$V(r) = -ar^{-\alpha} + br^{\alpha} + c \qquad (a, b, \alpha > 0)$$

occur frequently in the literature. Values for α are

$\alpha = \frac{1}{2}$ Ref. [Son87]
$\alpha = \frac{3}{4}$ Ref. [Lic89], the Turin potential
$\alpha = 1$ Ref. [Eic80], the Cornell potential.

The former two are purely phenomenological, while the latter is the QCD-motivated Coulomb-plus-linear potential.

- The purely phenomenological potential

$$V(r) = ar^{0.1} + c$$

(Ref. [Mar81]), which behaves almost like a logarithmic potential. The result of equation (1.39) was a motivation for the introduction of this potential.

- The QCD-motivated potentials

$$\begin{aligned} V(r) &= b\frac{(1-ar)^2}{r\ln(ar)} + c \text{ , the Indiana potential [Fog79]} \\ V(q^2) &= b\frac{1}{q^2}\frac{1}{\ln(1+q^2/a)} \text{ , the Richardson potential [Ric79]} \\ V(q^2) &= a\frac{\alpha_s(q^2)}{q^2} \text{ , with } \alpha_s \text{ the running coupling constant [Buc81],} \end{aligned}$$

that all have the asymptotic limits predicted by QCD.

Note that all these potentials are single-channel potentials, *i.e.* decay is not accounted for[2]. A selection of potentials is plotted in Figure 1.6. There where the potentials for charmonium and bottomonium were not equal, the potential for charmonium was plotted. The parameters of the Nijmegen potential can be found in Chapter 3.

A realistic model cannot be complete without the incorporation of hadronic decay. How could decay be described and are there any models that do so?

1.5.2 Hadronic decay

The addition of non-diagonal terms to the potential, that is, coupling the bound state to a set of (virtual) decay channels[3], causes a shift in the energy of the bound state. This shift can be well over 100 MeV, so one has to be careful with the interpretation of the results of the single-channel models: the calculated energy levels should not

[2] In [Eic80] coupled channels are added to the single-channel model (called the "naive model"), so the Cornell model is in fact a multi-channel model. Most references to this model, however, apply to the naive model.

[3] Virtual decay channels are channels to which decay is forbidden energetically. Even coupling to these virtual channels causes a shift in the energy. These virtual channels are important for particles that lie below the threshold for hadronic decay and it is these particles that we are interested in: the ψ and Υ family.

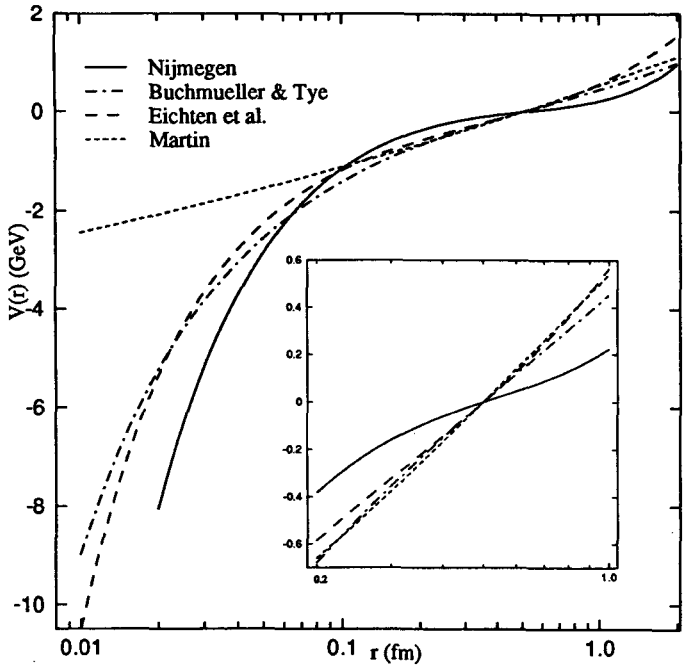

Figure 1.6: Comparison between various potentials, shifted in such a way that $V(r = 0.5 \text{ fm}) = 0$. The small inserted plot shows the potentials in the region where the charmonium and bottomonium states reside. References can be found in the text.

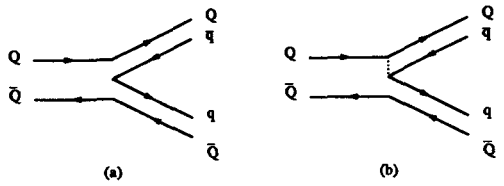

Figure 1.7: Hadronic decay via (a) the $^3P_0$-mechanism, and (b) the $^1S_0$-mechanism.

agree too precisely with the data! Moreover, the shifts are different for different particles and their excitations. Our model learns that the 1^3S_1 state has a larger shift than the 2^3S_1 and 3^3S_1 states. The question arises what the validity is of conclusions drawn from potential models in general and single-channel models in particular. Especially, does it make sense to compare χ^2-fits for various models (see for example [Lic90])? I will come back to this point in Chapter 6.

The way hadronic decay is incorporated is to create a $q\bar{q}$ pair out of the vacuum and to recombine the four quarks into two mesons (see Fig. 1.7). Note that OZI-forbidden decays (where the $Q\bar{Q}$ pair annihilates into gluons from which new $Q\bar{Q}$ and $q\bar{q}$ pairs are formed) are neglected. In the Cornell model [Eic78, Eic80] the $q\bar{q}$ pair is created in a $^1S_0$ state (as a pseudoscalar), in the model of Heikkilä *et al.* [Hei84] and in the model of the Nijmegen group (see Chapter 2 and 3) the pair is created in a $^3P_0$ state (scalar). The shifts between the so called *bare* masses (the energy eigenvalues of the single-channel model) and the physical masses range from -50 to -180 MeV in the model of the Cornell group, from -20 to -200 MeV (-30 to -75 MeV) in the model of Heikkilä *et al.* and -30 to -500 MeV (-90 to -370 MeV) in the Nijmegen model for charmonium (bottomonium). Another recent multi-channel model is that by Bicudo and Ribeiro [Bic89], but no numerical results are available yet.

Although the precise form of the transition potential is unknown, and effects like final-state interactions are neglected, the success of the models that account for hadronic decay is such that it encourages to explore these models further. In my opinion the time of the single-channel models is over and a successful phenomenological model should contain hadronic decay.

1.5.3 The spin structure of the Hamiltonian

So far the spin structure of the quark-antiquark interaction has been neglected. These spin-dependent interactions induce the fine and hyperfine splitting of the mass spectra. These additional terms—the spin-orbit term, the spin-spin term,

and the tensor term—are in fact relativistic corrections (up to order v^2/c^2) to the spin-independent Hamiltonian, H_0

$$H = H_0 + H_{SO} + H_{SS} + H_T \ . \tag{1.41}$$

The precise form of these spin terms depends on the nature of the quark-antiquark interaction: is it a vector or a scalar interaction.

As the spin terms are essential for the description of the P states and because these are the subject of Chapter 3, I refer to that chapter and for a more extensive treatment to [Met90], and leave this subject here for what it is.

1.5.4 Reliability of a non-relativistic description

At the end of this rather extensive Introduction I will address the issue of the reliability of a non-relativistic description of quarkonium.

The fundamental problem of the whole potential-model approach is the non-relativistic reduction inherent to the Schrödinger formalism. Non-relativistic here implies that the velocity v of the quarks in the bound state is small compared to the speed of light, c,

$$\frac{v^2}{c^2} = \frac{\boldsymbol{p}^2 c^2}{E^2} \ll 1, \tag{1.42}$$

in which case the higher-order terms in the expansion of the relativistic kinetic energy

$$E = \sqrt{\boldsymbol{p}^2 c^2 + m^2 c^4} = mc^2 + \frac{\boldsymbol{p}^2}{2m} + \ldots \tag{1.43}$$

may be neglected. The question is to what extent this approximation is justified. For different models v^2/c^2 varies somewhere between 0.2–0.4 for charmonium and around 0.1 for bottomonium. One place where we can see that charmonium is a somewhat less non-relativistic system than bottomonium—as expected from the figures above—is in the calculation of the radiative widths (see Chapter 5). Especially the wave function is sensitive for relativistic corrections. For bottomonium a non-relativistic treatment seems justified.

In contrast, light quarks very likely move with relativistic velocities. This circumstance is usually ignored without a moment of hesitation. Note, however, that the only justification of the application of non-relativistic potential models are their phenomenologically successful predictions—especially in the case of light quarks.

Yet there are some other hints why the description of bound states by the non-relativistic Schrödinger equation is not complete nonsense (see [Luc89]). First of all,

consider the two-particle Hamiltonian with relativistic kinematics

$$H_{\mathrm{R}} = 2\sqrt{\boldsymbol{p}^2 + m^2} + W \ , \tag{1.44}$$

for equal masses and in the center-of-mass system (and $c \equiv 1$). According to $|\langle \mathcal{O} \rangle| \leq \sqrt{\langle \mathcal{O}^2 \rangle}$ valid for any hermitian operator $\mathcal{O}$, the relativistic kinetic energy satisfies $\langle \sqrt{\boldsymbol{p}^2 + m^2} \rangle \leq \sqrt{\langle \boldsymbol{p}^2 \rangle + m^2}$. From this one finds for the expectation value of H_{R}

$$\begin{aligned} \langle H_{\mathrm{R}} \rangle &= 2\langle \sqrt{\boldsymbol{p}^2 + m^2} \rangle + \langle W \rangle \leq 2\sqrt{\langle \boldsymbol{p}^2 \rangle + m^2} + \langle W \rangle \\ &= 2\frac{\langle \boldsymbol{p}^2 \rangle + m^2}{\sqrt{\langle \boldsymbol{p}^2 \rangle + m^2}} + \langle W \rangle = \left\langle 2\frac{\boldsymbol{p}^2 + m^2}{\sqrt{\langle \boldsymbol{p}^2 \rangle + m^2}} + W \right\rangle \ . \end{aligned} \tag{1.45}$$

Consequently, the relativistic energy eigenvalue $E \equiv \langle H_{\mathrm{R}} \rangle$ is bounded from above by

$$E \leq \left\langle 2\frac{\boldsymbol{p}^2 + m^2}{\sqrt{\langle \boldsymbol{p}^2 \rangle + m^2}} + W \right\rangle \ . \tag{1.46}$$

The operator on the right-hand side of this inequality is of the same structure as the non-relativistic Schrödinger Hamiltonian

$$H_{\mathrm{NR}} = 2\hat{m} + \frac{\boldsymbol{p}^2}{2\mu} + V \tag{1.47}$$

with, however, an effective mass

$$\hat{m} = 2\mu = \frac{1}{2}\sqrt{\langle \boldsymbol{p}^2 \rangle + m^2} \tag{1.48}$$

and the non-relativistic potential

$$V = \frac{2m^2}{\sqrt{\langle \boldsymbol{p}^2 \rangle + m^2}} - \sqrt{\langle \boldsymbol{p}^2 \rangle + m^2} + W = 2\hat{m} - \frac{\langle \boldsymbol{p}^2 \rangle}{\hat{m}} + W \ . \tag{1.49}$$

The effective mass as well as the potential depend on the average momentum $\langle \boldsymbol{p}^2 \rangle$ and will thus vary from level to level.

Secondly, there exists a kind of duality between an ultra-relativistic Hamiltonian with harmonic-oscillator potential and a non-relativistic Hamiltonian with linear potential. The ultra-relativistic Hamiltonian

$$H_{\mathrm{UR}} = 2\sqrt{\boldsymbol{p}^2} + \kappa r^2 \tag{1.50}$$

is converted into the non-relativistic Hamiltonian

$$H_{\mathrm{NR}} = \frac{\boldsymbol{p}^2}{2\mu} + ar \tag{1.51}$$

by means of the duality transformation

$$|\boldsymbol{p}| \to \frac{a}{2} r \,, \qquad r \to \frac{2}{a} |\boldsymbol{p}| \,, \tag{1.52}$$

provided the parameters κ, a, and μ are related by

$$\kappa = \frac{a^2}{8\mu} \,. \tag{1.53}$$

The eigenfunctions in the corresponding wave equations,

$$H_{\mathrm{UR}} \phi(\boldsymbol{x}) = E \phi(\boldsymbol{x}) \tag{1.54}$$

and

$$H_{\mathrm{NR}} \psi(\boldsymbol{y}) = E \psi(\boldsymbol{y}) \,, \tag{1.55}$$

respectively, are then connected by the Fourier transformation

$$\phi(\boldsymbol{x}) = \int d^3y e^{ia/2\, \boldsymbol{x}\cdot\boldsymbol{y}} \psi(\boldsymbol{y}) \,. \tag{1.56}$$

Integrating by parts and taking advantage of the fact that the surface terms vanish, one finds

$$\begin{aligned} H_{\mathrm{UR}} \phi(\boldsymbol{x}) &= (2\sqrt{-\Delta_{\boldsymbol{x}}} + \kappa |\boldsymbol{x}^2|) \int d^3y e^{ia/2\, \boldsymbol{x}\cdot\boldsymbol{y}} \psi(\boldsymbol{y}) \\ &= \int d^3y \left[\left(a|\boldsymbol{y}| - \frac{4\kappa}{a^2} \Delta_y \right) e^{ia/2\, \boldsymbol{x}\cdot\boldsymbol{y}} \right] \psi(\boldsymbol{y}) \\ &= \int d^3y e^{ia/2\, \boldsymbol{x}\cdot\boldsymbol{y}} \left(-\frac{\Delta_y}{2\mu} + a|\boldsymbol{y}| \right) \psi(\boldsymbol{y}) \\ &= \int d^3y e^{ia/2\, \boldsymbol{x}\cdot\boldsymbol{y}} H_{\mathrm{NR}} \psi(\boldsymbol{y}) \,. \end{aligned} \tag{1.57}$$

Thirdly, for a central potential $W(r)$ and equal masses of the constituents the relativistic virial theorem [Luc90] reads

$$\left\langle r \frac{d}{dr} W(r) \right\rangle = 2 \left\langle \frac{\boldsymbol{p}^2}{\sqrt{\boldsymbol{p}^2 + m^2}} \right\rangle \,, \tag{1.58}$$

where the expectation values are understood to be taken with respect to normalized eigenstates of the Hamiltonian (1.44). With the decomposition

$$\frac{\boldsymbol{p}^2}{\sqrt{\boldsymbol{p}^2 + m^2}} = \sqrt{\boldsymbol{p}^2 + m^2} - \frac{m^2}{\sqrt{\boldsymbol{p}^2 + m^2}} \tag{1.59}$$

the corresponding eigenvalues E are given by

$$\begin{aligned} E &\equiv \langle H_{\mathrm{R}} \rangle = 2\langle \sqrt{\boldsymbol{p}^2 + m^2} \rangle + \langle W(r) \rangle \\ &= \left\langle r \frac{d}{dr} W(r) \right\rangle + \langle W(r) \rangle + 2 \left\langle \frac{m^2}{\sqrt{\boldsymbol{p}^2 + m^2}} \right\rangle . \end{aligned} \tag{1.60}$$

In the ultra-relativistic case $m = 0$ the last expectation value in the above expression drops out,

$$E_{\mathrm{UR}} = \left\langle r \frac{d}{dr} W(r) \right\rangle + \langle W(r) \rangle . \tag{1.61}$$

As an example, let us consider a potential consisting of a Coulomb term and a confining term in the form of a power-law potential

$$W(r) = -\frac{4}{3} \frac{\alpha_s}{r} + \lambda r^{\nu} \qquad (\nu \geq 0) . \tag{1.62}$$

The ultra-relativistic eigenvalue becomes

$$E_{\mathrm{UR}} = (\nu + 1) \lambda \langle r^{\nu} \rangle . \tag{1.63}$$

That is, despite the presence of the Coulomb term in the potential the quarks only feel the confining part. Consequently, for light masses of the constituents, the non-relativistic treatment of bound states with a purely confining potential $V = \lambda r^{\nu}$ is equivalent to the relativistic treatment with the confining plus Coulomb potential. In other words, ignoring in a non-relativistic computation the Coulomb part of the potential for light particles simulates a relativistic calculation. That might be the reason why no Coulomb term was needed in our model until we wanted to describe the heavy P states in Chapter 3. And this might be an explanation for the, sometimes, astonishing success of non-relativistic potential models, even for light quarks.

The remainder of this thesis is organized as follows: Chapter 2 deals with the Unitarized Meson model of the Nijmegen group. In Chapter 3 this model is extended to include the P states in charmonium and bottomonium. A Coulomb-like interaction is built into the model. In Chapter 4 the theory of the electromagnetic transitions in quarkonium is presented, both for the single-channel as for the multi-channel case. In Chapter 5 the results from our model are given, and in Chapter 6 some conclusions are drawn and the lines along which future research should proceed—in my opinion—are discussed.

Chapter 2

The Model

In this chapter the main features of the unitarized meson model will be sketched. I will not give an extensive description of this model, for this has been done before [Rup82, Bev83d, Met90]. I will limit myself to a description of a simplified version of the model, in which all calculations can be performed analytically and to a short enumeration of the characteristics of the full model. The references to the unitarized meson model are: [Bev80, Bev83a, Bev83b, Bev83c, Bev84c, Dul82].

The fact that the confining potential in our model is a harmonic oscillator and not a linear potential as suggested by QCD[1], is made plausible by referring to a geometrical model [Bev84a, Bev84b, Bev84d, Bev86b, Bor88, Dul84a, Dul84b, Dul88a, Dul88b, Dul88c]. The idea of geometrical confinement of quarks offers a natural explanation for the similarity in structure of the charmonium and bottomonium spectra, which otherwise would require the existence of logarithmic or almost logarithmic potentials, for which a justification from first principles is lacking.

[1]The form of the linear plus Coulomb potential is motivated from QCD asymptotic behaviours. For short distances, the running coupling constant α_s becomes so small that one gluon exchange is expected to be a good approximation. This yields a (colour) Coulomb potential. For large separation of a quark and an antiquark, the intermediate gluon fields are thought to form a linear tube so that the potential increases linearly with distance. However, since the experimental data of heavy quarkonium systems are mostly in the region from short distances to the intermediate distances, it is uncertain whether the confining potential has the linear form. See also Chapter 1.

2.1 A simple model for hadronic decay of mesons

2.1.1 Introduction

At present, several models exist that describe the properties of mesons [Eic75, Mar80, Qui77, Buc81, Bev80]. These models share at least one aspect: the static quark-antiquark potential is described by a confining potential, but this potential has different forms in the various models. Sometimes a Coulomb potential is present to account for the one-gluon-exchange between the quark and the antiquark [Qui77, Eic75, Buc81] and sometimes the hadronic decay of the mesons is taken into account [Bev80, Eic75].

The simple model presented here is a simplification of the model of the Nijmegen group (see [Bev80, Bev83b, Bev83c]). It has the same confining potential, *viz.* a harmonic oscillator, no Coulomb part (although this will be added in the full model in Chapter 3) and it takes into account hadronic decay. The simplification consists of considering just one decay channel instead of many and instead of a transition potential, a δ-shell will give the coupling between the confined channel ($q\bar{q}$) and the free channel ($M\bar{M}$: meson-meson).

This simple model has proven to give insight in many features of the Nijmegen model [Dul77]. It has been used as a test model in order to see roughly the impact of new effects, about to be built in into the full model. As an introduction to the full model we will calculate the energy levels, phase-shifts, cross-sections, leptonic widths and electromagnetic transitions in charmonium in this simplified model.

2.1.2 Solving the Schrödinger equation

The radial Schrödinger equation reads:

$$\left\{ \frac{1}{2M} \left(-\frac{d^2}{dr^2} + \frac{L(L+1)}{r^2} \right) + V(r) \right\} u_L(r) = E\, u_L(r) \,, \tag{2.1}$$

where

$$M = \begin{pmatrix} \mu_c & 0 \\ 0 & \mu_f \end{pmatrix}$$

denotes the reduced mass matrix,

$$L = \begin{pmatrix} l_c & 0 \\ 0 & l_f \end{pmatrix}$$

denotes the angular momentum matrix, and

$$V(r) = \begin{pmatrix} \frac{1}{2}\mu_c\omega^2 r^2 + C_1 & g\delta(r-a) \\ g\delta(r-a) & C_2 \end{pmatrix} . \tag{2.2}$$

V_{11} is a harmonic oscillator potential (with universal oscillator frequency ω), that acts as a confining potential in the permanently closed channel (subscript "c"). $V_{12} = V_{21}$ is a one delta-shell interaction potential, that couples the closed channel to the open channel (subscript "f") with a constant potential — no final state interactions —, *i.e.* a threshold.

The energy (the eigenvalue of this differential equation) is defined by

$$E = \frac{k^2}{2\mu_f} + C_2 . \tag{2.3}$$

Let's write the wave function $u_L(r)$ as

$$u_L(r) = \begin{pmatrix} u_{l_c}(r) \\ u_{l_f}(r) \end{pmatrix} .$$

Now we can rewrite (2.1) as a set of two coupled Schrödinger equations:

$$\begin{aligned} \left(-\frac{d^2}{dr^2} + \frac{l_c(l_c+1)}{r^2} + \mu_c^2\omega^2 r^2 + 2\mu_c(C_1 - E)\right) u_{l_c}(r) 2\mu_c\, g\, \delta(r-a) u_{l_f}(r) &= 0 \\ \left(-\frac{d^2}{dr^2} + \frac{l_f(l_f+1)}{r^2} - k^2\right) u_{l_f}(r) 2\mu_f\, g\, \delta(r-a) u_{l_c}(r) &= 0 \end{aligned} \tag{2.4}$$

For $r \neq a$ equation (2.4) decouples, because the δ-function is zero. Now it is easy to write down the solutions. Write

$$u_{l_c}(r) = \begin{pmatrix} c_1\psi_<(r) \\ c_2\psi_>(r) \end{pmatrix} \text{ and } \quad u_{l_f}(r) = \begin{pmatrix} c_3\phi_<(r) \\ c_4\phi_>(r) \end{pmatrix} ,$$

where "$<$" stands for $r < a$ and "$>$" for $r > a$. Then

$$\psi_<(r) = (\mu_c\omega r^2)^{\frac{1}{2}(l_c+1)} e^{-\frac{1}{2}\mu_c\omega r^2} \Phi(-n, l_c + \frac{3}{2}; \mu_c\omega r^2)/\Gamma(l_c + \frac{3}{2}) \tag{2.5a}$$

$$\psi_>(r) = (\mu_c\omega r^2)^{\frac{1}{2}(l_c+1)} e^{-\frac{1}{2}\mu_c\omega r^2} \Psi(-n, l_c + \frac{3}{2}; \mu_c\omega r^2) \tag{2.5b}$$

$$\phi_<(r) = kr\, j_{l_f}(kr) \tag{2.5c}$$

$$\phi_>(r) = kr\, (\, j_{l_f}(kr)\, \cos\delta_{l_f} - n_{l_f}(kr)\, \sin\delta_{l_f}) \tag{2.5d}$$

with

$$\Phi(a,c;x) = {}_1F_1(a,c;x)$$
$$\Psi(a,c;x) = \frac{\Gamma(1-c)}{\Gamma(a-c+1)}\Phi(a,c;x) + \frac{\Gamma(c-1)}{\Gamma(a)}x^{1-c}\Phi(a-c+1,2-c;x)$$
$$E = \omega(2n + l_c + \frac{3}{2}) + C_1$$

with n the radial quantum number. Continuity at $r = a$ requires:

$$\begin{aligned} c_1\,\Phi(-n,l_c+\tfrac{3}{2};\mu_c\omega a^2)/\Gamma(l_c+\tfrac{3}{2}) &= c_2\,\Psi(-n,l_c+\tfrac{3}{2};\mu_c\omega a^2) \\ c_3\,ka\,j_{l_f}(ka) &= c_4\,ka\,(\,j_{l_f}(ka)\,\cos\delta_{l_f} - n_{l_f}(ka)\,\sin\delta_{l_f}) \end{aligned} \tag{2.6}$$

If we integrate equations (2.4) over r from $r = a - \varepsilon$ to $r = a + \varepsilon$ and then take the limit $\varepsilon \to 0$, we obtain an expression for the discontinuity of the derivatives at $r = a$. Writing

$$\begin{aligned} &\psi_<(r) \equiv \tilde{\Phi}(r)/\Gamma(l_c+\tfrac{3}{2}), && \phi_<(r) \equiv J_{l_f}(kr) \\ &\psi_>(r) \equiv \tilde{\Psi}(r), && \phi_>(r) \equiv (\,J_{l_f}(kr)\,\cos\delta_{l_f} - N_{l_f}(kr)\,\sin\delta_{l_f})\,, \end{aligned}$$

we get

$$\begin{aligned} &c_1\,\tilde{\Phi}'(a)/\Gamma(l_c+\frac{3}{2}) - c_2\,\tilde{\Psi}'(a) + 2\mu_c\,g\,c_4\,(\,J_{l_f}(ka)\,\cos\delta_{l_f} - N_{l_f}(ka)\,\sin\delta_{l_f}) &&= 0 \\ &c_3\,J'_{l_f}(ka) - c_4\,(\,J'_{l_f}(ka)\,\cos\delta_{l_f} - N'_{l_f}(ka)\,\sin\delta_{l_f}) + 2\mu_f\,g\,c_2\,\tilde{\Psi}(a) &&= 0 \end{aligned} \tag{2.7}$$

Combining the sets of equations (2.6) and (2.7) yields:

$$c_2 = c_4\frac{2\mu_c\,g\,\tilde{\Phi}(a)\,(\,J_{l_f}(ka)\,\cos\delta_{l_f} - N_{l_f}(ka)\,\sin\delta_{l_f})}{W(\tilde{\Phi},\tilde{\Psi})\,|_a} \tag{2.8}$$

$$c_4\,W(J_{l_f},N_{l_f})\,|_a\,\sin\delta_{l_f} + 2\mu_f\,g\,c_2\,\tilde{\Psi}(a)\,J_{l_f}(ka) = 0 \tag{2.9}$$

where $W(f,g)\,|_a$ is the Wronskian of f and g determined in $r = a$.

If we combine and rewrite the last two equations, we get an expression for $\cot\delta_{l_f}$:

$$\cot\delta_{l_f} = -\frac{W(\tilde{\Phi},\tilde{\Psi})\,|_a\;W(J_{l_f},N_{l_f})\,|_a}{4\mu_c\mu_f\,g^2\,J^2_{l_f}(ka)\,\tilde{\Phi}(a)\,\tilde{\Psi}(a)} + \frac{N_{l_f}(ka)}{J_{l_f}(ka)}\,. \tag{2.10}$$

Next we will calculate the Wronskians. Define

$$\begin{aligned} \tilde{\Phi}(z) &= z^{l/2}\,e^{-z/2}\,\Phi(-n,l+\tfrac{3}{2};z) \\ \tilde{\Psi}(z) &= z^{l/2}\,e^{-z/2}\,\Psi(-n,l+\tfrac{3}{2};z)\,. \end{aligned}$$

Then

$$W(\tilde{\Phi}(z), \tilde{\Psi}(z)) \;=\; z^l\, e^{-z}\, W(\Phi(z), \Psi(z))$$

and

$$W(\Phi(z), \Psi(z)) \;=\; -\frac{\Gamma(l+\frac{3}{2})}{\Gamma(-n)}\, z^{-(l+\frac{3}{2})}\, e^z \;.$$

The relation between the Wronskians with argument z and $\mu_c \omega r^2$ is simple:

$$W(\tilde{\Phi}(r), \tilde{\Psi}(r))\,|_a \;=\; 2\mu_c \omega a\, W(\tilde{\Phi}(z), \tilde{\Psi}(z))\,|_a \;.$$

Now we see

$$W(\tilde{\Phi}(r), \tilde{\Psi}(r))\,|_a \;=\; -\frac{\Gamma(l_c+\frac{3}{2})}{\Gamma(-n)}\, \frac{2}{a\sqrt{\mu_c \omega a^2}} \;.$$

We know that $W(J_l(z), N_l(z)) = 1$, so

$$W(J_{l_f}(kr), N_{l_f}(kr))\,|_a \;=\; k \;.$$

Thus we can write down the final expression for $\cot \delta_{l_f}$:

$$\cot \delta_{l_f} \;=\; \frac{1}{2\mu_c \mu_f\, g^2\, k a^3\, j_{l_f}^2(ka)\, \bar{\mathcal{A}}(n, l_c)} \;+\; \frac{n_{l_f}(ka)}{j_{l_f}(ka)} \;, \tag{2.11}$$

where

$$\begin{aligned} \bar{\mathcal{A}}(n, l_c) \;&=\; \frac{\Gamma(-n)}{\Gamma(l_c+\frac{3}{2})}\, (\mu_c \omega a^2)^{l_c+\frac{1}{2}}\, e^{-\mu_c \omega a^2} \\ &\quad \cdot\; \Phi(-n, l_c+\frac{3}{2}; \mu_c \omega a^2)\, \Psi(-n, l_c+\frac{3}{2}; \mu_c \omega a^2) \;. \end{aligned} \tag{2.12}$$

2.1.3 The S-matrix

Now that we know the expression for $\cot \delta_{l_f}$, we can determine the S-matrix. (Note: the S-matrix is in fact a matrix, because this is a 2×2 problem, but we are only interested in the phase-shift in the meson-meson channel, *i.e.* the S-matrix under consideration is a number, not a matrix.) Let's drop the subscript "f" in l_f.

$$\begin{aligned} \mathcal{S} \;&\equiv\; e^{2i\delta_l} \\ &=\; \tfrac{\cot \delta_l + i}{\cot \delta_l - i} \\ &=\; 1 \;+\; \tfrac{2i}{\cot \delta_l - i} \\ &\equiv\; 1 \;+\; \mathcal{T} \;. \end{aligned} \tag{2.13}$$

Bound states occur when the S-matrix and the T-matrix have poles: $\cot \delta_l = i$ and $k = i\kappa$, $\kappa > 0$ (because for bound states $k^2 < 0$).

Write $\mathcal{T} = \frac{A}{B}$ with $B = 0$ on a pole, then we find for the residue $\mathcal{C}$:

$$\begin{aligned}\mathcal{C}^{-1} &= \frac{d\mathcal{T}^{-1}}{dE}\Big|_{E=E_0} \\ &= \frac{1}{A}\frac{dB}{dE}\Big|_{E=E_0} \\ &= -\frac{\mu_f}{\kappa A}\frac{dB}{d\kappa}\Big|_{E=E_0} \ .\end{aligned}$$

with E_0 the position of the pole (in the complex energy plane).

$$\begin{aligned}\frac{dB}{d\kappa} &= \frac{d}{d\kappa}\cot\delta_l \\ &= -\frac{1}{\kappa}\left[2\mu_c\mu_f g^2 i\kappa a^3 j_{l_f}^2(i\kappa a)\,\bar{\mathcal{A}}(n,l_c)\right]^{-1} + \frac{i}{a\kappa^2 n_l^2(i\kappa a)} \ .\end{aligned}$$

Using $\cot\delta_l = i$ $(B = 0)$ on a pole, we find for the inverse of the residue:

$$\mathcal{C}^{-1} = \frac{\mu_f}{2\kappa^2}\left(\frac{j_l(i\kappa a) + in_l(i\kappa a)}{j_l(i\kappa a)} - \frac{1}{a\kappa\, n_l^2(i\kappa a)}\right) . \tag{2.14}$$

2.1.4 Pole tracing

If we increase the value of the coupling constant g, *i.e.* the $q\bar{q}$ channel couples stronger to the $M\bar{M}$ channel, the eigenvalues of the Schrödinger equation shift. This shift depends on the original position of the eigenvalues. These eigenvalues correspond to poles of the S-matrix. In this section we will trace these poles and see what their behaviour is.

In the previous sections we derived expressions for the S-matrix, the phase-shift δ_l and the energy (eigenvalue). We can express the radial quantum number n in terms of the energy, the oscillator frequency and the angular momentum of the confined channel:

$$n = \tfrac{1}{2}\left(\frac{E - C_1}{\omega} - l_c - \frac{3}{2}\right) . \tag{2.15}$$

Looking at the expression for $\cot\delta_l$ (remember: for poles $\cot\delta_l = i$), we observe that j_l, n_l, Φ and Ψ are slowly varying functions of $n(\sim E)$, in contrast to $\Gamma(-n)$. For the pure harmonic oscillator "poles" occur for positive integer values of n. If we turn on the coupling strength g, we find poles for

$$n = n_0 + \triangle n \ ,$$

with n_0 a positive integer and small g. In this case we are able to make the following approximation for $\Gamma(-n)$:

$$\Gamma(-n) = \Gamma(-n_0 - \triangle n) \approx \frac{(-1)^{n_0+1}}{n_0!\,\triangle n} . \tag{2.16}$$

Let

$$\bar{\mathcal{A}}_0(n_0, l_c) = \frac{1}{\Gamma(l_c + \frac{3}{2})} (\mu_c \omega a^2)^{l_c + \frac{1}{2}} e^{-\mu_c \omega a^2} \cdot \Phi(-n_0, l_c + \frac{3}{2}; \mu_c \omega a^2)\, \Psi(-n_0, l_c + \frac{3}{2}; \mu_c \omega a^2) \,. \quad (2.17)$$

Substitution of (2.16) and (2.17) into the expression for $\cot \delta_l = i$ yields:

$$\triangle n = \frac{(-1)^{n_0}}{n_0!} 2\mu_c \mu_f g^2 k_0 a^3 \bar{\mathcal{A}}_0(n_0, l_c) \left(j_l(k_0 a) n_l(k_0 a) - i\, j_l^2(k_0 a) \right) \,, \quad (2.18)$$

where k_0 is the value of k belonging to $E_0 = C_1 + \omega(2n_0 + l_c + \frac{3}{2})$. Now $E = E_0 + 2\omega \triangle n \equiv E_0 + \triangle E$.

Behaviour of $\triangle n$:

For n_0 a positive integer, $1/\Gamma(-n_0) = 0$, so we can rewrite $\bar{\mathcal{A}}_0(n_0, l_c)$:

$$\bar{\mathcal{A}}_0(n_0, l_c) = (\mu_c \omega a^2)^{l_c + \frac{1}{2}} e^{-\mu_c \omega a^2} \frac{\Gamma(-l_c - \frac{1}{2})}{\Gamma(-n_0 - l_c - \frac{1}{2})} \Phi^2(-n_0, l_c + \frac{3}{2}; \mu_c \omega a^2) \,. \quad (2.19)$$

Here we used the fact that

$$\Gamma(-l - \tfrac{1}{2}) / \Gamma(-n_0 - l - \tfrac{1}{2}) = (-1)^{n_0} \Gamma(n_0 + l + \frac{3}{2}) / \Gamma(l + \frac{3}{2}) \,.$$

So we find

$$\bar{\mathcal{A}}_0(n_0, l_c) = (-1)^{n_0} |\bar{\mathcal{A}}_0(n_0, l_c)| \,. \quad (2.20)$$

In order to determine the behaviour of the poles, we still have to look at the expression $-ik_0 a\, j_l(k_0 a) h_l^{(1)}(k_0 a)$. We discriminate between energies above and below the threshold.

I. $E > C_2$, $k_0 > 0$:

Using (2.18) and (2.20) we find for $\triangle n$:

$$\triangle n = \frac{1}{n_0!} 2\mu_c \mu_f g^2 k_0 a^3 |\bar{\mathcal{A}}_0(n_0, l_c)| \left(j_l(k_0 a) n_l(k_0 a) - i\, j_l^2(k_0 a) \right) \,. \quad (2.21)$$

Thus we can extract an expression for $\mathrm{Im}(\triangle n)$ and conclude:

$$\mathrm{Im}(\triangle n) < 0 \,. \quad (2.22)$$

The real part may be anything, but we see that poles tend to go into the negative imaginary energy plane ($E \sim \triangle n$) for poles that lie above the meson-meson threshold!

g	E(1S)	E(1P)	E(2S)
0	3.408	3.598	3.787
0.1	3.407	3.597	3.785 -0.000286 i
0.5	3.364	3.565	3.738 -0.004672 i
1.0	3.155	3.342	3.642 -0.001462 i
1.4	2.794	2.946	3.601 -0.000004 i
1.5	2.677	2.822	3.595
2.0	1.955	2.070	3.576

Table 2.1: The energy eigenvalues (in GeV) for different values of the coupling.

II. $E < C_2$, $k_0 = i\kappa_0$, $\kappa_0 > 0$:

Using [Abr65, Bat53] we find:

$$-ik_0a\, j_l(k_0a)\, h_l^{(1)}(k_0a) \;=\; -\mathrm{I}_{l+\frac{1}{2}}(\kappa_0a)\,\mathrm{K}_{l+\frac{1}{2}}(\kappa_0a)\;.$$

In this case

$$\mathrm{Im}(\triangle n) = 0 \;\text{ and }\; \mathrm{Re}(\triangle n) < 0\;, \tag{2.23}$$

which means that poles tend to move along the real axis towards smaller energy values as the strength of the coupling increases.

Note that $\mathrm{I}_{l+\frac{1}{2}}(x)$ and $\mathrm{K}_{l+\frac{1}{2}}(x)$ are both positive for positive x.

2.1.5 Energy shifts

We have seen how the energy levels can be calculated when the coupling of the meson-meson channel to the $q\bar{q}$ channel is increased. In Table 2.1 the energy levels for some values of g are listed. Note that for values of the energy above the threshold — taken to be twice the meson mass ($M = 1.8$ GeV, $m_c = 1.562$ GeV) — the energy becomes complex due to the coupling (as we saw in the previous section). Once the energy comes below the threshold, the energy becomes real again.

2.1.6 Wave functions for bound states

In one of the previous sections we calculated the residue of the S-matrix for bound state poles. Now it's easy to calculate the normalized wave functions for bound

states using this residue. The wave functions for bound states may be obtained by solving the Schrödinger equation (2.1) for bound state energies: $E = -\kappa^2/2\mu_f + C_2$. The wave functions are analogous to those for "positive" energies (see (2.5)):

$$\psi_<(r) = c_1\,(\mu_c\omega r^2)^{(l_c+1)/2} e^{-\frac{1}{2}\mu_c\omega r^2}\,\Phi(-n, l_c+3/2; \mu_c\omega r^2)/\Gamma(l_c+3/2) \quad (2.24a)$$

$$\psi_>(r) = c_2\,(\mu_c\omega r^2)^{(l_c+1)/2} e^{-\frac{1}{2}\mu_c\omega r^2}\,\Psi(-n, l_c+3/2; \mu_c\omega r^2) \quad (2.24b)$$

$$\phi_<(r) = c_3\, i\kappa r\, j_{l_f}(i\kappa r) \quad (2.24c)$$

$$\phi_>(r) = c_4\, i\kappa r\,(\, h^{(2)}_{l_f}(i\kappa r) \,+ h^{(1)}_{l_f}(i\kappa r)\,\mathcal{S}) \quad (2.24d)$$

Now $E = -\omega(2n + l_c + \frac{3}{2}) + C_1$. With $\mathcal{S} = 1 + \mathcal{T}$, and $\mathcal{T} = \frac{\mathcal{C}}{E-E_0}$ on a pole we find for $\phi_>(r)\,|_{pole}$:

$$\phi_>(r) = c_4\, i\kappa r\, h^{(1)}_{l_f}(i\kappa r)\,\frac{\mathcal{C}}{E-E_0}\,.$$

Using the fact that the residue is proportional to the square of the asymptotic normalization constant: $c_4^2 = \mu_f/\kappa\,\mathcal{C}$, and using the relations for the (dis)continuity of the wave functions and their derivatives, we obtain expressions for the normalization constants:

$$\begin{aligned} c_3 &= c_4\,\left(1 + i n_{l_f}(i\kappa a)/j_{l_f}(i\kappa a)\right) \\ c_2 &= c_4\,\mu_c\, g\, a(\mu_c\omega a^2)^{\frac{1}{2}(l_c-1)} e^{-\frac{1}{2}\mu_c\omega a^2}\,\Phi(-n, l_c+\frac{3}{2}; \mu_c\omega a^2)\, i\kappa a\, h^{(1)}_{l_f}(i\kappa a) \\ &\quad \cdot\,\Gamma(-n)/\Gamma(l_c+\frac{3}{2})^2 \\ c_1 &= c_2\,\Gamma(l_c+\frac{3}{2})\,\Psi(-n, l_c+\frac{3}{2}; \mu_c\omega a^2)/\Phi(-n, l_c+\frac{3}{2}; \mu_c\omega a^2) \end{aligned} \quad (2.25)$$

Note that the factor $\frac{\mathcal{C}}{E-E_0}$ disappears in the normalization, because it is an overall factor.

Combining (2.24c) and (2.25) yields the expressions for the normalized wave functions for bound states, which we will use in calculating the leptonic widths[2] and electromagnetic transitions (see Chapter 4). In Figure 2.1 the 1S, 1P and 2S (corresponding to J/ψ, χ_0^c , and ψ' respectively) radial wave functions are plotted for a value of the coupling constant $g = 1.0$. Note the discontinuity of the derivatives of the wave functions at $r = a \simeq 1.4$ GeV^{-1}, where the coupling of the two channels takes place due to the delta-function $\delta(r-a)$. Because of the conservation of angular momentum an S wave in the confined channel yields automatically a P wave in the free channel (*i.e.* the mesons are in a relative $l = 1$ motion) and vice-versa.

[2] via the van Royen-Weisskopf formula [Roy67]: $\Gamma_{ee} = 16\pi e_q^2\alpha^2\frac{|\psi(0)|^2}{M^2}$, where $\psi(0) = R(0)\,Y_0^0(\vartheta,\varphi)$

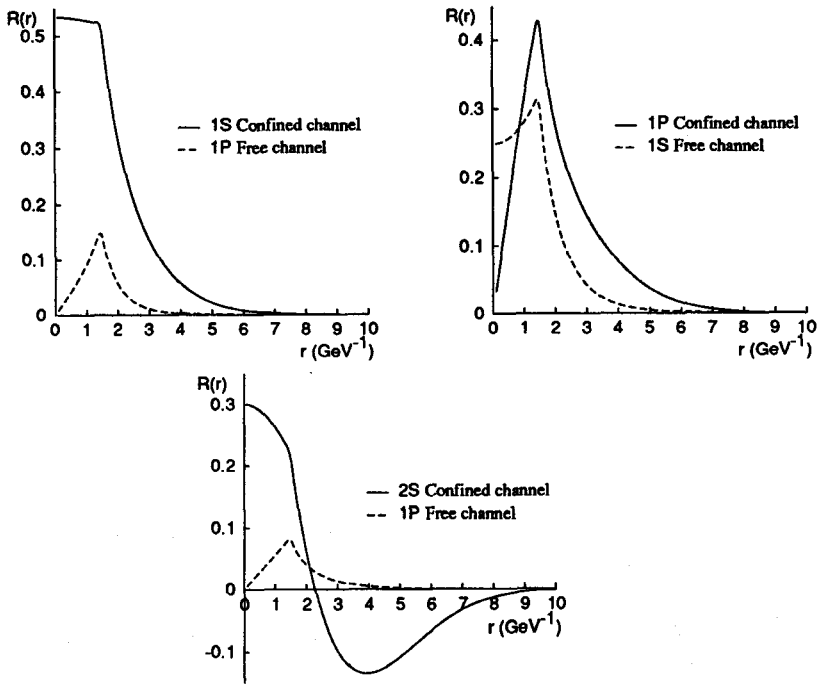

Figure 2.1: The 1S, 1P and 2S two-channel radial wave functions for $g = 1.0$.

	$g = 0.001$	$g = 1.0$	*experiment*
$\Gamma_{J/\psi \to ee}$ (keV)	1.3	2.7	4.72 ± 0.35
$\Gamma_{\psi' \to ee}$ (keV)	1.3	0.6	2.15 ± 0.21

Table 2.2: Leptonic widths of J/ψ and ψ'.

Γ (keV)	$g = 0.001$	$g = 1.0$	*experiment*
$J/\psi \to \eta_c + \gamma$	2.7	2.7	0.86 ± 0.23
$\psi' \to \eta_c + \gamma$	11.9	0.007	0.68 ± 0.19
$\psi' \to \eta_c' + \gamma$	1.4	1.4	0.43 - 2.8
$\eta_c' \to J/\psi + \gamma$	3.8	1.4	
$\psi' \to \chi_0^c + \gamma$	46	24	22.6 ± 4.4
$\psi' \to \chi_1^c + \gamma$	48	24	21.1 ± 4.2
$\psi' \to \chi_2^c + \gamma$	38	19	19.0 ± 3.9
$\chi_0^c \to J/\psi + \gamma$	265	139	95 ± 46
$\chi_1^c \to J/\psi + \gamma$	525	294	< 355
$\chi_2^c \to J/\psi + \gamma$	909	520	$351\ ^{+165}_{-125}$

Table 2.3: Electromagnetic decay widths of M1 and E1 transitions in charmonium.

In Table 2.2 the decay widths are displayed for the decay $J/\psi \to e^+e^-$ and $\psi' \to e^+e^-$ for $g = 0.001$ (*i.e.* a harmonic oscillator) and $g = 1.0$. We clearly see the influence of hadronic decay on the decay widths: for a harmonic oscillator the width decreases for increasing radial quantum number n, but the effect of the decay into mesons reverses this behaviour. In Table 2.3 the electromagnetic decay widths are calculated. Experimental data are taken from [PDG88].

We observe from Table 2.3 that the decay widths decrease due to the coupling to the meson-meson channel. We expect that in the full model these widths will decrease even further, because a larger part of the total wave function will go from the quark-quark wave function to the meson-meson wave function. (This argument also holds for the leptonic decay widths.) But on the other hand there will also be contributions from processes like $(M\bar{M}) \to (M\bar{M})' + \gamma$ to the total width. We see that the widths for the E1 transitions agree very well with experiment.

2.1.7 Phase-shifts and Cross-sections

With the information we have obtained so far we are able to plot the phase-shifts δ_l as a function of the energy for different values of the coupling constant g (Figure 2.2).

As the partial wave cross-section is related to the phase-shift, it is very easy to calculate:

$$\sigma_l = \frac{4\pi}{k^2}(2l_f + 1)\sin^2\delta_l \,. \tag{2.26}$$

In Figure 2.3 the cross-sections are plotted in the same way as the phase-shifts.

If we compare Figure 2.2 with Figure 2.3 we see that every time the phase-shift passes 90 degrees (modulo 180 degrees), the cross-section reaches a maximum ($\sin\delta = 1$). In each interval of 2ω (= 0.379 GeV in our case) a maximum occurs, corresponding to increasing radial quantum number n.

If we look at Fig. 2.3 we might suspect that the resonances can be described by the Breit-Wigner formula. Let us show that this is indeed the case for small coupling constants. We can write the cross-section as

$$\sigma_l = \frac{4\pi}{k^2}(2l_f + 1)\left|\frac{\mathcal{S}-1}{2i}\right|^2 \,, \tag{2.27}$$

with $\mathcal{S}$ the S-matrix as defined in (2.13). We write out $\mathcal{S} - 1$ for small coupling constant g (using (2.11), (2.16) and (2.17))

$$\begin{aligned}\mathcal{S} - 1 &= 2i\left(\frac{(-1)^{n_0+1}n_0!\triangle n}{2\mu_c\mu_f g^2 k_0 a^3 j_l^2(k_0a)\bar{A}_0} + \frac{n_l(k_0a)}{j_l(k_0a)} - i\right)^{-1} \\ &= \frac{4i\beta\omega j_l(k_0a)\bar{A}_0}{E - E_0 + 2\beta\omega n_l(k_0a)\bar{A}_0 - 2i\beta\omega\bar{A}_0 j_l(k_0a)} \,,\end{aligned}$$

with

$$\begin{aligned}\triangle n &= \frac{E - E_0}{2\omega} \,, \\ \beta &= \frac{(-1)^{n_0+1}}{n_0!} 2\mu_c\mu_f g^2 k_0 a^3 j_l(k_0a) \,.\end{aligned}$$

At a resonance $\delta = 90^o$, hence $\cot\delta = 0$. This yields

$$\cot\delta = \frac{1}{\frac{1}{\triangle n}\beta j_l(k_0a)\bar{A}_0} + \frac{n_l(k_0a)}{j_l(k_0a)} = 0 \,, \tag{2.28}$$

where now $\triangle n = (E_R - E_0)/2\omega$. So we write

$$E_R - E_0 = -2\beta\omega n_l(k_0a)\bar{A}_0 \,, \tag{2.29}$$

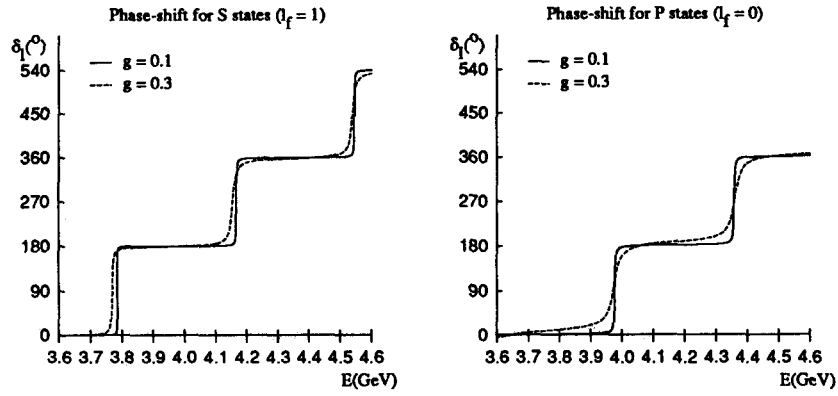

Figure 2.2: The phase-shift versus the energy.

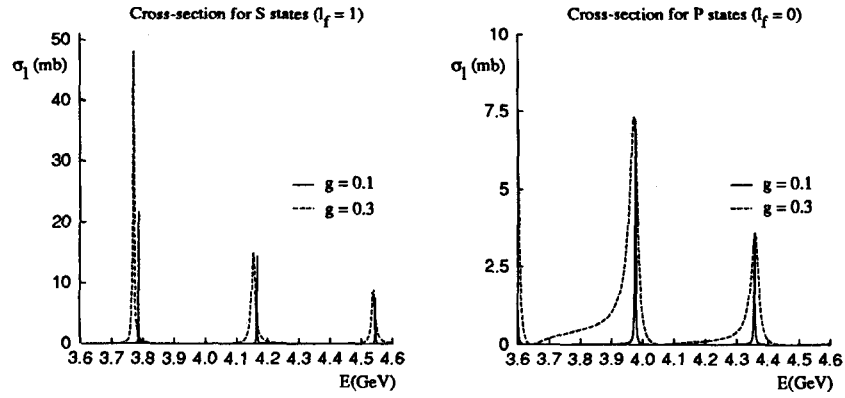

Figure 2.3: The cross-section versus the energy.

and if we define

$$\Gamma/2 = -2\beta\omega j_l(k_0 a)\bar{A}_0 \,, \tag{2.30}$$

then we find

$$\mathcal{S} - 1 = \frac{i\Gamma}{E_R - E - i\Gamma/2} \,. \tag{2.31}$$

Note that if we examine the expression for β and use (2.20) and (2.30), we see that $\Gamma \geq 0$.

This gives the Breit-Wigner formula for the cross-section:

$$\sigma_l = \frac{4\pi}{k^2}(2l_f + 1)\frac{\Gamma^2/4}{(E - E_R)^2 + \Gamma^2/4} \,. \tag{2.32}$$

Indeed, from Fig. 2.3 we see that for a small coupling constant the cross-section has the Breit-Wigner form.

2.2 The unitarized meson model

The Unitarized Meson model of the Nijmegen group differs from the above presented simple model on several points. First of all the number of channels is enlarged to n confined (permanently closed) channels and m free (scattering) channels. The notion of several confined channels instead of one enables us to describe states that are mixtures of different quark flavours, for example the η and the η'. In case of charmonium and bottomonium there is only one confined channel. The m free channels represent different (virtual) decay channels, each with its own threshold and coupling strength. The latter originates from the recoupling of the four quarks into two mesons (refer to [Bev83a, Bev86a]).

Secondly, the central equation is still the Schrödinger equation, but some relativistic dynamics are added. This is done by deriving the Schrödinger equation from a Bethe-Salpeter equation via a Blankenbecler-Sugar–Logunov-Tavkhelidze equation and a Lippmann-Schwinger equation (refer to [Bev83b]). This means that the energy, E, and the reduced mass, μ, are defined by

$$\begin{aligned} E &= \sqrt{k^2 + m_1^2} + \sqrt{k^2 + m_2^2} \,, \\ \mu &= \frac{1}{2}\frac{dk^2}{dE} \,, \end{aligned} \tag{2.33}$$

where $\boldsymbol{k}$ is the propagation vector. In the confined channels, however, the non-relativistic limit of (2.33) is used and also in the free channels for energies lower

than the threshold. The Schrödinger equation now reads

$$\left\{-\frac{d^2}{dr^2}+\frac{L(L+1)}{r^2}+2\mu(E)V(r)-\boldsymbol{k}^2(E)\right\}\phi_E(r)=0\ . \tag{2.34}$$

where L, μ, and $\boldsymbol{k}^2$ are $(n+m)\times(n+m)$ diagonal matrices and V is the $(n+m)\times(n+m)$ potential matrix. The potential matrix has the form

$$V(r)=\begin{pmatrix} V_c(r) & V_{\rm int} \\ V_{\rm int} & T \end{pmatrix}\ , \tag{2.35}$$

where $V_c(r)=\frac{1}{2}\mu\omega^2r^2$ is the diagonal confining harmonic oscillator potential matrix, T is the diagonal threshold matrix, and $V_{\rm int}$ can be written as

$$(V_{\rm int})_{ij}=\tilde{g}\omega c_{ij}V_{\rm emp}v_{\rm int}(r)\ , \tag{2.36}$$

where $\tilde{g}$ is the dimensionless overall coupling constant, ω the universal harmonic oscillator frequency, c_{ij} are the recoupling coefficients ($\tilde{g}c_{ij}$ are the coupling strengths mentioned above for the separate decay channels), $V_{\rm emp}$ is an empirical factor [3]

$$V_{\rm emp}=\sqrt{\frac{E}{T_j}}\ , \tag{2.37}$$

that suppresses the influence of the higher thresholds, T_j, and $v_{\rm int}(r)$ contains the radial dependence of $V_{\rm int}(r)$, given by

$$v_{\rm int}(r)=\frac{r}{r_0}e^{-\frac{1}{2}(\frac{r}{r_0})^2}\ , \tag{2.38}$$

with $r_0=\rho_0/\sqrt{\mu_i\omega}$ and ρ_0 a constant. The justification for (2.38) to be proportional to r lies in the fact that the transition potential couples states that differ by one unit of orbital angular momentum. Because (2.38) has a maximum for $r=r_0$, r_0 can be regarded as the "transition radius".

The parameters in our model are the quark masses m_n, m_s, m_c, m_b (where m_n stands for $m_u=m_d$) and ω, $\tilde{g}$, and ρ_0. In Chapter 3 we will introduce a few additional parameters in order to describe the P states in charmonium and bottomonium. These parameters are determined in a fitting procedure.

[3] For the pseudo-scalar and vector mesons the square root in $V_{\rm emp}$ contained an additional term that governed the spin-spin splitting (see [Bev83b]). This term was already absent for the scalar mesons (see [Bev86a]) and proves to be superfluous for the heavy pseudo-scalar and vector mesons once spin-dependent terms are introduced in the potential (see Chapter 3).

The Schrödinger equation is solved numerically and to this end the potential $v_{\rm int}(r)$ is replaced by a number of delta-shells with such a strength that the original shape of $v_{\rm int}(r)$ is maintained (see Fig. 2.4 and [Dul82]).

I will make a little digression on the wave functions generated by the model, because these are so important for the calculation of the radiative widths, the main topic of this thesis. The general form of the wave function reads

$$\varphi(r) = c_1 F(r) + c_2 G(r) , \tag{2.39}$$

where $F(r)$ and $G(r)$ are regular at the origin and at infinity, respectively, and the coefficients c_1 and c_2 are chosen in such a way that $\varphi(r)$ is regular in $[0, \infty]$ by matching F and G at every delta-shell position. For the free channels F and G are Bessel functions. In order to let $\varphi(r)$ approach zero for $r \to \infty$, c_1 and c_2 have to satisfy (for the free channels, see [Dul82])

$$c_1/c_2 \to ik^{2l+1} , \tag{2.40}$$

where k and l are the momentum and angular momentum in the free channel. If we require that relation (2.40) holds exactly for r greater than the "interaction radius", then φ will behave properly.

Now follows a technical story about the way relation (2.40) was imposed on the wave function in the computer program of our model (HADRON).

Let us have a look at Figure 2.4. The coefficients c_1 and c_2 are calculated for every channel (ICHAN=1,NCHAN) and every delta-shell position (IDELTA=1,NDELTA+1) in subroutine COEFF; the functions F and G are calculated for every channel and every integration step (IX=1,NX) in subroutine FGFUN1. In subroutine WAVEFN the wave function is calculated according to equation (2.39) in all R(IX), (IX=1,NX), after the corresponding delta-shell has been determined.

The ratio $x \equiv c_1/c_2$ differs from $-ik^{2l+1}$ less than 1% at R=R(NDELTA). For R(NDELTA) < r < RMAX the coefficients are all equal to those at R=R(NDELTA), so an inaccuracy in the ratio x causes the wave function to blow up for large r. And this proved to be the case for the P states.

The solution is simply to make the coefficients at R=R(NDELTA) satisfy equation (2.40) exactly by redefining c_1 and c_2:

$$c_1' = c_1 \sqrt{\frac{-ik^{2l+1}}{x}}$$
$$c_2' = c_2 \sqrt{\frac{x}{-ik^{2l+1}}}$$

In this way all wave functions of the free channels are forced to approach zero for large r.

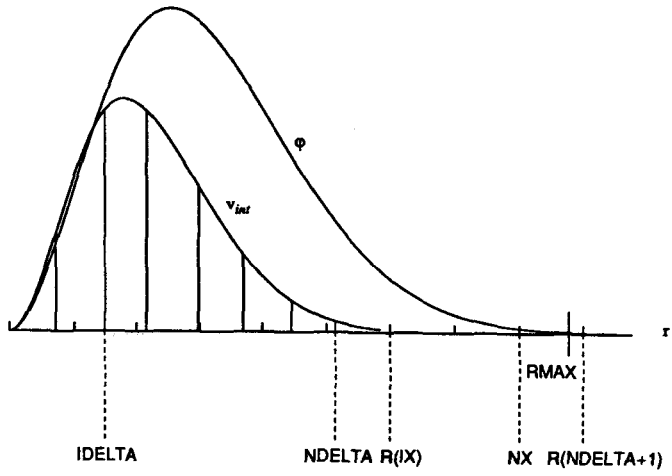

Figure 2.4: The wave function and interaction potential according to the computer program.

Chapter 3

The Extended Model [1]

3.1 Introduction

This paper is devoted to the study of the colour interactions at short distances in heavy quarkonia. To this aim we investigate in detail the properties of the interquark wave functions near the origin in the framework of a previously developed meson model.

Charmonium and bottomonium serve as testing ground for studies of quarkonia in terms of effective interquark-potential models. In a recent study by Lichtenberg *et al.* [Lic90] the properties of various models have been compared. A similar study has been made in the past by Buchmüller *et al.* [Buc81]. The strategy behind these models is to determine the form of the potential as to reproduce the spin-averaged spectra of charmonium and bottomonium. A common feature of the resulting potentials is that the effective interquark interaction is singular and attractive near the origin and confining at larger distances. Another common feature is that the influence of hadronic decay has been ignored for the spectroscopy of heavy quarkonia. In the following we will refer to these models as single-channel models.

The effects of hadronic decay, *i.e.* the coupling of $q\bar{q}$ states to their two-meson decay channels, has been studied in the Unitarized Meson Model of the Nijmegen group (UMMN) (see Ref. [Bev86a] and references therein, and [Bev83b]). The conclusion from that work was that the effects of the attractive singular interactions at short distances can be ignored once hadronic decay is accounted for as far as the S- and D-state spectra for light and heavy quarkonia are concerned.

[1] Co-authors: K. Metzger, E. van Beveren, and C. Dullemond. THEF-NYM Report 90.12. To be published under the title *The influence of color-Coulomb interactions on the spectra and leptonic decay widths of charmonium and bottomonium.*

Apparently the S-state spectra are described by either a single-channel potential with a pure (colour-) Coulomb term [Ric79], or a multi-channel description without such a term. This means that we have to be careful with conclusions about the influence of a Coulomb term or the influence of decay in either model type. For example, estimating the influence of decay within a single-channel model with a pure Coulomb term will result in the conclusion that the influence of decay is small, because the bound state positions of such a model are already fitted to the S-state quarkonia spectra without the implementation of unitarity effects. Analogously, trying to incorporate a pure Coulomb potential into the UMMN model will result in the conclusion that there is no need for such an interaction.

For the P-state spectrum the situation is different. The influence of the Coulomb interaction and the influence of unitarity effects on the P-state spectrum is not the same. Because P-state wave functions and S-state wave functions behave differently in the origin, the positions of the P states relative to the S states are strongly influenced by the presence of the Coulomb interaction. One may expect to measure this effect by comparing the charmonium and bottomonium spectra. Note that within UMMN the low position of the ground state is not caused by the singularity of the Coulomb potential but finds its origin in the coupling to the meson-meson scattering channels [Bev83c].

In addition to the relative position of the P states also the fine and hyperfine splittings of the P states play an important role. We found that these splittings have to be studied simultaneously with the confinement force and the unitarization effects.

A larger influence of the Coulomb interaction can be expected on properties which are more closely related to the shape of the wave function. Such properties are the leptonic and the radiative decay widths. Because of the success of UMMN in the heavy and light meson spectroscopy, we feel that a test of these more delicate properties connected to the wave functions is justified.

Previous calculations within the Unitarized Meson model without a Coulomb contribution pointed out that the leptonic decay widths of the charmonium and bottomonium states come out roughly a factor two smaller than the experimental data. However, it should be noted that the ratios for higher recurrencies were already correct within the unitarization scheme [Bev83c]. It may be expected that when a colour-Coulomb term is introduced, the wave functions in the origin are enhanced which improves the resulting leptonic decay widths. However, as we will see later on, due to the limitation on the colour charge in order not to disturb mass-scale invariance of the level splittings for the $J^{PC}= 1^{--}$ spectrum, this enhancement

turns out to be insufficient if the Coulomb potential is just inversely proportional to the interquark distance. This observation is by no means in conflict with QCD, since only at very short distances one-gluon-exchange dominates for heavy pointlike quarks. Higher-order QCD contributions suggest that screening effects may occur at larger interquark distances. These characteristics are combined in the expression:

$$V_{\text{Coulomb}}(r) = -\frac{\kappa e^{-\lambda r}}{r} \,. \tag{3.1}$$

In the following we will see that a colour-exchange potential of the form (3.1) does not destroy the S- and P-state spectrum but causes an extra enhancement of the wave function in the origin.

The main experimental data that can provide us with clues about the contribution of (3.1) are summarized below:

- The leptonic decay widths of the 1S and 2S states of both charmonium and bottomonium.
- The position of the 1P state between the 1S and the 2S states.
- The fine and hyperfine splittings of the P states.

The remainder of this paper is organized as follows: In Section 3.2 we will briefly summarize the characteristics of UMMN; in Section 3.3 the spin-dependent forces are discussed, and in Section 3.4 the influence of decay on the P-state spectrum is studied. In Section 3.5 the results of a fit to the data are presented and Section 3.6 is devoted to a comparison between the model presented here and two models that also try to describe the light and heavy mesons simultaneously. Section 3.7 contains our conclusions.

3.2 The model

In UMMN all mesons are treated as bound states and resonances in elastic and inelastic meson-meson scattering in the sense of S-matrix theory. Consequently, UMMN is rather a model for the description of the scattering of mesons, than a model for permanently bound quarks and antiquarks. This does not mean that these mesonic bound states and resonances are to be considered as pure meson-meson states. Quark-antiquark systems enter the model under the assumption that mesons dominantly interact via the creation and annihilation of valence quark pairs. This so-called quark pair creation mechanism, QPC [Mic69, Car70], couples the systems

of two interacting mesons to the systems of one quark permanently bound to one antiquark. Hence the bound and resonant states of the model are a mixture of pure meson-meson molecules (in the terminology of [Wei90]) and pure quark-antiquark states. In this approach it is essential that confinement is separated from other effects and appears in the model as an exact property.

A zero'th-order approximation to the light and heavy meson spectra is in UMMN obtained by placing a quark and an antiquark in a harmonic-oscillator potential which is proportional to the flavour mass [Bev83b], *i.e.*

$$V(r) = \tfrac{1}{2}\mu\omega^2 r^2 \ , \tag{3.2}$$

where μ represents the reduced effective valence flavour mass of the quark-antiquark system under consideration. Confinement is in this model described by one parameter, the universal oscillator frequency, ω, which is found to be about 0.2 GeV.

In the limit of infinitely heavy quark masses, the confinement potential derived from QCD resembles at small distances the ordinary Coulomb potential of electrostatics. Although the spectra of ψ and Υ already somewhat exhibit this Coulomb spectrum, a more striking signature is the almost equal and flavour-independent spacing of the $J^{PC}= 1^{--}$ states. The basic idea behind UMMN is, that this signature is the key to the confinement mechanism and therefore has to be build into the potential in an exact way. The only potential which exhibits the equal and flavour independent spacing in an exact way, is the harmonic-oscillator potential (3.2). A possible scenario for harmonic forces in QCD is based on a quark-confinement model using Anti-De Sitter transformations as an internal symmetry for the quark-gluon condensate as indicated in Refs. [Bev84b, Dul84a, Bev84d, Bev86b, Dul88a].

The bound states and resonances in meson-meson scattering are somehow related to the bare states, *i.e.* to the energy eigenstates of the confinement potential (3.2). Their central positions and hadronic widths are strongly influenced by the transition potential which represents the QPC mechanism. The mass differences between the bare spectrum of (3.2) and the "physical" spectrum of UMMN are in some cases of the order of the level spacings of the spectrum of the confining potential.

In estimating the effects of the QPC mechanism, we should keep in mind that the strong coupling constant α_s which is the main parameter for the short range behaviour (Coulomb potential) of QCD, not necessarily has to determine the creation rate of $q\bar{q}$ pairs out of the non-perturbative vacuum in case of large kinetic energies of the constituent quarks. In fact, those effects cannot be determined from first principles because of the same basic problems that make a calculation of the $q\bar{q}$ potential at intermediate ranges impossible. The transition potential has there-

fore to be determined empirically and depends on the choice which is made for the confining potential. In this way we are modeling two phenomenological aspects of the non-perturbative vacuum: *i.e.* the way it is responsible for confinement and the way it governs the creation and annihilation of $q\bar{q}$ pairs.

In UMMN the transition potential for all mesonic systems of pseudoscalar and vector type (in which the $q\bar{q}$ system is in an S state) contains a universal dimensionless parameter $\tilde{g}$ representing the coupling strength of the QPC mechanism (see [Bev83b, Bev84c] for a precise definition of $\tilde{g}$). In [Bev83b, Bev84c], the value of $\tilde{g}$ has been chosen such that an overall fit of the experimental data is obtained for this type of mesons. Since we now want to make an overall fit to the S state as well as the P-state data the value of $\tilde{g}$ may change. In what follows a comparison of the newly determined value of $\tilde{g}$, which we shall call g, is made with the value of $\tilde{g}$ determined in [Bev83b]. This g is not universal: a distinction is made between the g-value for the S states, called g_S, and for the P states, called g_P. Apart from g there is one other dimensionless parameter determining the transition potential. This is $\rho_0 = \sqrt{\mu\omega}r_0$ where r_0 is the r-value for the potential maximum. The parameter ρ_0 is universal if flavour independence of the spectra is an exact property.

3.3 Spin-dependent forces

As mentioned in the introduction the Coulomb interaction strongly influences the relative position of the P-state spectrum with respect to the S-state spectrum and therefore we have to extend our model to incorporate the P states as well.

However, the study of P states cannot be complete without a discussion of the influence of the spin-dependent forces. In this section we will do some investigations on the splitting of the P states in charmonium and bottomonium. In Table 3.1 the main experimental data that measure the contribution of the spin-dependent forces are tabulated. For vector interactions one finds

$$V = V_0(r) + \frac{3}{2}\frac{\mathbf{L}\cdot\mathbf{S}}{m^2}\frac{V_0'(r)}{r} + \frac{2}{3}\frac{\mathbf{S_1}\cdot\mathbf{S_2}}{m^2}\Delta V_0 \qquad (3.3)$$

$$-\frac{1}{m^2}\left(\frac{(\mathbf{r}\cdot\mathbf{S_1})(\mathbf{r}\cdot\mathbf{S_2})}{r^2} - \frac{\mathbf{S_1}\cdot\mathbf{S_2}}{3}\right)\left(V_0'' - \frac{V_0'}{r}\right) .$$

For scalar interactions we find

$$V = V_0(r) - \frac{\mathbf{L}\cdot\mathbf{S}}{2m^2}\frac{V_0'(r)}{r} . \qquad (3.4)$$

Charmonium states		Bottomonium states	
State	Mass in MeV	State	Mass in MeV
J/ψ	3096.9	$\Upsilon(1S)$	9460.3
$\psi(2S)$	3686.0	$\Upsilon(2S)$	10023.3
$\psi(3S)$	4040.0	$\Upsilon(3S)$	10355.3
η_c	2979.6	η_b	
η_c'	3594.0		
χ_c^0	3415.1	χ_b^0	9859.8
χ_c^1	3510.6	χ_b^1	9891.9
χ_c^2	3556.3	χ_b^2	9913.2
$M_c^{cog}(1P)$	3524	$M_b^{cog}(1P)$	9900.3
h_c	3525	h_b	9895
		$\chi_b^0(2P)$	10235.3
		$\chi_b^1(2P)$	10255.2
		$\chi_b^2(2P)$	10269.0
		$M_b^{cog}(2P)$	10260.2

Table 3.1: Main charmonium and bottomonium S and P states. Data are from [PDG88] and [Bow87] for h_c and [Bag86] for h_b.

Here $\boldsymbol{S}_1$ and $\boldsymbol{S}_2$ are the quark spin operators, $\boldsymbol{S} = \boldsymbol{S}_1 + \boldsymbol{S}_2$, $V_0(r)$ is some central potential and m is the quark mass. In case we choose $V_0 = -\kappa/r$ for the vector interaction a Darwin term of the form

$$\frac{\pi\kappa}{m^2}\delta(\mathbf{r}) \tag{3.5}$$

should be included. This term was in first instance neglected in Eq. (3.3) but can be recovered by a more detailed procedure as given by Gromes [Gro77]. The singular terms can then be combined into:

$$(\tfrac{2}{3}\sigma_1\cdot\sigma_2 + 1)\frac{\pi\kappa}{m^2}\delta(\mathbf{r})\ . \tag{3.6}$$

These terms present a difficulty when the coupled Schrödinger equations are exactly solved or solved in a numerical way, since they do not influence the physical parameters and they only influence the wave functions exactly at the point $\boldsymbol{r} = 0$, *i.e.* they generate a removable singularity. The Darwin terms must therefore be treated differently. Their influence on the physical parameters is defined as due to lowest-order perturbation theory or lowest Born approximation. In order to reconcile these nonzero effects with the vanishing effects mentioned earlier one must think of replacing the delta function by a smeared-out potential, wide enough for first-order perturbation contributions to be dominant over higher order contributions, but sufficiently narrow for suppressing contributions to other than S states. Corrections due to (3.6) and other singular terms will therefore be carried out in first-order perturbation theory using the $q\bar{q}$ part of the normalized, unitarity-corrected, wave functions.

If a screened Coulomb term of the form (3.1) is used, the Darwin terms stay the same. For a more general analysis of the contribution of the spin-dependent forces on the splitting of the P states it is convenient to split off the quantum number dependence as follows

$$\begin{aligned} M(^3P_2) &= M_{cog} + c_{LS} - \tfrac{1}{10}c_T \\ M(^3P_1) &= M_{cog} - c_{LS} + \tfrac{1}{2}c_T \\ M(^3P_0) &= M_{cog} - 2c_{LS} - c_T \end{aligned} \tag{3.7}$$

in which

$$c_{LS} = \frac{1}{2m^2}\langle\frac{3V_v'}{r} - \frac{V_s'}{r}\rangle \tag{3.8}$$

$$c_T = -\frac{1}{m^2}\langle V_v'' - \frac{V_v'}{r}\rangle \tag{3.9}$$

and M_{cog} is the center of gravity of the P triplet:

$$M_{cog} = \frac{1}{9}\{M(^3P_0) + 3M(^3P_1) + 5M(^3P_2)\} \ . \tag{3.10}$$

Here V_v and V_s denote the parts of the potential that are caused by vector interactions and scalar interactions respectively.

In our model, as mentioned before, the central potential describing the interaction between the quarks is a combination of a pure harmonic oscillator and a screened Coulomb potential. The harmonic oscillator part, which we shall consider as purely of V_s type, is obtained by considering the non-relativistic limit of a description based on the anti-De Sitter geometry. The spectrum of quasi-free quarks moving in such a geometry is the spectrum of an irreducible representation of the CAdS group which is known to be equidistant under all circumstances, *i.e.* it always resembles the non-relativistic spectrum and does not exhibit any splitting of P states. So when the quark masses are increased in order to approach the non-relativistic limit no $\boldsymbol{L}\cdot\boldsymbol{S}$ terms as appearing in (3.4) will be produced. Apparently the Thomas precession term is then completely compensated.

The Coulomb term is considered to be of V_v type. Its contribution to (3.10) and (3.13) are consequently given by:

$$c_{LS} = \frac{3}{8}\frac{\kappa}{\mu^2}\left\{\langle\frac{e^{-\lambda r}}{r^3}\rangle + \lambda\langle\frac{e^{-\lambda r}}{r^2}\rangle\right\} \tag{3.11}$$

$$c_T = \frac{1}{4}\frac{\kappa}{\mu^2}\left\{3\langle\frac{e^{-\lambda r}}{r^3}\rangle + 3\lambda\langle\frac{e^{-\lambda r}}{r^2}\rangle + \lambda^2\langle\frac{e^{-\lambda r}}{r}\rangle\right\} \tag{3.12}$$

Introducing a variable which denotes the magnitude of the Darwin terms,

$$c_D = \frac{\pi\kappa}{m^2}|\Psi(0)|^2 \ , \tag{3.13}$$

where $\Psi(0)$ is the value of the normalized wave function in the origin, we can write the expectation value of (3.6) as

$$(\tfrac{2}{3}\sigma_1\cdot\sigma_2 + 1)c_D \ , \tag{3.14}$$

which is the first-order perturbation contribution. The Darwin term has no influence on the P states because for these states the $q\bar{q}$ wave function vanishes in the origin. The meson-meson wave function then does not vanish in the origin, but in the spirit of neglecting all direct meson-meson interactions it is supposed not to contribute. This implies an effective absence of spin-spin dependence of the P-state spectrum and will cause the singlet-P state ($^1P_1$) to coincide with the center of gravity of

the triplet P-states (^3P_J). The recently discovered h_c and h_b indeed adhere to this relation.

As far as the S states are concerned the term (3.14) causes the hyperfine-splitting between the triplet-S state ($^3S_1$ for which $\sigma_1 \cdot \sigma_2 = 1$) and the singlet-S state ($^1S_0$ for which $\sigma_1 \cdot \sigma_2 = -3$). Between these states we have a splitting that is proportional to $\Delta(\sigma_1 \cdot \sigma_2) = 4$ and it reads

$$M(^3S_1) - M(^1S_0) = \tfrac{8}{3} c_D \ . \tag{3.15}$$

In charmonium the singlet state is η_c but in bottomonium it is not yet found.

3.4 Influence of decay on the P-state spectrum

The spectrum of the P states is shifted by the presence of decay. Unfortunately we do not know the decay potential that is present in case of P states with sufficient precision. Of course, it is possible to derive a decay potential within the harmonic-oscillator framework as was done in [Bev83a] and this at least gives a hint as to its shape and magnitude. Within UMMN, however, we followed a more empirical approach and used a transition potential for the heavy-quarkonia states of the following form [Bev83b]

$$V_{tr,ij}(r) \propto g\omega \frac{r}{r_0} c_{ij} \exp\left[-\frac{1}{2}\left(\frac{r}{r_0}\right)^2\right] \ . \tag{3.16}$$

The c_{ij} are numerical constants indicating the relative couplings of the pure quark-antiquark states to the decay channels and are normalized such that

$$\sum_j c_{ij}^2 = 1 \ . \tag{3.17}$$

For the charmonium P-states only the final meson states involving D, D^* and D_S have been taken into account. Values for c_{ij}^2 are tabulated in Table 3.2.

The relative couplings to the free channels in case of the bottomonium states χ_b^0, χ_b^1, χ_b^2 and h_b are of course exactly the same, albeit that the channels are replaced by BB, BB^*, B^*B^*, B_sB_s, $B_sB_s^*$ and $B_s^*B_s^*$.

The coupling constants g appearing in (3.16) are in fact overlap integrals of the initial and final four-quark states (see [Bev83a] for details) and their relative magnitudes can be estimated. It can then be concluded that the influence of decay on the P states is certainly smaller than its influence on the S states because we are dealing with $l = 1$ states which will result in smaller overlap integrals. However, the

Decay Channel	χ_c^0	χ_c^1	χ_c^2	h_c
DD	$\frac{1}{2}$			
DD^*		$\frac{2}{3}$		$\frac{1}{3}$
D^*D^*	$\frac{1}{6}$		$\frac{2}{3}$	$\frac{1}{3}$
D_sD_s	$\frac{1}{4}$			
$D_sD_s^*$		$\frac{1}{3}$		$\frac{1}{6}$
$D_s^*D_s^*$	$\frac{1}{12}$		$\frac{1}{3}$	$\frac{1}{6}$
Spin	0	1	2	1

Table 3.2: Relative couplings c_{ij}^2 of the charmonium P states to the decay channels.

precise coupling to the free channels in the case of P states has to be determined empirically. Using the relative couplings we calculated the shift that a possible decay is causing. Within this calculation we used the pure harmonic oscillator in the confined channel and all the parameters that we used before to fit the S states (see [Bev83b]).

In Table 3.3 we show the influence of decay on the 2P-1P splitting for the bottomonium system. From this table we see that the coupling that corresponds to the experimental splitting is rather small—note that $\tilde{g}$ is the value of the coupling constant needed for the pseudo-scalars and vector mesons—resulting in a smaller influence of decay on the P-state spectrum. This agrees with what we expected.

The fine-splitting of the $^3P_2$, $^3P_1$ and $^3P_0$ states is not only caused by the spin-dependent forces as described in the previous section. Because the $^3P_2$, $^3P_1$ and $^3P_0$ states couple differently to the decay channels they will be split if the coupling strength is not zero. In Table 3.4 the splittings due to decay only are explicitly given.

3.5 Results

As far as the light meson sector is concerned, there are no relevant changes with respect to the previous predictions of [Bev83b, Bev86a]. The reason is that light quarks do not probe the interior region of the interquark potential and thus allow for the smearing procedure of the spin-dependent effects which has been used in

$g^2/\tilde{g}^2$	h_b(1P) (GeV)	h_b(2P) (GeV)	h_b(2P) - h_b(1P) (MeV)
0.0	9.936	10.316	380
0.2	9.883	10.240	357
0.4	9.818	10.188	370
0.6	9.747	10.152	405
0.8	9.674	10.127	353
1.0	9.602	10.107	505
Exp.	9.900	10.260	360

Table 3.3: Influence of decay on the 2P-1P splitting.

	Charmonium		Bottomonium	
$g^2/\tilde{g}^2$	χ_c^2 - χ_c^1 (MeV)	χ_c^1 - χ_c^0 (MeV)	χ_b^2 - χ_b^1 (MeV)	χ_b^1 - χ_b^0 (MeV)
0.0	0.0	0.0	0.0	0.0
0.2	19.5	18.1	3.0	1.8
0.4	33.8	26.5	6.6	3.8
0.6	42.6	30.5	9.8	5.5
0.8	48.1	32.6	12.3	6.8
1.0	51.7	33.8	14.2	7.8
Exp.	45	95	21	32

Table 3.4: Influence of decay on the splitting of the 1P states.

those works. In [Bev83b] the $J^{PC}= 0^{-+}$ and 1^{--} predictions for bound states and resonances in the light-meson sector are shown to be in good agreement with the data, as well as P-wave scattering data for elastic $\pi\pi$ and $K\pi$ scattering. Only the pion mass is not reproduced very well in that work, as hardly had to be expected. In [Bev86a] the $J^{PC}= 0^{++}$ resonances are discussed; especially the surprisingly good results of the predicted cross sections and phase shifts for S-wave $\pi\pi$, $K\pi$ and $\eta\pi$ elastic scattering in a model with basically no free parameters.

The model was fitted against the following observables of the heavy quarkonia:

- The first triplet-S states of charmonium and bottomonium J/ψ, ψ', Υ, Υ' and Υ''.
- The leptonic decay width of the first two S states $\Gamma(J/\psi)$, $\Gamma(\psi')$, $\Gamma(\Upsilon)$, $\Gamma(\Upsilon')$.
- The P-state triplets of charmonium and bottomonium χ_c^0, χ_c^1, χ_c^2, χ_b^0, χ_b^1, χ_b^2.
- The first singlet-S state of charmonium η_c.

In table 3.5 a description of the parameters and their values after fitting is given. Note that we need a smaller value for κ_b than for κ_c. This can be expected because also the related α_s is a running coupling constant that decreases with Q^2. Because we restricted ourselves in this work to the charmonium and bottomonium systems we did not make a parametrization like was done in [God85]. Moreover, as already mentioned in the Introduction, there is not necessarily a direct relation between α_s and the strength of the Coulomb potential that describes a bound state system of quarks. The results of the model for these values of the parameters are compared to experiment in Table 3.6. From this table we see that the overall fit for the heavy quarkonia in this model is rather good.

In Table 3.7 the theoretical leptonic decay widths are compared to their experimental values. From this table we see that the leptonic decay widths are considerably improved compared to the results without a Coulomb term (Ref. [Bev80]). As remarked before this is due to the increased wave function at the origin caused by the presence of the colour-Coulomb interaction.

From Table 3.6 we see that the $\psi(2S) - \psi(1S)$ splitting is 13 MeV too small and the $\Upsilon(2S) - \Upsilon(1S)$ splitting is 33 MeV too large. The difference is 46 MeV. Within the Unitarized Model without Coulomb this difference was 22 MeV. We can conclude that the mass dependence that is introduced by the colour-Coulomb potential amounts to approximately 24 MeV in the charmonium and bottomonium systems. The leptonic decay widths improved considerably.

Symbol	Value	Description
ω	154 MeV	universal harmonic-oscillator frequency
m_c	1.609 GeV	mass of the constituent charmed quark
m_b	4.795 GeV	mass of the constituent bottom quark
g_S	$1.06\tilde{g}$	decay coupling constant for the S-state spectra
g_P	$0.15\tilde{g}$	decay coupling constant for the P-state spectra
κ_c	0.89	the Coulomb coupling strength for the charmonium system
κ_b	0.78	the Coulomb coupling strength for the bottomonium system
σ	2.4	dimensionless screening parameter, related to the parameter λ of equation (3.1) given by $\sigma = \lambda/\sqrt{\mu\omega}$

Table 3.5: The model parameters.

When we study the results for the P states we see that as far as the absolute positions are concerned, the center of gravity of the χ_c states is slightly lower and that of the χ_b states is higher than in the pure harmonic-oscillator case.

3.6 Comparison of models

In the introduction a rough sketch was given of the different possible descriptions of the quarkonia spectra using a potential model. In this section the Nijmegen model will be compared with two other models that try to fit the light and heavy mesons simultaneously. These are the models of Brayshaw [Bra87] and of Godfrey and Isgur [God85].

3.6.1 Qualitative picture

In general any potential model will have to cope with the large differences between the light and the heavy mesons. The *light meson* sector is characterized by a more relativistic behaviour of its supposed constituents. The sector of the *heavy mesons* exhibit less relativistic effects, can easier be described using a Schrödinger equation

	Experimental (GeV)	Theoretical (GeV)	Exp - Theor (MeV)
J/ψ	3.097	3.113	-16
ψ'	3.686	3.683	4
ψ''	4.040	4.009	20
η_c	2.980	2.989	-9
η_c'	3.594	3.561	33
χ_c^0	3.415	3.434	-19
χ_c^1	3.511	3.494	17
χ_c^2	3.556	3.540	16
M_{cog}	3.524	3.513	11
Υ	9.460	9.442	18
Υ'	10.023	10.038	-15
Υ''	10.355	10.355	0
χ_b^0	9.860	9.864	4
χ_b^1	9.892	9.892	0
χ_b^2	9.913	9.913	0
M_{cog}	9.900	9.901	-1
$\chi_b^{0'}$	10.235	10.168	67
$\chi_b^{1'}$	10.255	10.195	60
$\chi_b^{2'}$	10.269	10.215	54

Table 3.6: Model compared to experiment after fitting.

	$\Gamma_{e^+e^-}$ (keV)	
	Model	Experiment
J/ψ	5.45	4.72 $\pm$ 0.35
ψ'	3.35	2.15 $\pm$ 0.21
Υ	1.62	1.34 $\pm$ 0.05
Υ'	1.14	0.60 $\pm$ 0.04

Table 3.7: Leptonic decay width of the lowest charmonium and bottomonium states. The experimental data are from [PDG88].

and probes the short range behaviour of the potential. All three models discussed here have their own characteristic way of linking the sectors of the light and heavy mesons.

- The model of Brayshaw takes as a starting point the light mesons and treats them in a Dirac formalism thus taking the relativistic kinematics directly into account. As far as the long range behaviour of the potential is concerned, the light quarks can be considered to be confined within some radius R_p. Because this confinement radius will result in the wrong splittings for the heavy quarkonia (they will be much too small) the heavy mesons are treated differently using a linear potential. The linking of the two regimes is done by means of a term in the potential that can be interpreted as a kind of r *dependent mass.* In this model it is clearly necessary that the light and heavy regimes are treated differently. This makes it possible to identify the $\rho'(1600)$ as the first excitation of the $\rho(770)$.

- The Nijmegen model treats the light and heavy mesons in a unified way. There are no exceptional parameters that act exclusively in either regime. The basis of the model is the flavour dependent harmonic-oscillator. Because of this treatment this model identifies $\rho'(1250)$ as the first excitation of the $\rho(770)$.

- Godfrey and Isgur adopt a Schrödinger equation using a Coulomb plus linear term as the non-relativistic potential. Apart from using relativistic kinematics they build a *semiquantitative model of relativistic effects.* This model describes the momentum dependence and the non-locality of the potentials. This has the disadvantage that the parameters of the model have mainly to do with the technicalities of the smearing process that is necessary to arrive at a useful interpretation of the singularities in the model.

  In the way it links the light and heavy meson sectors the model of Godfrey and Isgur can be regarded as an intermediate model between the Nijmegen and the Brayshaw model. Contrary to the model of Brayshaw it starts off from the non-relativistic description of the heavy meson spectra (using the Coulomb plus linear term as done in [Eic78]). It is of no surprise that it reproduces the shape of the bottomonium spectrum rather well.

  It does not make a definite distinction between the light and heavy meson regimes. Therefore it finds level spacings for the light mesons that are considerably larger than those of the Nijmegen model but considerably lower than

state	J^{PC}	Exp.	Nijmegen		Brayshaw		Godfrey	
		(MeV)	theor	diff	theor	diff	theor	diff
J/ψ	1^{--}	3097	3113	-16	3129	-32	3100	-3
ψ'	1^{--}	3686	3683	3	3680	6	3680	6
ψ''	1^{--}	4029	4009	20	4246	-216	4100	-71
η_c	0^{-+}	2980	2989	-9	3011	-30	2970	11
η_c'	0^{-+}	3594	3561	33	3580	14	3620	-26
χ_c^0	0^{++}	3415	3434	-19	3410	5	3440	-25
χ_c^1	1^{++}	3511	3494	17	3514	-3	3510	1
χ_c^2	2^{++}	3556	3540	16	3540	16	3550	6
M_{cog}		3524	3513	11	3517	7	3524	0
Υ	1^{--}	9460	9442	18	9452	8	9460	0
Υ'	1^{--}	10023	10038	-15	10007	16	10000	23
Υ''	1^{--}	10355	10355	0	10342	14	10350	6
χ_b^0	0^{++}	9860	9864	-4	9866	-6	9850	10
χ_b^1	1^{++}	9892	9892	0	9910	-18	9880	12
χ_b^2	2^{++}	9913	9913	0	9926	-13	9900	13
M_{cog}		9900	9901	-1	9914	-14	9888	12

Table 3.8: Comparison of the three models with experiment.

those of the Brayshaw model. Therefore it needs a $\rho'(1450)$ as the first excitation of the $\rho(770)$.

3.6.2 Quantitative picture

In Table 3.8 we give the theoretical results of the three potential models for the charmonium and bottomonium systems. What we see is that the three models roughly exhibit the same descriptive power as far as the heavy meson systems are concerned. Unfortunately in the paper of Brayshaw the leptonic decay widths are not given and therefore it is more difficult to compare his results to the results of the other two models. In Table 3.9 we give therefore separately the results for the leptonic decay widths for the Nijmegen model and the model of Godfrey and Isgur.

The main difference between the Nijmegen model and the other two is that the

	Exp.	Nijmegen		Godfrey	
	(keV)	theor	diff	theor	diff
J/ψ	4.72 ± 0.35	5.45	0.7	9.95	5.2
ψ'	2.15 ± 0.21	3.35	1.3	3.26	1.2
Υ	1.34 ± 0.05	1.62	0.4	1.43	0.2
Υ'	0.60 ± 0.04	1.14	0.6	0.65	0.1

Table 3.9: Comparison of the leptonic decay widths to experiment.

discrepancies between model and experiment are not uniformly distributed in the Nijmegen model as they are in the other two models. As far as the leptonic decay widths are concerned the Nijmegen model and the model of Godfrey and Isgur are comparable except for the width of the J/ψ state. In the last model this value is much too high which indicates that the wave function in the origin is too high in their model.

3.7 Conclusion

As mentioned in the Introduction it is our goal to build a model that can help to uncover to mechanisms that cause confinement. In fact, confinement is built into our model by means of a permanently closed channel governed by a mass dependent harmonic-oscillator potential. The results clearly indicate that this picture of confinement can be maintained when confronted with the experimental results in the domain of the P-state spectrum and leptonic decay widths.

In our interpretation of the meson spectra the decay mechanism contributes an essential part of the description of the hadron spectra. This means that when we are studying the form of the potential more closely by incorporating fine-tuning effects like the colour-Coulomb interaction we should realize that the way the decay mechanism is taken into account becomes increasingly important. This can most clearly be seen in the splittings of the P states of the charmonium system which are strongly influenced by the presence of the decay channels.

Within the Unitarized model the decay potential is kept simple. The localized potentials that were calculated within the harmonic-oscillator framework [Bev83a] were not built into the model in that form. Instead, an overall $gre^{-\beta r^2}$ shape was used. Although the correct decay potential is unknown to us, it will possess non-

local and essentially energy-dependent terms[1]. A more thorough study of the decay potential could explain the effective suppression of the influence of higher channels. This suppression is at the moment built into our model in a phenomenological way. It could also explain the almost absent influence of decay on the overall position of the P states, that was observed in Chapter 6 and possibly lead to a better description of the P-state splitting in the charmonium system (where the influence of decay is largest).

Along with an introduction of the final state interactions these improvements of the model can be regarded as *fine tuning* the model. They do not alter the main conclusions that can be drawn from the Unitarized model. These main conclusions concern the shape of the potential that is responsible for the confining mechanism (the mass dependent harmonic-oscillator potential), and the influence of decay on the meson spectra.

Acknowledgements

We like to acknowledge Dr. Th.A. Rijken for suggesting the use of screening in the Coulomb potential.

[1]The non-local potentials should also describe in a more detailed way the relation between the spatial coordinate r in the confined channel, denoting the separation of the confined quarks, and the coordinate r in the decay channels describing the separation of the decaying mesons.

Chapter 4

Radiative transitions

In this chapter the theory of the electromagnetic transitions in quarkonium will be presented. In the first part the expressions for the radiative widths will be derived for the single-channel case. Then this formalism is applied to the multi-channel model and finally the magnetic moments of the mesons involved are determined. In order to make this chapter not entirely unreadable part of the calculations is given in appendices.

Part of this chapter is based on previous work by Berens [Ber82] and Aerts [Aer75].

4.1 The interaction Hamiltonian

Our goal is to describe the interaction of non-relativistically moving quarks and the radiation field for charmonium and bottomonium. To do so, we start off with the following Hamiltonian

$$H_0 = H_{q\bar{q},0} + H_{em} \,, \tag{4.1}$$

where (in Gaussian units)

$$H_{q\bar{q},0} = \frac{p_1^2}{2m_1} + \frac{p_2^2}{2m_2} + V(r) \tag{4.2}$$

$$H_{em} = \frac{1}{8\pi} \int d^3r \, (E^2 + B^2) \qquad (\textit{in vacuum}) \,. \tag{4.3}$$

The subscript 1 (2) refers to the (anti)quark, and $V(r)$ is the confining potential. When we take into account the spin character of the quarks and apply the principle of minimal substitution, we can rewrite $H_{q\bar{q},0}$:

$$H_{q\bar{q}} = \frac{(\boldsymbol{\sigma}_1 \cdot (\boldsymbol{p}_1 - q_1 \boldsymbol{A}_1/c))^2}{2m_1} + \frac{(\boldsymbol{\sigma}_2 \cdot (\boldsymbol{p}_2 - q_2 \boldsymbol{A}_2/c))^2}{2m_2} + V(r) \,. \tag{4.4}$$

$\boldsymbol{A}_{1(2)}$ refers to the vector potential at the position of the quark with charge $q_{1(2)}$. Using

$$(\boldsymbol{\sigma}\cdot\boldsymbol{a})(\boldsymbol{\sigma}\cdot\boldsymbol{b}) = \boldsymbol{a}\cdot\boldsymbol{b} + i\boldsymbol{\sigma}\cdot(\boldsymbol{a}\times\boldsymbol{b}) \tag{4.5}$$

and

$$\boldsymbol{p}\times\boldsymbol{A} + \boldsymbol{A}\times\boldsymbol{p} = -i\hbar\boldsymbol{B}\ , \tag{4.6}$$

we obtain

$$H_{q\bar{q}} = \frac{(\boldsymbol{p}_1 - q_1\boldsymbol{A}_1/c)^2}{2m_1} + \frac{(\boldsymbol{p}_2 - q_2\boldsymbol{A}_2/c)^2}{2m_2} - \frac{q_1\hbar}{2m_1c}\boldsymbol{\sigma}_1\cdot\boldsymbol{B}_1 - \frac{q_2\hbar}{2m_2c}\boldsymbol{\sigma}_2\cdot\boldsymbol{B}_2 + V(r)\ . \tag{4.7}$$

In this expression the magnetic moment is $q_i\hbar/2m_ic$. Because $\boldsymbol{S}_i = \frac{\hbar}{2}\boldsymbol{\sigma}_i$, we have a gyromagnetic ratio $g = 2$. Generalizing this ratio to g_i, the magnetic term becomes

$$H_{magn} = -\mu_1\boldsymbol{S}_1\cdot\boldsymbol{B}_1 - \mu_2\boldsymbol{S}_2\cdot\boldsymbol{B}_2\ , \tag{4.8}$$

where

$$\mu_i = \frac{q_i}{2m_ic}g_i\ . \tag{4.9}$$

Because the emission of γ-rays is an internal process, not depending on the motion of the $q\bar{q}$-system, we choose the center-of-mass frame of the quarks as our reference frame. The center-of-mass effects do not contribute to the transition amplitude in any reference frame of physical interest, because these effects give rise to longitudinal contributions, which vanish in the transverse gauge that we will use (see Ref. [Mos87]). We will take into account the effects of recoil of the final state by taking for the photon momentum

$$p = \frac{M_i^2 - M_f^2}{2M_i}c\ , \tag{4.10}$$

where $M_{i(f)}$ denotes the mass of the initial (final) state.

To split off the C.M. motion, we first define

$$M = m_1 + m_2, \qquad \mu = \frac{m_1m_2}{m_1+m_2} \tag{4.11a}$$

$$\boldsymbol{R} = \frac{m_1\boldsymbol{r}_1 + m_2\boldsymbol{r}_2}{m_1+m_2}, \qquad \boldsymbol{r}_i = (-1)^{i+1}\frac{\mu}{m_i}\boldsymbol{r} \tag{4.11b}$$

$$\boldsymbol{P} = \boldsymbol{p}_1 + \boldsymbol{p}_2, \qquad \boldsymbol{p} = \mu\left(\frac{\boldsymbol{p}_1}{m_1} - \frac{\boldsymbol{p}_2}{m_2}\right)\ . \tag{4.11c}$$

This gives

$$\frac{p_1^2}{2m_1} + \frac{p_2^2}{2m_2} = \frac{P^2}{2M} + \frac{p^2}{2\mu}\ . \tag{4.12}$$

If we define an expression for the vector potential analogously to equation (4.11c)

$$Q\boldsymbol{\mathcal{A}} = q_1\boldsymbol{A}_1 + q_2\boldsymbol{A}_2 \tag{4.13a}$$

$$q\boldsymbol{A} = \mu\left(\frac{q_1\boldsymbol{A}_1}{m_1} - \frac{q_2\boldsymbol{A}_2}{m_2}\right) , \tag{4.13b}$$

we obtain an analogue of equation (4.12)

$$\frac{(\boldsymbol{p}_1 - q_1\boldsymbol{A}_1/c)^2}{2m_1} + \frac{(\boldsymbol{p}_2 - q_2\boldsymbol{A}_2/c)^2}{2m_2} = \frac{(\boldsymbol{P} - Q\boldsymbol{\mathcal{A}}/c)^2}{2M} + \frac{(\boldsymbol{p} - q\boldsymbol{A}/c)^2}{2\mu} . \tag{4.14}$$

Now we subtract the kinetic term for the C.M. motion to obtain the Hamiltonian that we will use for our calculations

$$H = H_{q\bar{q}} + H_{em} + H_{int} \tag{4.15}$$

where

$$H_{q\bar{q}} = \frac{p^2}{2\mu} + V(r) , \tag{4.16}$$

$$H_{int} = -\frac{q}{\mu c}\boldsymbol{p}\cdot\boldsymbol{A} + H_{magn} + \frac{q^2}{2\mu c^2}A^2 . \tag{4.17}$$

Here we used $[\boldsymbol{p}, \boldsymbol{A}] = 0$, which holds due to our choice of gauge $\boldsymbol{\nabla}\cdot\boldsymbol{A} = 0$.

4.2 Choice of basis

To calculate the transition probabilities, we will use a representation in which H_0 is diagonal. Our Hilbert space will be the tensor product of the two Hilbert spaces spanned by the complete sets of eigenfunctions of $H_{q\bar{q}}$ and H_{em}. Then H_{int} can be considered as a perturbation. Because we consider the emission of single quanta, we only have to perturb to first order in the coupling constant. Thus we can neglect the term of H_{int} proportional to q^2. First we will find all eigenstates of $H_{q\bar{q}}$ and H_{em} separately and we simply have to multiply them to find the eigenstates of $H_{q\bar{q}} \oplus H_{em}$.

Starting with the eigenfunctions of $H_{q\bar{q}}$, we make the assumption that they can be described by the quantum numbers E_{JLS}, J, L, S, M, and P, which means that we must have, as is the case in our model,

$$\left[H_{q\bar{q}}, \boldsymbol{J}^2\right] = \left[H_{q\bar{q}}, \boldsymbol{L}^2\right] = \left[H_{q\bar{q}}, \boldsymbol{S}^2\right] = \left[H_{q\bar{q}}, J_z\right] = \left[H_{q\bar{q}}, P\right] = 0 \tag{4.18}$$

where $\boldsymbol{L}$, $\boldsymbol{S} = \boldsymbol{S}_1 + \boldsymbol{S}_2$ and $\boldsymbol{J}$ are the total orbital angular momentum, the total spin and the total angular momentum respectively and P the parity.

In the coordinate representation we can use as basis

$$\langle \boldsymbol{r}|E_{JLS},J,L,S,M,P\rangle = R(r)\sum_{m,\mu} C^{\,l\ \ s\ \ J}_{\,m\ \ \mu\ \ M}\, Y^l_m(\hat{\boldsymbol{r}})\chi^s_\mu \tag{4.19}$$

where

$$\chi^s_\mu = \sum_{\mu_1,\mu_2} C^{\,\frac{1}{2}\ \ \frac{1}{2}\ \ s}_{\,\mu_1\ \ \mu_2\ \ \mu}\, \chi^{\frac{1}{2}}_{\mu_1}\chi^{\frac{1}{2}}_{\mu_2}\,, \tag{4.20}$$

is the spin function, Y^l_m are the spherical harmonics, $C^{\,\frac{1}{2}\ \ \frac{1}{2}\ \ s}_{\,\mu_1\ \ \mu_2\ \ \mu}$ is the Clebsch-Gordan coefficient, and R satisfies the radial Schrödinger equation $H_{q\bar{q}}R = E_{JLS}R$.

For the eigenstates of H_{em} we notice that they must satisfy the vector Helmholtz equation, which follows from the Maxwell equations for regions where there are no sources present:

$$\left(\triangle + k^2\right)\boldsymbol{A} = 0\,. \tag{4.21}$$

It is convenient to introduce the spherical basis vectors in $\mathbb{R}^3$

$$\begin{aligned} \boldsymbol{e}_\pm &= \mp\tfrac{1}{\sqrt{2}}(\boldsymbol{e}_x \pm i\boldsymbol{e}_y) \\ \boldsymbol{e}_0 &= \boldsymbol{e}_z\,. \end{aligned} \tag{4.22}$$

These vectors will be chosen such that $\boldsymbol{e}_\pm$ coincides with the right (left) handed polarization vectors of the photon and $\boldsymbol{e}_0$ with the direction of propagation of the photon.

Any vector can be written as

$$\boldsymbol{a} = \sum_\mu (-1)^\mu a_\mu \boldsymbol{e}_{-\mu} \tag{4.23}$$

and we have the relations

$$\begin{aligned} \boldsymbol{e}^*_\mu &= (-1)^\mu \boldsymbol{e}_{-\mu} \\ \boldsymbol{e}^*_\mu \cdot \boldsymbol{e}_{\mu'} &= (-1)^\mu \boldsymbol{e}_{-\mu}\cdot\boldsymbol{e}_{\mu'} = \delta_{\mu\mu'} \\ a_\mu &= \boldsymbol{e}_\mu \cdot \boldsymbol{a}\,. \end{aligned} \tag{4.24}$$

If we define the spherical vector harmonics

$$\boldsymbol{Y}^J_{LM}(\hat{\boldsymbol{r}}) = \sum_m C^{\,L\ \ 1\ \ J}_{\,M-m\ \ m\ \ M}\, Y^L_{M-m}(\hat{\boldsymbol{r}})\boldsymbol{e}_m\,, \tag{4.25}$$

we are able to write down a complete set of solutions $\boldsymbol{f}$ of equation (4.21)

$$\boldsymbol{f}^J_{kLM}(\boldsymbol{r}) = 2kj_L(kr)\boldsymbol{Y}^J_{LM}(\hat{\boldsymbol{r}}) \tag{4.26}$$

with

$$\int d^3r \boldsymbol{f}^{J*}_{kLM}(\boldsymbol{r})\boldsymbol{f}^{J'}_{k'L'M'}(\boldsymbol{r}) = 2\pi\delta(k-k')\delta_{JJ'}\delta_{LL'}\delta_{MM'}\,. \tag{4.27}$$

With an eye on the transversality condition $\nabla \cdot \boldsymbol{A} = 0$, we can define three linear combinations of the $\boldsymbol{f}$'s for fixed J (see Ref. [Ros55])

$$\boldsymbol{f}^{(m)}_{kJM}(\boldsymbol{r}) = \boldsymbol{f}^{J}_{kJM}(\boldsymbol{r}) \tag{4.28}$$

$$\boldsymbol{f}^{(e_\perp)}_{kJM}(\boldsymbol{r}) = \sqrt{\frac{J+1}{2J+1}}\boldsymbol{f}^{J}_{kJ-1M}(\boldsymbol{r}) - \sqrt{\frac{J}{2J+1}}\boldsymbol{f}^{J}_{kJ+1M}(\boldsymbol{r}) \tag{4.29}$$

$$\boldsymbol{f}^{(e_\parallel)}_{kJM}(\boldsymbol{r}) = \sqrt{\frac{J}{2J+1}}\boldsymbol{f}^{J}_{kJ-1M}(\boldsymbol{r}) + \sqrt{\frac{J+1}{2J+1}}\boldsymbol{f}^{J}_{kJ+1M}(\boldsymbol{r}) \,. \tag{4.30}$$

The first two combinations are transversal

$$\nabla \cdot \boldsymbol{f}^{(m)}_{kJM} = \nabla \cdot \boldsymbol{f}^{(e_\perp)}_{kJM} = 0 \tag{4.31}$$

and the last combination is longitudinal

$$\nabla \times \boldsymbol{f}^{(e_\parallel)}_{kJM} = 0 \,. \tag{4.32}$$

We will only consider the transversal combinations (because of our gauge), which satisfy in addition to equation (4.31)

$$\begin{aligned} \nabla \times \boldsymbol{f}^{(e)}_{kJM} &= -ik\boldsymbol{f}^{(m)}_{kJM} \\ \nabla \times \boldsymbol{f}^{(m)}_{kJM} &= ik\boldsymbol{f}^{(e)}_{kJM} \end{aligned} \tag{4.33}$$

where we dropped the subscript $\perp$ from $e_\perp$, as we will do in the remainder of this work.

Now we are able to write down the expression for the vector potential in this basis (see Appendix A)

$$\boldsymbol{A}(\boldsymbol{r}_j, t) = \sqrt{4\pi}\hbar c \sum_{l,m,i} \int \frac{dk}{2\pi} \sqrt{\frac{1}{2\hbar\omega}} \boldsymbol{f}^{(i)}_{klm}(\boldsymbol{r}_j) a^{(i)}_{lm}(k) e^{-i\omega t} + h.c. \,, \tag{4.34}$$

with $i \in \{e, m\}$ and $a^{(i)}_{lm}(k)$ the annihilation operator of a photon with momentum k and quantum numbers l, m.

It is possible to derive a different expression for the $\boldsymbol{f}^{(i)}$'s, using the fact that

$$\frac{1}{\sqrt{l(l+1)}} \boldsymbol{L} Y^l_m(\hat{\boldsymbol{r}}) = \boldsymbol{Y}^l_{lm}(\hat{\boldsymbol{r}}) \,. \tag{4.35}$$

This yields

$$\boldsymbol{f}^{(m)}_{klm}(\boldsymbol{r}) = \frac{2k}{\sqrt{l(l+1)}} j_l(kr) \boldsymbol{L} Y^l_m(\hat{\boldsymbol{r}}) \tag{4.36}$$

and

$$\begin{aligned} \boldsymbol{f}^{(e)}_{klm}(\boldsymbol{r}) &= \frac{1}{ik}\boldsymbol{\nabla}\times\boldsymbol{f}^{(m)}_{klm}(\boldsymbol{r}) \\ &= \frac{1}{ik}\boldsymbol{\nabla}\times\boldsymbol{L}\frac{2k}{\sqrt{l(l+1)}}j_l(kr)Y^l_m(\hat{\boldsymbol{r}})\ . \end{aligned} \tag{4.37}$$

Using

$$\boldsymbol{\nabla}\times\boldsymbol{L} = -i\left(-\boldsymbol{\nabla}(1+\boldsymbol{r}\cdot\boldsymbol{\nabla})+\boldsymbol{r}\boldsymbol{\nabla}^2\right) \tag{4.38}$$

we can define the vector-potential density amplitudes

$$\begin{aligned} \boldsymbol{A}^{(e)}_{klm}(\boldsymbol{r}_i,t) &= \frac{1}{k}\sqrt{4\pi}\sqrt{2\hbar\omega}\left(\boldsymbol{\nabla}_i(1+r\frac{\partial}{\partial r})+k^2\boldsymbol{r}_i\right) \\ &\quad\cdot\frac{1}{\sqrt{l(l+1)}}j_l(kr_i)Y^l_m(\hat{\boldsymbol{r}}_i)a^{(e)}_{lm}(k)e^{-i\omega t}+h.c. \end{aligned} \tag{4.39}$$

$$\boldsymbol{A}^{(m)}_{klm}(\boldsymbol{r}_i,t) = \sqrt{4\pi}\sqrt{2\hbar\omega}\frac{1}{\sqrt{l(l+1)}}j_l(kr_i)\boldsymbol{L}Y^l_m(\hat{\boldsymbol{r}}_i)a^{(m)}_{lm}(k)e^{-i\omega t}+h.c. \tag{4.40}$$

Because our expression for H_{int} only contains the vector potential $\boldsymbol{A}$ and the magnetic field $\boldsymbol{B}$, we only need the field amplitudes $\boldsymbol{A}^i_{klm}$ and $\boldsymbol{B}^i_{klm}$, which can be calculated with the help of $\boldsymbol{B}=\boldsymbol{\nabla}\times\boldsymbol{A}$ and relations (4.33), (4.36) and (4.37).

$$\boldsymbol{B}^{(e)}_{klm}(\boldsymbol{r}_i,t) = -ik\sqrt{4\pi}\sqrt{2\hbar\omega}\frac{1}{\sqrt{l(l+1)}}j_l(kr_i)\boldsymbol{L}Y^l_m(\hat{\boldsymbol{r}}_i)a^{(e)}_{lm}(k)e^{-i\omega t}+h.c. \tag{4.41}$$

$$\begin{aligned} \boldsymbol{B}^{(m)}_{klm}(\boldsymbol{r}_i,t) &= i\sqrt{4\pi}\sqrt{2\hbar\omega}\left(\boldsymbol{\nabla}_i(1+r\frac{\partial}{\partial r})+k^2\boldsymbol{r}_i\right) \\ &\quad\cdot\frac{1}{\sqrt{l(l+1)}}j_l(kr_i)Y^l_m(\hat{\boldsymbol{r}}_i)a^{(m)}_{lm}(k)e^{-i\omega t}+h.c. \end{aligned} \tag{4.42}$$

4.3 The matrix elements of H_{int}

We are going to calculate the matrix elements for the following type of transition

$$(q\bar{q})_{E_{JLS},J,L,S,M,P} \rightarrow (q\bar{q})_{E'_{J'L'S'},J',L',S',M',P'}+\gamma_{klmi}\ . \tag{4.43}$$

We write the matrix elements as

$$\langle\varphi',klmi|H_{int}|\varphi,0\rangle \equiv \langle\varphi'|H_{int}(klmi)|\varphi\rangle \tag{4.44}$$

where

$$H_{int}(klmi) = \langle klmi|H_{int}|0\rangle \ , \tag{4.45}$$

where is understood that H_{int} only acts on the photon vacuum, and

$$|\varphi\rangle = |E_{JLS}, J, L, S, M, P\rangle_{q\bar{q}} \ . \tag{4.46}$$

First we will calculate the potential amplitudes in the notation $H^{(i)}_{j,lm}$, with $i \in \{m, e\}$ and $j \in \{o, s\}$; o for orbital, s for spin. We define

$$H^{(i)}_{o,lm} = \langle klmi| - \frac{q}{\mu c}\boldsymbol{p}\cdot\boldsymbol{A}|0\rangle \tag{4.47}$$

$$H^{(i)}_{s,lm} = \langle klmi| - \mu_1 \boldsymbol{S}_1\cdot\boldsymbol{B}_1 - \mu_2\boldsymbol{S}_2\cdot\boldsymbol{B}_2|0\rangle \ . \tag{4.48}$$

Let

$$q = q_1 = -q_2 \tag{4.49}$$

and using $Y^{l}_{m}{}^{*} = (-1)^m Y^{l}_{-m}$ and equations (4.11b), (4.13b), (4.39)-(4.42), we can write for the orbital potential amplitudes

$$\begin{aligned} H^{(e)}_{o,lm} = {} & (-1)^{m+1}\frac{q}{\sqrt{l(l+1)}}\sqrt{4\pi}\sqrt{2\hbar\omega} \\ & \left\{\frac{1}{m_1c^2}\left(\frac{m_1}{\mu}\frac{\boldsymbol{\nabla}}{k}(1 + r\frac{\partial}{\partial r}) + \frac{\mu}{m_1}k\boldsymbol{r}\right) j_l(\frac{\mu}{m_1}kr)\right. \\ & \left. -(-1)^l\frac{1}{m_2c^2}\left(\frac{m_2}{\mu}\frac{\boldsymbol{\nabla}}{k}(1 + r\frac{\partial}{\partial r}) + \frac{\mu}{m_2}k\boldsymbol{r}\right) j_l(\frac{\mu}{m_2}kr)\right\} \\ & \cdot Y^{l}_{-m}(\hat{\boldsymbol{r}})e^{i\omega t}\cdot(-i\hbar c\boldsymbol{\nabla}) \end{aligned} \tag{4.50}$$

$$\begin{aligned} H^{(m)}_{o,lm} = {} & (-1)^{m}\frac{q}{\sqrt{l(l+1)}}\sqrt{4\pi}\sqrt{2\hbar\omega} \\ & \left\{\frac{1}{m_1c^2}j_l(\frac{\mu}{m_1}kr) + (-1)^l\frac{1}{m_2c^2}j_l(\frac{\mu}{m_2}kr)\right\}\boldsymbol{L}Y^{l}_{-m}(\hat{\boldsymbol{r}})e^{i\omega t}\cdot(-i\hbar\boldsymbol{\nabla}) \end{aligned} \tag{4.51}$$

We observe that the parity of $H^{(e)}_{o,lm}$ is $P = (-1)^l$, so $H^{(e)}_{o,lm}$ contributes to E_l radiation. The parity of $H^{(m)}_{o,lm}$ is $P = (-1)^{l+1}$, so $H^{(m)}_{o,lm}$ contributes to M_l radiation. Note that for equal masses $m_1 = m_2$, $H^{(e)}$ vanishes for even l and $H^{(m)}$ for odd l.

The expressions for $H^{(i)}$ in the above notation are not hermitian, but this is a matter of notation (only the creation part is written down)—of course the operators are still hermitian. Note that the ∇/k's and $\boldsymbol{L}$'s act up to $Y^{l}_{-m}(\hat{\boldsymbol{r}})$. The $i\hbar\nabla$'s act upon the wave functions, between which these potential amplitudes are to be sandwiched in order to obtain the matrix elements.

For the spin potential amplitudes we obtain the following expressions

$$H^{(e)}_{s,lm} = (-1)^m \frac{iq\hbar\omega}{\sqrt{l(l+1)}}\sqrt{4\pi}\sqrt{2\hbar\omega}$$
$$\left\{\frac{g_1}{2m_1c^2} j_l(\frac{\mu}{m_1}kr)\boldsymbol{S}_1 - (-1)^l \frac{g_2}{2m_2c^2} j_l(\frac{\mu}{m_2}kr)\boldsymbol{S}_2\right\} \boldsymbol{L}Y^l_{-m}(\hat{\boldsymbol{r}})e^{i\omega t} \tag{4.52}$$

$$H^{(m)}_{s,lm} = (-1)^m \frac{iq\hbar\omega}{\sqrt{l(l+1)}}\sqrt{4\pi}\sqrt{2\hbar\omega}$$
$$\left\{\frac{g_1}{2m_1c^2}\left(\frac{m_1}{\mu}\frac{\boldsymbol{\nabla}}{k}(1+r\frac{\partial}{\partial r}) + \frac{\mu}{m_1}k\boldsymbol{r}\right) j_l(\frac{\mu}{m_1}kr)\cdot\boldsymbol{S}_1\right.$$
$$\left.+(-1)^l\frac{g_2}{2m_2c^2}\left(\frac{m_2}{\mu}\frac{\boldsymbol{\nabla}}{k}(1+r\frac{\partial}{\partial r}) + \frac{\mu}{m_2}k\boldsymbol{r}\right) j_l(\frac{\mu}{m_2}kr)\cdot\boldsymbol{S}_2\right\}$$
$$\cdot Y^l_{-m}(\hat{\boldsymbol{r}})e^{i\omega t}\,, \tag{4.53}$$

contributing to E_l and M_l radiation respectively.

The calculation of the matrix elements $\langle\varphi'\left|H^{(i)}_{lm}\right|\varphi\rangle$ $(i \in \{e,m\})$ is tedious but straightforward. In Appendix B some steps in the derivation are listed.

Summing the two contributions from equations (4.50) and (4.52), we get for the total electric matrix element

$$\langle\varphi'|H^{(e)}_{lm}|\varphi\rangle = iq\sqrt{4\pi}\sqrt{2\hbar\omega}e^{it(\hbar\omega+E'-E)/\hbar}$$
$$(-1)^{m+L'}C^{\,J\ \ l\ \ J'}_{M\ \ m\ \ M'}\sqrt{\frac{(2J+1)(2L+1)(2l+1)(2L'+1)}{4\pi}}\begin{pmatrix} L' & l & L \\ 0 & 0 & 0\end{pmatrix}$$
$$\cdot\left\{(-1)^{J+L'+S'+l}\frac{\delta_{SS'}}{\sqrt{l(l+1)}}\begin{bmatrix} J & l & J' \\ L' & S' & L\end{bmatrix}(R_1+R_2)\right.$$
$$+(-1)^{S_1+S_2+1}\sqrt{(2l+1)(2S+1)(2S'+1)}\begin{bmatrix} L & l & L' \\ S & 1 & S' \\ J & l & J'\end{bmatrix}$$
$$\cdot\left\{(-1)^S g_1\frac{\hbar\omega}{m_1c^2}\sqrt{S_1(S_1+1)(2S_1+1)}\begin{bmatrix} S & 1 & S' \\ S_1 & S_2 & S_1\end{bmatrix}R^{(1)}_{0,l}-\right.$$
$$\left.\left.(-1)^{l+S'}g_2\frac{\hbar\omega}{m_2c^2}\sqrt{S_2(S_2+1)(2S_2+1)}\begin{bmatrix} S & 1 & S' \\ S_2 & S_1 & S_2\end{bmatrix}R^{(2)}_{0,l}\right\}\right\} \tag{4.54}$$

where $R^{(i)}_j$ are radial integrals:

$$R^{(i)}_{0,l} = \int_0^\infty dr\, u^*_{\varphi'}(r) j_l(\frac{\mu}{m_i}kr)u_\varphi(r) \tag{4.55}$$

$$R_1 = \int_0^\infty dr u^*_{\varphi'}(r) \left(1 + r\frac{\partial}{\partial r}\right) \left(j_l(\frac{\mu}{m_1}kr) - (-1)^l j_l(\frac{\mu}{m_2}kr)\right) u_\varphi(r) \tag{4.56}$$

$$R_2 = \int_0^\infty dr u^*_{\varphi'}(r) \left(\frac{\mu}{m_1}\frac{\hbar\omega}{m_1c^2} j_l(\frac{\mu}{m_1}kr) - (-1)^l \frac{\mu}{m_2}\frac{\hbar\omega}{m_2c^2} j_l(\frac{\mu}{m_2}kr)\right) r\frac{\partial}{\partial r} u_\varphi(r) \tag{4.57}$$

with $u_\varphi(r) = rR(r)$; $R(r)$ satisfies the radial Schrödinger equation $H_{q\bar{q}}R = E_{JLS}R$ for the state $|\varphi\rangle$.

Summing the two contributions from equations (4.51) and (4.53), we get for the total magnetic matrix element

$$\begin{aligned}
\langle\varphi'|H^{(m)}_{lm}|\varphi\rangle = {} & iq\sqrt{4\pi}\sqrt{\hbar\omega}e^{it(\hbar\omega+E'-E)/\hbar} \\
& (-1)^{m+L'+1} C^{J\ \ l\ \ J'}_{M\ \ m\ \ M'} \sqrt{\frac{(2J+1)(2L'+1)}{4\pi}} \\
& \cdot \Bigg[\delta_{SS'}(-1)^{J+L+S'}(2l+1) \begin{bmatrix} L' & L & l \\ J & J' & S \end{bmatrix} \\
& \Bigg\{ \sqrt{(2L+3)(L+1)} \begin{pmatrix} L' & l & L+1 \\ 0 & 0 & 0 \end{pmatrix} \begin{bmatrix} L' & L & l \\ 1 & l & L+1 \end{bmatrix} R_{3,-L} \\
& - \sqrt{(2L-1)L} \begin{pmatrix} L' & l & L-1 \\ 0 & 0 & 0 \end{pmatrix} \begin{bmatrix} L' & L & l \\ 1 & l & L-1 \end{bmatrix} R_{3,L+1} \Bigg\} \\
& + 2(-1)^{S_1+S_2+1} \sqrt{(2L+1)(2S+1)(2S'+1)} \\
& \cdot \Bigg\{ g_1 \frac{\hbar\omega}{2m_1c^2} (-1)^S \sqrt{S_1(S_1+1)(2S_1+1)} \begin{bmatrix} S & 1 & S' \\ S_1 & S_2 & S_1 \end{bmatrix} \\
& \Bigg(\sqrt{l(2l+3)} \begin{bmatrix} L & l+1 & L' \\ S & 1 & S' \\ J & l & J' \end{bmatrix} \begin{pmatrix} L' & l+1 & L \\ 0 & 0 & 0 \end{pmatrix} R^{(1)}_{0,l+1} - \\
& \sqrt{(l+1)(2l-1)} \begin{bmatrix} L & l-1 & L' \\ S & 1 & S' \\ J & l & J' \end{bmatrix} \begin{pmatrix} L' & l-1 & L \\ 0 & 0 & 0 \end{pmatrix} R^{(1)}_{0,l-1} \Bigg) \\
& + (-1)^l g_2 \frac{\hbar\omega}{2m_2c^2} (-1)^{S'} \sqrt{S_2(S_2+1)(2S_2+1)} \begin{bmatrix} S & 1 & S' \\ S_2 & S_1 & S_2 \end{bmatrix} \\
& \Bigg(\sqrt{l(2l+3)} \begin{bmatrix} L & l+1 & L' \\ S & 1 & S' \\ J & l & J' \end{bmatrix} \begin{pmatrix} L' & l+1 & L \\ 0 & 0 & 0 \end{pmatrix} R^{(2)}_{0,l+1} -
\end{aligned}$$

$$\sqrt{(l+1)(2l-1)} \begin{bmatrix} L & l-1 & L' \\ S & 1 & S' \\ J & l & J' \end{bmatrix} \begin{pmatrix} L' & l-1 & L \\ 0 & 0 & 0 \end{pmatrix} R^{(2)}_{0,l-1} \Bigg) \Bigg\} \Bigg] \tag{4.58}$$

where

$$R_{3,L} = \int_0^\infty dr u^*_{\varphi'}(r) \left(\frac{\hbar}{m_1 c} j_l(\frac{\mu}{m_1} kr) + (-1)^l \frac{\hbar}{m_2 c} j_l(\frac{\mu}{m_2} kr) \right) \left(\frac{\partial}{\partial r} + \frac{L}{r} \right) u_\varphi(r) \tag{4.59}$$

Note that the matrix elements above contain a factor q, because we wrote the magnetic moment $\mu \sim q$. This implies that uncharged particles give vanishing matrix elements. However, uncharged particles with an anomalous magnetic moment may contribute. In this case we will have to write the magnetic moment μ explicitly in the expressions above.

4.4 Transitions in a multi-channel model

Now that we have derived the expressions for the matrix elements, we have to check what must be done to apply this formalism to a multi-channel model. The specific way in which the radiative decays are incorporated depends on the details of the model. As far as strong decay is concerned, however, there are only a few possibilities for the transitions in these decay channels. In general the Hamiltonian in matrix form looks like

$$H = \begin{pmatrix} H_{q\bar{q}_1} & \cdots & V_{q\bar{q}_1 q\bar{q}_k} & V_{q\bar{q}_1 M\bar{M}_1} & \cdots & V_{q\bar{q}_1 M\bar{M}_l} \\ \vdots & \ddots & \vdots & \vdots & \ddots & \vdots \\ V_{q\bar{q}_1 q\bar{q}_k} & \cdots & H_{q\bar{q}_k} & V_{q\bar{q}_k M\bar{M}_1} & \cdots & V_{q\bar{q}_k M\bar{M}_l} \\ V_{q\bar{q}_1 M\bar{M}_1} & \cdots & V_{q\bar{q}_k M\bar{M}_1} & H_{M\bar{M}_1} & \cdots & V_{M\bar{M}_1 M\bar{M}_l} \\ \vdots & \ddots & \vdots & \vdots & \ddots & \vdots \\ V_{q\bar{q}_1 M\bar{M}_l} & \cdots & V_{q\bar{q}_k M\bar{M}_l} & V_{M\bar{M}_1 M\bar{M}_l} & \cdots & H_{M\bar{M}_l} \end{pmatrix} \tag{4.60}$$

if there are k $q\bar{q}$ channels and l $M\bar{M}$ channels and V_{ij} denotes the coupling between the channels i and j. Our Unitarized Meson model [Bev80, Bev83b, Bev83c] has one quark-antiquark channel and eight meson-meson channels for charmonium and bottomonium (see also Table 4.2), and there is no mixing between the meson-meson channels, so $V_{M\bar{M}_i M\bar{M}_j} = 0$ (all i, j).

When we are dealing with electromagnetic transitions, we have to substitute

$$H_{\alpha\bar{\alpha}_i} \rightarrow H_{0,\alpha\bar{\alpha}_i} + H_{int,\alpha\bar{\alpha}_i} \; . \tag{4.61}$$

pair(s)	*charmonium*	*bottomonium*
$(q\bar{q})$	$J/\psi,\ \eta_c,\ \chi_c^J$	$\Upsilon,\ (\eta_b),\ \chi_b^J$
$(q\bar{n}),(n\bar{q})$	$D^0\bar{D}^0; D^{*0}\bar{D}^{*0};$	$B^-B^+; B^{*-}B^{*+};$
	$D^{*0}\bar{D}^0, D^0\bar{D}^{*0};$	$B^{*-}B^+, B^-B^{*+};$
	$D^+D^-; D^{*+}D^{*-};$	$B^0\bar{B}^0; B^{*0}\bar{B}^{*0};$
	$D^{*+}D^-, D^+D^{*-}$	$B^{*0}\bar{B}^0, B^0\bar{B}^{*0}$
$(q\bar{s}),(s\bar{q})$	$D_s^+D_s^-; D_s^{*+}D_s^{*-};$	$B_s^0\bar{B}_s^0; B_s^{*0}\bar{B}_s^{*0};$
	$D_s^{*+}D_s^-, D_s^+D_s^{*-}$	$B_s^0\bar{B}_s^{*0}, B_s^{*0}\bar{B}_s^0$

Table 4.1: Possible $(q\bar{q})$ and $(q\bar{Q})$,$(Q\bar{q})$ pairs for charmonium and bottomonium.

This means that we get two types of transitions:

$$(q\bar{q}) \rightarrow (q\bar{q})' + \gamma\ , \tag{4.62}$$

and

$$(M_1M_2) \rightarrow (M_1M_2)' + \gamma\ , \tag{4.63}$$

where the prime expresses the fact that the quantum numbers of the final quark-antiquark (meson-meson) state have changed with respect to the initial state. Because we took $V_{M\bar{M},M\bar{M}_j} = 0$, we will not consider processes like

$$(M_1^*M_2) \rightarrow (M_1M_2) + \gamma\ . \tag{4.64}$$

In other words, we neglect the internal structure of the mesons. The processes that remain ((4.62) and (4.63)) are nevertheless essential in any model with a coupling of quark-antiquark channels to strong decay channels. Thus the following treatment of radiative transitions in a multi-channel model is of general interest.

Let us look at the possible channels for charmonium and bottomonium (only OZI-allowed quark-pair creation is taken into account) in Table 4.1, where n denotes non-strange quarks. For details on our multi-channel model, see the references mentioned above.

The pairs in a separate channel have the same values for the quantum numbers E, J, J_z, P, C, and I (C is C-parity and I is isospin). The c and b quarks are isospin

singlets, so all channels must have $I = 0$. This yields for the D and D^* mesons the following $I = 0$ wave functions

$$\begin{aligned}
\xi^{I=0}_{D\bar{D}} &= \tfrac{1}{\sqrt{2}}\left(\xi_{D^+}\xi_{D^-} - \xi_{D^0}\xi_{\bar{D}^0}\right) \\
\xi^{I=0}_{D^*\bar{D}} &= \tfrac{1}{\sqrt{2}}\left(\xi_{D^{*+}}\xi_{D^-} - \xi_{D^{*0}}\xi_{\bar{D}^0}\right) \\
\xi^{I=0}_{D\bar{D}^*} &= \tfrac{1}{\sqrt{2}}\left(\xi_{D^+}\xi_{D^{*-}} - \xi_{D^0}\xi_{\bar{D}^{*0}}\right) \\
\xi^{I=0}_{D^*\bar{D}^*} &= \tfrac{1}{\sqrt{2}}\left(\xi_{D^{*+}}\xi_{D^{*-}} - \xi_{D^{*0}}\xi_{\bar{D}^{*0}}\right)
\end{aligned} \tag{4.65}$$

and analogous wave functions for the B and B^* mesons.

For the D_s, D_s^*, B_s, and B_s^* mesons we simply have

$$\xi^{I=0}_{XY} = \xi_X \xi_Y \ , \tag{4.66}$$

where X is one of D_s^+, D_s^{*+}, B_s^0, or B_s^{*0} and Y one of their antiparticles.

For a state consisting of a particle and its own antiparticle we know that the C-parity

$$C = (-1)^{L+S} \tag{4.67}$$

with L the relative orbital momentum and S the total spin. So the $M\bar{M}$, $M^*\bar{M}^*$, $M_s\bar{M}_s$, and $M_s^*\bar{M}_s^*$ (with $M = D$ or $M = B$) and $q\bar{q}$ states are C-parity eigenstates and C can easily be computed:

$$C\eta^C_{X\bar{X}} = (-1)^{L+S}\eta^C_{X\bar{X}} \tag{4.68}$$

where X refers to any of the above mentioned particles.

For the other states we had liked to have an analogue of equation (4.68):

$$C\eta^C_{XY} = (-1)^{L+S}\eta^C_{\bar{X}\bar{Y}} \ . \tag{4.69}$$

Let's write

$$\begin{aligned}
\eta^C_{M^*\bar{M},M\bar{M}^*} &= \tfrac{1}{\sqrt{2}}\left(\eta^C_{M^*\bar{M}} \pm \eta^C_{M\bar{M}^*}\right) \\
\eta^C_{M_s^*\bar{M}_s,M_s\bar{M}_s^*} &= \tfrac{1}{\sqrt{2}}\left(\eta^C_{M_s^*\bar{M}_s} \pm \eta^C_{M_s\bar{M}_s^*}\right)
\end{aligned} \tag{4.70}$$

which are eigenstates of C with $C = (-1)^{L+S}$ for the plus sign and $C = (-1)^{L+S+1}$ for the minus sign. So we can always construct a state with the desired C-parity.

Now we can decide what particles can be in the different channels. We have $q\bar{q}$ channels, channels with a mixture of D^+D^- and $D^0\bar{D}^0$ (B^+B^- and $B^0\bar{B}^0$), channels with $D^{*+}D^-$, $D^{*0}\bar{D}^0$, D^+D^{*-}, and $D^0\bar{D}^{*0}$ ($B^{*+}B^-$, $B^{*0}\bar{B}^0$, B^+B^{*-}, and $B^0\bar{B}^{*0}$),

channels with $D^{*0}\bar{D}^{*0}$ and $D^{*+}D^{*-}$ ($B^{*+}B^{*-}$ and $B^{*0}\bar{B}^{*0}$), channels with $D_s^+D_s^-$ ($B_s^0\bar{B}_s^0$), channels with $D_s^{*+}D_s^-$ and $D_s^+D_s^{*-}$ ($B_s^{*0}\bar{B}_s^0$ and $B_s^0\bar{B}_s^{*0}$), and channels with $D_s^{*+}D_s^{*-}$ ($B_s^{*0}\bar{B}_s^{*0}$). We will neglect the mass differences between the charged and uncharged mesons.

In general a wave function can now be written as (*cf.* equation (4.19))

$$\langle \boldsymbol{r}|\psi\rangle = R_{E_{JLS}}(r)Y_M^{J(LS)}(\hat{\boldsymbol{r}})\xi^{I=0}\eta^C \tag{4.71}$$

where $Y_M^{J(LS)}(\hat{\boldsymbol{r}})$ is composed of the orbital angular momentum and the spin function according to

$$Y_M^{J(LS)}(\hat{\boldsymbol{r}}) = \sum_m C^{\,L\;\;S\;\;J}_{M-m\;\;m\;\;M}\, Y_{M-m}^L(\hat{\boldsymbol{r}})\chi_m^s \tag{4.72}$$

and χ_m^s is composed of the spin functions of the different particles. Furthermore we have to keep in mind that for the quark (fermion) channels we have $P = (-1)^{L+1}$ and for the meson (boson) channels $P = (-1)^L$.

If we limit ourselves to transitions with a relative orbital angular momentum of the mesons L equal to 0 or 1, we see that we can think of the problem in terms of a 9-component wave function and a 9x9-matrix that represents the interaction Hamiltonian. Then this matrix has a diagonal block form. In Table 4.2 the different channels with their relative L and S values are listed. Note that for bottomonium we take the same channels as for charmonium, *i.e.* we do not look at transitions involving $b\bar{c}$ mesons.

We write the state vector as

$$\begin{aligned}|\psi_{EJPC}\rangle = {} & |\psi_{q\bar{q}}\rangle + |\psi_{M\bar{M}}\rangle + |\psi_{M^*\bar{M},M\bar{M}^*}\rangle + |\psi_{M^*\bar{M}^*}\rangle + \\ & |\psi_{M_s\bar{M}_s}\rangle + |\psi_{M_s^*\bar{M}_s,M_s\bar{M}_s^*}\rangle + |\psi_{M_s^*\bar{M}_s^*}\rangle\,.\end{aligned} \tag{4.73}$$

Here we have to bear in mind that $|\psi_{M^*\bar{M}^*}\rangle$ and $|\psi_{M_s^*\bar{M}_s^*}\rangle$ are composed of two parts:

$$|\psi\rangle = |\psi_1\rangle_{L_1S_1} + |\psi_2\rangle_{L_2S_2} \tag{4.74}$$

because we have two possible L, S combinations for these channels (see Table 4.2). The normalization of this state vector is, of course,

$$\langle\psi_{EJPC}|\psi_{EJPC}\rangle = \langle\psi_{q\bar{q}}|\psi_{q\bar{q}}\rangle + \ldots + \langle\psi_{M_s^*\bar{M}_s^*}|\psi_{M_s^*\bar{M}_s^*}\rangle = 1\,, \tag{4.75}$$

for all wave functions are normalized separately. This yields for the transition matrix element

$$\langle\psi'_{EJPC}|H_{int}|\psi_{EJPC}\rangle = \langle\psi'_{q\bar{q}}|H_{int,q\bar{q}}|\psi_{q\bar{q}}\rangle + \ldots + \langle\psi'_{M_s^*\bar{M}_s^*}|H_{int,M_s^*\bar{M}_s^*}|\psi_{M_s^*\bar{M}_s^*}\rangle\,. \tag{4.76}$$

	J^{PC} =	0^{+-}	1^{--}	0^{++}	1^{++}	2^{++}
channel	*contents*	$L\ S$	$L\ S$	$L\ S$	$L\ S$	$L\ S$
1	$q\bar{q}$	0 0	0 1	1 1	1 1	1 1
2	$M\bar{M}$	x	1 0	0 0	x	x
3	$M^*\bar{M}, M\bar{M}^*$	1 1	1 1	x	0 1	x
4	$M^*\bar{M}^*$	1 1	1 0	0 0	x	0 2
5	$M^*\bar{M}^*$	x	1 2	x	x	x
6	$M_s\bar{M}_s$	x	1 0	0 0	x	x
7	$M_s^*\bar{M}_s, M_s\bar{M}_s^*$	1 1	1 1	x	0 1	x
8	$M_s^*\bar{M}_s^*$	1 1	1 0	0 0	x	0 2
9	$M_s^*\bar{M}_s^*$	x	1 2	x	x	x

Table 4.2: Possible channels for charmonium and bottomonium states with $J^{PC} = 0^{+-}, 1^{--}, 0^{++}, 1^{++}, 2^{++}$. An x indicates an empty channel.

$H_{int,q\bar{q}}$ links states with different C-parity and does not affect the isospin. So if we have states with different C-parity, we can extract the C- and I-parts of the wave function (after the action of H_{int} on these parts), which yields a factor 1. States with equal C-parity give vanishing matrix elements. This means that we have the situation of Section 4.3:

$$\langle \psi'_{q\bar{q}} | H_{int,q\bar{q}} | \psi_{q\bar{q}} \rangle = \langle \varphi'_{q\bar{q}} | H_{int,q\bar{q}} | \varphi_{q\bar{q}} \rangle \ , \tag{4.77}$$

where φ refers only to the E, J, L, S, M, P part of the wave function.

For channels containing more than one pair of particles, The C- and I-parts of the wave function may give extra factors. We will start with the $M\bar{M}$ channels:

$$\begin{aligned}
\langle \psi'_{M\bar{M}} | H_{int,M\bar{M}} | \psi_{M\bar{M}} \rangle &= \langle \varphi'_{M\bar{M}} | H_{int,M\bar{M}} | \varphi_{M\bar{M}} \rangle \\
&\quad \cdot \tfrac{1}{2} \left(\xi_{M^+} \xi_{M^-} - \xi_{M^0} \xi_{\bar{M}^0} \right) \left(\xi_{M^+} \xi_{M^-} - \xi_{M^0} \xi_{\bar{M}^0} \right) \eta^{C'}_{M\bar{M}} \eta^{C}_{M\bar{M}} \\
&= \tfrac{1}{2} \langle \varphi'_{M\bar{M}} | H_{int,M\bar{M}} | \varphi_{M\bar{M}} \rangle \left(\xi_{M^+} \xi_{M^-} \xi_{M^+} \xi_{M^-} + \xi_{M^0} \xi_{\bar{M}^0} \xi_{M^0} \xi_{\bar{M}^0} \right) \\
&= \tfrac{1}{2} \langle \varphi'_{M\bar{M}} | H_{int,M\bar{M}} | \varphi_{M\bar{M}} \rangle \ .
\end{aligned} \tag{4.78}$$

In the last step we used the fact that the uncharged M mesons don't contribute, because H_{int} is proportional to the charge. In exactly the same way we obtain a factor $\frac{1}{2}$ for the $M^*\bar{M}^*$ channel, but here is a problem because of the possible anomalous magnetic moment of the uncharged vector mesons. A discussion of this problem will be postponed until Section 4.5.

For the $(M_s^*\bar{M}_s),(M_s\bar{M}_s^*)$ channels the isospin part yields a factor 1 and the C-part gives the following contribution:

$$\begin{aligned}
&\langle \psi'_{M_s^*\bar{M}_s,M_s\bar{M}_s^*} \mid H_{int,M_s^*\bar{M}_s,M_s\bar{M}_s^*} \mid \psi_{M_s^*\bar{M}_s,M_s\bar{M}_s^*} \rangle \\
&\quad = \langle \varphi'_{M_s^*\bar{M}_s,M_s\bar{M}_s^*} | H_{int,M_s^*\bar{M}_s,M_s\bar{M}_s^*} | \varphi_{M_s^*\bar{M}_s,M_s\bar{M}_s^*} \rangle \tfrac{1}{2} \left(\eta^C_{M_s^*\bar{M}_s} \pm \eta^C_{M_s\bar{M}_s^*} \right)^2 \\
&\quad = \tfrac{1}{2} \left(\langle \varphi'_{M_s^*\bar{M}_s} | H_{int,M_s^*\bar{M}_s} | \varphi_{M_s^*\bar{M}_s} \rangle + \langle \varphi'_{M_s\bar{M}_s^*} | H_{int,M_s\bar{M}_s^*} | \varphi_{M_s\bar{M}_s^*} \rangle \right) \\
&\quad = \langle \varphi'_{M_s^*\bar{M}_s} | H'_{int,M_s^*\bar{M}_s} | \varphi_{M_s^*\bar{M}_s} \rangle \ , \qquad (4.79)
\end{aligned}$$

where we used in the last step equations (4.54) and (4.58), the explicit values for l, S, and S' for the transitions we will consider (see Figure 4.1 of Section 4.6) and the fact that we simply have to exchange the indices 1 and 2 in the matrix element for $M_s^*\bar{M}_s$ to get the matrix element for $M_s\bar{M}_s^*$. Note that for magnetic transitions the part of $H_{int}^{(m)}$ proportional to the radial integral R_3 vanishes, because the terms with the indices exchanged cancel the original terms for $l = 1$. This is indicated by the accent in H_{int}.

The $M_s\bar{M}_s$ and $M_s^*\bar{M}_s^*$ channels cause no problems and yield factors 1, but the B_s^* mesons only contribute through their anomalous magnetic moments.

The last channel we have to look at is the $(M^*\bar{M}),(M\bar{M}^*)$ channel. Following the same reasoning as the one that led to equations (4.78) and (4.79), we conclude in this case

$$\langle \psi'_{M^*\bar{M},M\bar{M}^*} | H_{int,M^*\bar{M},M\bar{M}^*} | \psi_{M^*\bar{M},M\bar{M}^*} \rangle = \tfrac{1}{2} \langle \varphi'_{M^*\bar{M}} | H'_{int,M^*\bar{M}} | \varphi_{M^*\bar{M}} \rangle \ . \qquad (4.80)$$

Summarizing this section, we conclude:

- The $q\bar{q}$ channels can be treated as was done in Section 4.3.
- All channels with M or M^* mesons get an extra factor $\frac{1}{2}$ due to the isospin and the fact that the uncharged mesons don't contribute (see Section 4.5 for an exception).
- All channels with M_s or M_s^* don't get extra factors from the isospin or C-parity part of the wave function.

- Attention should be paid to the channels with two or more meson pairs. In our case the terms in $H_{int}^{(m)}$ proportional to R_3 cancel, but this result does not hold for arbitrary magnetic transitions. Thus equations (4.79) and (4.80) are not generally valid.

4.5 Magnetic moments

In this section we will calculate the magnetic moments of the M^* and M_s^* mesons. The M and M_s mesons are pseudoscalars and hence they don't have a magnetic moment. The uncharged M^* and M_s^* mesons don't have a normal magnetic moment either, but they possess an anomalous moment. We will neglect a possible internal structure of the quarks and assume that they have a normal magnetic moment

$$\mu_q = g_q \frac{q_q}{2m_q c} = \frac{q_q}{m_q c} , \tag{4.81}$$

with $g_q = 2$.

The next step is to write down the SU(3) and spin parts of the wave functions for the M^* and M_s^* mesons. The spin function describes the spin-1 state of the mesons. In our calculations we take $S_z = 1$ and $\boldsymbol{\mu}$ in the z-direction. The state vectors read

$$\begin{aligned}
|D^{*+}\rangle &= |c\bar{d}\rangle \chi_{\frac{1}{2}}^{\frac{1}{2}}(c)\chi_{\frac{1}{2}}^{\frac{1}{2}}(\bar{d}) \ , \ |B^{*+}\rangle = |u\bar{b}\rangle \chi_{\frac{1}{2}}^{\frac{1}{2}}(u)\chi_{\frac{1}{2}}^{\frac{1}{2}}(\bar{b}) \\
|D^{*-}\rangle &= |\bar{c}d\rangle \chi_{\frac{1}{2}}^{\frac{1}{2}}(\bar{c})\chi_{\frac{1}{2}}^{\frac{1}{2}}(d) \ , \ |B^{*-}\rangle = |\bar{u}b\rangle \chi_{\frac{1}{2}}^{\frac{1}{2}}(\bar{u})\chi_{\frac{1}{2}}^{\frac{1}{2}}(b) \\
|D^{*0}\rangle &= |c\bar{u}\rangle \chi_{\frac{1}{2}}^{\frac{1}{2}}(c)\chi_{\frac{1}{2}}^{\frac{1}{2}}(\bar{u}) \ , \ |B^{*0}\rangle = |d\bar{b}\rangle \chi_{\frac{1}{2}}^{\frac{1}{2}}(d)\chi_{\frac{1}{2}}^{\frac{1}{2}}(\bar{b}) \\
|\bar{D}^{*0}\rangle &= |\bar{c}u\rangle \chi_{\frac{1}{2}}^{\frac{1}{2}}(\bar{c})\chi_{\frac{1}{2}}^{\frac{1}{2}}(u) \ , \ |\bar{B}^{*0}\rangle = |\bar{d}b\rangle \chi_{\frac{1}{2}}^{\frac{1}{2}}(\bar{d})\chi_{\frac{1}{2}}^{\frac{1}{2}}(b) \\
|D_s^{*+}\rangle &= |c\bar{s}\rangle \chi_{\frac{1}{2}}^{\frac{1}{2}}(c)\chi_{\frac{1}{2}}^{\frac{1}{2}}(\bar{s}) \ , \ |B_s^{*0}\rangle = |s\bar{b}\rangle \chi_{\frac{1}{2}}^{\frac{1}{2}}(s)\chi_{\frac{1}{2}}^{\frac{1}{2}}(\bar{b}) \\
|D_s^{*-}\rangle &= |\bar{c}s\rangle \chi_{\frac{1}{2}}^{\frac{1}{2}}(\bar{c})\chi_{\frac{1}{2}}^{\frac{1}{2}}(s) \ , \ |\bar{B}_s^{*0}\rangle = |\bar{s}b\rangle \chi_{\frac{1}{2}}^{\frac{1}{2}}(\bar{s})\chi_{\frac{1}{2}}^{\frac{1}{2}}(b) \ .
\end{aligned} \tag{4.82}$$

The magnetic moment operator for a particle consisting of two quarks is given by

$$\boldsymbol{\mu} = \sum_{i=1,2} g_i \frac{q_i}{2m_i c} \boldsymbol{S}_i = \frac{\hbar}{2} \sum_{i=1,2} \frac{q_i}{m_i c} \boldsymbol{\sigma}_i \ , \tag{4.83}$$

where we used $g_q = 2$. The operator $q_i/m_i c$ acts on the SU(3) part and gives the value of $q_i/m_i c$ for the quark it acts on. For the z-component we have

$$\mu_z = \frac{\hbar}{2} \sum_{i=1,2} \frac{q_i}{m_i c} \sigma_{iz} \ . \tag{4.84}$$

Let's start with the magnetic moment of the D^{*+} meson

$$\begin{aligned}\mu_{D^{*+}} &= \langle D^{*+}|\mu_z|D^{*+}\rangle \\ &= \frac{\hbar}{2}\sum_{i=1,2}\langle c\bar{d}|\frac{q_i}{m_i c}|c\bar{d}\rangle = \frac{e\hbar}{2c}\left(\frac{2}{3m_c}+\frac{1}{3m_d}\right) ,\end{aligned} \tag{4.85}$$

which yields for the gyromagnetic ratio

$$g_{D^{*+}} = \frac{2m_{D^{*+}}c}{e\hbar}\mu_{D^{*+}} = \frac{m_{D^{*+}}}{3}\left(\frac{2}{3m_c}+\frac{1}{3m_d}\right) . \tag{4.86}$$

For the D^{*-} we obtain

$$\mu_{D^{*-}} = -\mu_{D^{*+}} \Rightarrow g_{D^{*-}} = g_{D^{*+}} . \tag{4.87}$$

Using the same procedure for the D^{*0} and $\bar{D}^{*0}$ mesons we get

$$\mu_{D^{*0}} = -\mu_{\bar{D}^{*0}} = \frac{e\hbar}{2c}\left(\frac{2}{3m_c}-\frac{2}{3m_u}\right) . \tag{4.88}$$

For these uncharged particles we cannot define a gyromagnetic ratio, which is what we had liked to do because then we can use our previously derived expressions for the matrix elements. If we had written these expressions in terms of μ instead of $gq/2m$, we would have found for the channels with D^* mesons $\mu_{D^{*+}} + \mu_{D^{*0}}$ and $\mu_{D^{*-}} + \mu_{\bar{D}^{*0}}$ respectively instead of $\mu_{D^{*+}}$ and $\mu_{D^{*-}}$. To get around this difficulty we define

$$g_{D^*} \equiv \frac{2m_{D^{*+}}}{e\hbar}(\mu_{D^{*+}} + \mu_{D^{*0}}) = \frac{m_{D^{*+}}}{3}\left(\frac{4}{m_c}+\frac{1}{m_d}-\frac{2}{m_u}\right) \tag{4.89}$$

and we will use g_{D^*} rather than $g_{D^{*+}} = g_{D^{*-}}$. Thus we account for the anomalous magnetic moment of the uncharged D^* mesons in a natural way. Note that we neglect the small mass difference (3 MeV) between the D^{*+} and the D^{*0}.

We calculate the magnetic moments of the D_s^*, B^* and B_s^* mesons in the same way (Table 4.3). The only difference is that in case of the B_s^* mesons, we have an anomalous magnetic moment. The quark masses are fit parameters in the Unitarized Meson model and have the following values: $m_u = m_d = 406$ MeV, $m_s = 508$ MeV, $m_c = 1609$ MeV, and $m_b = 4795$ MeV.

4.6 The decay widths

The Fermi Golden Rule states that the transition probability per unit time is

$$\frac{1}{\tau_{lm}^{(j)}} = W_{fi} = \frac{2\pi}{\hbar}|\langle f|T_{lm}^{(j)}|i\rangle|^2\rho_f , \tag{4.90}$$

M	μ (units $\frac{e\hbar}{6c}$) and g (units $\frac{M}{3}$)
D^*	$\frac{4}{m_c} + \frac{1}{m_d} - \frac{2}{m_u}$
D_s^*	$\frac{2}{m_c} + \frac{1}{m_s}$
B^*	$\frac{2}{m_b} + \frac{2}{m_u} - \frac{1}{m_d}$
B_s^*	$\frac{1}{m_b} - \frac{1}{m_s}$

Table 4.3: (Anomalous) magnetic moments and our definition of the gyromagnetic ratio

where up to first order

$$\begin{aligned}\langle f|T_{lm}^{(j)}|i\rangle &= e^{-(\hbar\omega+E'-E)it/\hbar}\langle f|H_{lm}^{(j)}|i\rangle \\ &\equiv \langle f|\bar{H}_{lm}^{(j)}|i\rangle \ ,\end{aligned} \tag{4.91}$$

with $\langle f|\bar{H}_{lm}^{(j)}|i\rangle$ time independent. The density of states is $\rho_f = 1/2\pi\hbar c$. Summing over the magnetic quantum numbers of the photon and the final quarkonium state, we obtain the expression for the decay widths

$$\Gamma_l^{(i)} = \frac{1}{\hbar c}\sum_{m,M'} |\langle f|\bar{H}_{lm}^{(j)}|i\rangle|^2 \ . \tag{4.92}$$

Now we are able to examine what type of electromagnetic transitions can occur in charmonium and bottomonium. First let us have a look at the spectra (Figure 4.1). As a photon has quantum numbers $J^{PC} = 1^{--}$, we can see that due to C-parity conservation only transitions between a level with $J^{PC} = 1^{--}$ and a level in one of the other two columns in Figure 4.1 are possible. Because E_l radiation has parity $P = (-1)^l$ and M_l radiation has $P = (-1)^{l+1}$, we note that between the two levels at the left side of the figure only E_l transitions with even l and M_l transitions with odd l are possible, whereas between the two levels at the right side of the figure only E_l transitions with odd l and M_l transitions with even l are possible.

From the matrix elements for $H_{int}^{(e)}$ (equation (4.54)) and $H_{int}^{(m)}$ (equation (4.58)) we are able to decide which transitions are possible between the various quarkonium states. Note that these states determine also the transitions in the meson channels because of the coupling of the quark states with the meson states.

First we have the $n^3S_1 \leftrightarrow m^1S_0$ transitions. Are there electric-multipole transitions possible? The answer is no, for the first term in equation (4.54) vanishes

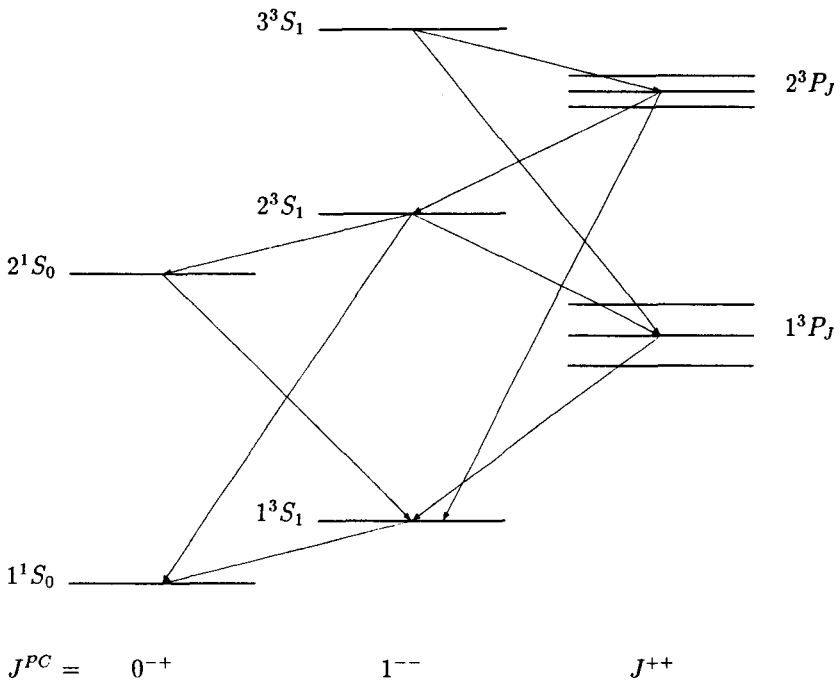

Figure 4.1: Quarkonium levels and their radiative transitions

because $S \neq S'$, so $\delta_{SS'} = 0$. The second term is proportional to

$$\begin{bmatrix} 0 & l & 0 \\ 1 & 1 & 0 \\ 1 & l & 0 \end{bmatrix} = \frac{(-1)^l}{\sqrt{3}} \delta_{l1} \begin{bmatrix} 0 & l & 0 \\ 1 & 1 & 1 \end{bmatrix}$$

and demands $l = 1$, but we saw above that only electric transitions with even l are allowed.

How about the magnetic-multipole transitions? The 3-J symbol

$$\begin{pmatrix} l_1 & l_2 & l_3 \\ 0 & 0 & 0 \end{pmatrix}$$

vanishes if $l_1 + l_2 + l_3$ is odd. So we must have, from equation (4.58), that $L' + l + L$ is odd so in this case l must be odd. From the 3-J symbols in equation (4.58), we see that only $l = 1$ yields some non-vanishing terms. We conclude that between the $^3S_1$ and $^1S_0$ levels only magnetic-dipole (M_1) radiation occurs.

Secondly we have the $n^3S_1 \leftrightarrow m^3P_J$ transitions. From the 3-J symbol in equation (4.54),

$$\begin{pmatrix} 1 & l & 0 \\ 0 & 0 & 0 \end{pmatrix},$$

we see that the only possibility is $l = 1$. Here we have electric-dipole (E_1) radiation. From the 3-J symbols in equation (4.58), we see that l must be even (as we already saw above), but then the 6-J symbols and the 9-J symbols all vanish. Thus for these transitions there is no magnetic-multipole radiation.

Remains to calculate the various coefficients in equations (4.54) and (4.58) for all transitions that are possible between the various channels. This yields for the electric-dipole decay widths for the transitions $n^3S_1 \rightarrow m^3P_J + \gamma$:

$$\Gamma^{(e)}(n^3S_1 \rightarrow m^3P_J + \gamma) = \tfrac{1}{3}(2J+1)\alpha\hbar\omega \left| \sum_{i=1,2} \int_0^\infty dr u^\dagger_{m^3P_J}(r) P_J^{(i)} E^{(i)}(r) u_{n^3S_1}(r) \right|^2 \tag{4.93}$$

(where $\alpha = e^2/\hbar c$) and with the help of the principle of detailed balancing we obtain for the transitions $n^3P_J \rightarrow m^3S_1 + \gamma$:

$$\Gamma^{(e)}(n^3P_J \rightarrow m^3S_1 + \gamma) = \alpha\hbar\omega \left| \sum_{i=1,2} \int_0^\infty dr u^\dagger_{n^3P_J}(r) P_J^{(i)} E^{(i)}(r) u_{m^3S_1}(r) \right|^2 , \tag{4.94}$$

where the coefficients $P_J^{(i)}$ and the operator matrices $E^{(i)}(r)$ are defined in Appendix C.

For the magnetic-dipole decay widths we obtain for the transitions $n^3S_1 \to m^1S_0 + \gamma$:

$$\Gamma^{(m)}(n^3S_1 \to m^1S_0 + \gamma) = \tfrac{1}{3}\alpha\hbar\omega \left| \sum_{i=1,2} \int_0^\infty dr u^\dagger_{m^1S_0}(r) Q^{(i)} M^{(i)}(r) u_{n^3S_1}(r) \right|^2 \quad (4.95)$$

and for the transitions $n^1S_0 \to m^3S_1 + \gamma$:

$$\Gamma^{(m)}(n^1S_0 \to m^3S_1 + \gamma) = \alpha\hbar\omega \left| \sum_{i=1,2} \int_0^\infty dr u^\dagger_{n^1S_0}(r) Q^{(i)} M^{(i)}(r) u_{m^3S_1}(r) \right|^2 , \quad (4.96)$$

where the coefficients $Q^{(i)}$ and the operator matrices $M^{(i)}(r)$ are defined in Appendix C.

By taking the first term in a Taylor-series expansion for the Bessel functions, we obtain the more familiar expressions for the electromagnetic decay widths in the long-wavelength approximation ($kr \ll 1$) in the one-channel case (see Appendix C).

Chapter 5

Results

In this chapter I will present the results as obtained by the Unitarized Meson model for the radiative widths in charmonium and bottomonium. This chapter is organized as follows: first of all, I will give the results of the full model. Secondly, I will make some approximations to the expressions for the widths and investigate what contributions the various terms in these expressions give. In Section 5.3 our model is going to be compared with other models and some concluding remarks are made.

5.1 Results from the model

Calculating the widths as given by formulas (4.54) and (4.58) yields the results as tabulated in Tables 5.1 and 5.2 (denoted by "full model"). The fact that two tables were made requires an explanation. The results in Table 5.2 are called "numerically unstable", in contrast to the as "numerically stable" denoted values in Table 5.1. By the term "numerically unstable" the fact is expressed that in the overlap integrals (in the expressions for the widths) appreciable cancellations occur, because the integrand has one or more nodes. (Refer to Figures 5.1 and 5.2, where the integrands are plotted as a function of the distance.) Because of the accuracy of the wave functions, I decided to put the widths with a cancellation of the overlap integral of more than 15–20%, say, in Table 5.2, where the percentage of cancellation can be found too. Obvious examples of large cancellations are the so called "hindered" magnetic dipole transitions $\psi' \to \eta_c + \gamma$ and $\eta_c' \to J/\psi + \gamma$, where the overlap integral vanishes almost completely. For a non-relativistic, one-channel model it will be very difficult to describe these hindered transitions properly. Moreover, most models calculate the radiative widths in long-wavelength approximation, with a magnetic dipole operator proportional to unity, yielding exactly zero widths for orthonormal states.

Two remarks have to be made at this point. The recoil of the final state was accounted for by taking for the photon momentum $k = (M_i^2 - M_f^2)/2M_i$, where $M_{i(f)}$ denotes the mass of the initial (final) state, and in a discussion of the results I will restrict myself to the transitions in Table 5.1.

The widths for the transitions $\psi' \to \eta_c' + \gamma$, $\chi_c^J \to J/\psi + \gamma$, $\Upsilon' \to \chi_b^J + \gamma$, and $\Upsilon'' \to \chi_b^{J'} + \gamma$ appear to agree with experiment, whereas those for the transitions $J/\psi \to \eta_c + \gamma$ and $\psi' \to \chi_c^J + \gamma$ are approximately a factor two too large. A discussion of these results is postponed until the next section.

5.2 Analysis of the results

In order to gain more insight in the results of the full model, the expressions for the decay widths are analyzed and some common approximations are made. This analysis may be useful to compare our results with those of other authors in Section 5.3.

Most phenomenological quark models are one-channel models that do not take into account the effects of strong decay. Therefore, let us calculate the radiative widths in one-channel approximation. The only thing one has to do is to substitute all wave functions for the meson-meson channels by zero. Hence $|\psi\rangle = |\psi_{q\bar{q}}\rangle$ (remember that one must set $\langle\psi_{q\bar{q}}|\psi_{q\bar{q}}\rangle = 1$). The results are in the first column of Tables 5.1 and 5.2 and in Table 5.3 the reduction on the widths due to coupled-channel effects is tabulated. We find that our coupled-channel reductions are somewhat larger than those of Eichten *et al.* [Eic80], which are often quoted when an estimation of the coupled-channel effects on electromagnetic transitions is given. Note that for bottomonium (and for some reactions in charmonium) the one-channel results are closer to experiment than the full model results. This phenomenon expresses the fact that the full model results are too low rather than that there is no need for meson-meson contributions to the radiative widths.

For an explanation of the differences in column *a* of Table 5.3, one must keep in mind that in our multi-channel model the contributions of the meson-meson channels are not the same for all particles (this depends on the number of decay channels and the positions of the thresholds). Remembering that the one-channel results were obtained by neglecting the contributions of the meson-meson channels and renormalizing the $q\bar{q}$-wave function, one sees that by combining Table 5.4 and the second column of Table 5.1, the results of column *a* of Table 5.3 are easily explained (qualitatively). Note that in calculating the radiative widths from the meson-meson channels only (Table 5.1, second column), the sum of the meson-meson wave functions are renormalized to unity: $\sum_M \langle\psi_{M\bar{M}}|\psi_{M\bar{M}}\rangle = 1$.

	width (keV)				
transition	1 channel[a]	$M\bar{M}$[b]	l.w.a.[c]	full model	experiment
$J/\psi \to \eta_c\gamma$	2.51	$2.1{\cdot}10^{-3}$	1.68	1.67	0.86 ± 0.23
$\psi' \to \eta_c'\gamma$	1.24	$1.4{\cdot}10^{-4}$	1.02	1.01	0.43 - 2.8
$\psi' \to \chi_c^0\gamma$	52.9	13.9	45.5	31.7	22.6 ± 4.4
$\psi' \to \chi_c^1\gamma$	58.7	7.37	56.2	49.8	21.1 ± 4.2
$\psi' \to \chi_c^2\gamma$	49.7	3.09	38.8	38.5	19.0 ± 3.9
$\chi_c^0 \to J/\psi\gamma$	118	62.0	91.6	51.7	95 ± 46
$\chi_c^1 \to J/\psi\gamma$	232	118	356	210	< 355
$\chi_c^2 \to J/\psi\gamma$	380	152	333	228	351^{+165}_{-125}
$\Upsilon' \to \chi_b^0\gamma$	1.64	0.93	1.69	1.59	1.89 ± 0.59
$\Upsilon' \to \chi_b^1\gamma$	2.66	1.44	2.22	2.14	2.95 ± 0.72
$\Upsilon' \to \chi_b^2\gamma$	2.73	1.34	2.64	2.64	2.90 ± 0.71
$\chi_b^0 \to \Upsilon\gamma$	19.8	38.2	25.9	20.9	
$\chi_b^1 \to \Upsilon\gamma$	25.4	50.3	19.8	15.8	
$\chi_b^2 \to \Upsilon\gamma$	31.7	63.7	36.6	33.2	
$\Upsilon'' \to \chi_b^{0'}\gamma$	1.69	0.31	1.67	1.59	1.25 ± 0.46
$\Upsilon'' \to \chi_b^{1'}\gamma$	3.02	0.52	2.67	2.59	3.12 ± 1.06
$\Upsilon'' \to \chi_b^{2'}\gamma$	3.30	0.51	3.11	3.10	3.38 ± 1.10
$\chi_b^{0'} \to \Upsilon'\gamma$	6.70	2.17	6.62	5.45	
$\chi_b^{1'} \to \Upsilon'\gamma$	8.63	2.80	9.75	8.14	
$\chi_b^{2'} \to \Upsilon'\gamma$	10.2	3.50	10.0	8.53	

[a] radiative widths from quark anti-quark channel only

[b] radiative widths from meson-meson channels only

[c] long-wavelength approximation (see Appendix C)

Table 5.1: Radiative widths for "numerically stable" transitions in charmonium and bottomonium.

	width (keV)					
transition	1 ch.[a]	$M\bar{M}$[b]	l.w.a.[c]	full	cancel.[d]	experiment
$\psi' \to \eta_c\gamma$	1.85	0.038	0.002	1.41	79	0.68 ± 0.19
$\eta_c' \to J/\psi\gamma$	0.53	0.080	0.006	0.43	90	
$\Upsilon'' \to \chi_b^0\gamma$	4.14	30.7	4.10	2.59	52	
$\Upsilon'' \to \chi_b^1\gamma$	11.6	79.5	17.5	14.1	34	0.041 ± 0.029 [e]
$\Upsilon'' \to \chi_b^2\gamma$	19.7	122	16.5	13.2	50	0.064 ± 0.045 [e]
$\chi_b^{0\prime} \to \Upsilon\gamma$	17.9	215	26.5	26.2	16	
$\chi_b^{1\prime} \to \Upsilon\gamma$	21.5	264	6.72	8.37	28	
$\chi_b^{2\prime} \to \Upsilon\gamma$	28.0	343	30.9	39.3	16	

[a] radiative widths from quark anti-quark channel only
[b] radiative widths from meson-meson channels only
[c] long-wavelength approximation (see Appendix C)
[d] cancellation of the overlap integral: $(1 - \frac{I}{\max(I_+, I_-)}) \times 100\%$, where $I_\pm$ is the positive/negative contribution to the total integral $I = I_+ - I_-$
[e] data from Kwong & Rosner [Kwo88]

Table 5.2: Radiative widths for "numerically unstable" transitions in charmonium and bottomonium.

We may conclude that the unitarization effects on the radiative widths are somewhat less for bottomonium than for charmonium. If one wants to study these effects in detail (*e.g.* differences for $J = 0, 1, 2$ transitions), one has to know the details of the multi-channel model. Nevertheless, these effects prove to be important.

Besides the fact that most models that try to describe the properties of (heavy) quarkonium are one-channel models, there is another feature shared by almost all models: electromagnetic transitions are calculated in the so called long-wavelength approximation (sometimes called dipole approximation). This approximation is said to be valid when the size of the bound state emitting the photon is small compared to the wavelength of the photon: $kR \ll 1$ (where k is the photon momentum and R the size of the bound state; see also Appendix C). If the size of the charmonium and bottomonium ground states is calculated via $R = \sqrt{\langle r^2 \rangle}$, one finds $R_{J/\psi} \simeq 0.4$ fm and $R_\Upsilon \simeq 0.2$ fm. The photon energy varies from 0.1–0.4 GeV for the

transitions we consider, so kR varies from 0.2–0.8 and 0.1–0.4 for charmonium and bottomonium respectively. By comparing the full model results with those from the long-wavelength approximation one is able to test how good this assumption is. Corrections to the long-wavelength approximation are called finite size or retardation effects. These corrections are expected to be smaller for bottomonium than for charmonium. One may also expect to see this effect clearly in transitions involving triplet-P states, because of the difference in photon energy for different values of J. In our case the long-wavelength approximation means that we take only terms up to order kr in the expressions for the dipole operators (Appendix C). The results are in the third column of Tables 5.1 and 5.2 and the relative size of this approximation is tabulated in Table 5.3.

It is clear that the long-wavelength approximation is very good for the M1-transitions in charmonium for non-orthonormal states. For orthogonal states ($n^3S_1 \leftrightarrow m^1S_0$, $n \neq m$ transitions) this approximation leads to vanishing matrix elements in the one-channel case. This means that the meson-meson channels supply for most of the total width in these cases. As expected, the finite-size corrections prove to be larger for charmonium than for bottomonium and the dependence of these corrections on the photon energy is evident from the E1-transitions: the larger the momentum, the larger the correction. Remarkable is the fact that I find rather large finite-size effects. Novikov *et al.* [Nov78] and McClary and Byers [McC83] claim that these effects are about 3% for charmonium and even less for bottomonium. To explain this discrepancy, let us look at the expressions for the dipole operators in more detail. Expanding the Bessel functions, one finds for these operators up to third order in kr

$$E^{(1)} \simeq \frac{2}{3}kr\left(1-\frac{(kr)^2}{20}\right)+\frac{(kr)^2}{6}\frac{1}{m}\frac{\partial}{\partial r} \equiv E_A^{(1)}+E_B^{(1)} \tag{5.1}$$

$$E^{(2)} \simeq \frac{2}{3}kr\left(1-\frac{(kr)^2}{20}\right) \tag{5.2}$$

(where $g = 2$ was assumed). Assuming kr to be of the order of one, we introduce an error of 5% by neglecting the second part of $E_A^{(1)}$. This is the analogue of the the approximation made by the above mentioned authors. But the other terms ($E_B^{(1)}$ and $E^{(2)}$) cannot be neglected! In our case k/m ranges from 0.1–0.3 for charmonium and so does $E^{(2)}/E_A^{(1)}$. $E_B^{(1)}$ gives a smaller contribution because $1/6m \simeq 0.1$ for charmonium.

Thus I come to the conclusion that the long-wavelength approximation is not a good approximation for E1-transitions in charmonium and a little bit less worse for bottomonium.

5.3 Comparison with other models

Starting with the magnetic dipole transitions in charmonium, I found that only very few authors give any results for these rates. Indeed, almost all models are unable to calculate the widths for the hindered transitions (because of the dipole approximation), while for the allowed transition $J/\psi \rightarrow \eta_c + \gamma$ the predictions are a factor of two too large compared with experiment (see Ref. [Kon86, God85]. Because of the large experimentally allowed range for the transition rate of $\psi' \rightarrow \eta_c' + \gamma$, no conclusions can be drawn from this reaction. While relativistic corrections will have a large influence on the hindered transition rate, because of the position of the node(s) in the wave function, they will probably not alter the results for the allowed M1-transitions significantly. Coupled-channel effects will also be of importance as we have seen in the previous section. The only way one is able to obtain smaller widths for the allowed transitions is by assuming a large anomalous magnetic moment for the charmed quark. However, this does not seem to be reasonable. We will have to wait for the discovery of the $b\bar{b}$ pseudoscalars and their electromagnetic transitions to enliven this sector.

From Table 5.5 can be seen that the non-relativistic models (*a*, *b*, *e*, and our model) give transition rates for $\psi' \rightarrow \chi_c^J + \gamma$ that are approximately a factor two too large compared to experiment. The model of McClary and Byer with relativistic corrections gives better results and the results of the relativized quark model of Godfrey and Isgur agrees very well with experiment. This is an indication that relativistic corrections have a fairly large influence on the wave functions in charmonium. Note that in most models the width for $\psi' \rightarrow \chi_c^0 + \gamma$ differs most from the experimental value, but in our model, however, it is closest of the triplet states. This is due to the fact that the coupled-channel reduction is largest for transitions involving scalars.

Looking at the transition $\chi_c^J \rightarrow J/\psi + \gamma$ one observes that the coupled-channel models (Eichten's and ours) and those with relativistic corrections (McClary's and Godfrey and Isgurs') yield the right widths.

Let us look at Table 5.6 for the electric transitions in bottomonium. The theoretical values are approximately the same for all models and agree well with experiment, except those of Godfrey and Isgur, which are too small. Our results are closest to experiment and I presume that this is due to the influence of the coupled channels. Moreover, our results include finite-size corrections, but it is clear that this effect is far less important than in the case of charmonium. There is a difference for the transition $\chi_b^{J(')} \rightarrow \Upsilon^{(')} + \gamma$, where our results are smaller than those of the other

models. Unfortunately, no experimental results exist yet for these transitions.

What can be concluded from this comparison between the various models? For charmonium there is certainly need for relativistic corrections to the wave functions in order to bring theory and experiment in agreement as far as the radiative transitions are concerned. For bottomonium this is not the case: relativistic corrections are very small. Moreover, the finite-size corrections are smaller, so here the dipole approximation is justified, as opposed to charmonium. Coupled-channel effects change the theoretical predictions in the right direction both for charmonium and bottomonium.

	transition	ccr[a]	fsc[b]
$c\bar{c}$:	$J/\psi \to \eta_c\gamma$	33	1
	$\psi' \to \eta_c'\gamma$	19	1
	$\psi' \to \chi_c^0\gamma$	40	30
	$\psi' \to \chi_c^1\gamma$	15	11
	$\psi' \to \chi_c^2\gamma$	23	1
	$\chi_c^0 \to J/\psi\gamma$	56	44
	$\chi_c^1 \to J/\psi\gamma$	9	41
	$\chi_c^2 \to J/\psi\gamma$	40	32
$b\bar{b}$:	$\Upsilon' \to \chi_b^0\gamma$	3	6
	$\Upsilon' \to \chi_b^1\gamma$	20	4
	$\Upsilon' \to \chi_b^2\gamma$	3	0
	$\chi_b^0 \to \Upsilon\gamma$	-6	19
	$\chi_b^1 \to \Upsilon\gamma$	38	20
	$\chi_b^2 \to \Upsilon\gamma$	-5	9
	$\Upsilon'' \to \chi_b^{0'}\gamma$	6	5
	$\Upsilon'' \to \chi_b^{1'}\gamma$	14	3
	$\Upsilon'' \to \chi_b^{2'}\gamma$	6	0
	$\chi_b^{0'} \to \Upsilon'\gamma$	19	18
	$\chi_b^{1'} \to \Upsilon'\gamma$	6	17
	$\chi_b^{2'} \to \Upsilon'\gamma$	16	15

[a] coupled-channel reduction: $\left(1 - \frac{\text{full model}}{\text{1 channel}}\right) \times 100\%$

[b] finite-size corrections: $\left(1 - \frac{\text{full model}}{\text{l.w.a.}}\right) \times 100\%$

Table 5.3: Analysis of the radiative widths in Table 5.1.

particle	part of wave function in $q\bar{q}$-channel (%)	particle	part of wave function in $q\bar{q}$-channel (%)
J/ψ, η_c	90	Υ	93
ψ', η_c'	95	Υ', Υ''	97
χ_c^0	89	$\chi_b^{0,1,2}$	97,97,97
χ_c^1	93	$\chi_b^{0,1,2,}$	97,97,98
χ_c^2	95		

Table 5.4: Ratio of the quark anti-quark channel wave function and the total multi-channel wave function.

	width (keV)						
transition	Eichten[a]	MR[b]	MB[c]	GI[d]	GRR[e]	this work	experiment
$\psi' \to \chi_c^0\gamma$	43.2 (50.0)	37	19	19.6	62.0	31.7 (52.9)	22.6 ± 4.4
$\psi' \to \chi_c^1\gamma$	34.4 (45.3)	48	31	22.5	50.5	49.8 (58.7)	21.1 ± 4.2
$\psi' \to \chi_c^2\gamma$	23.7 (28.9)	41	27	19.6	32.0	38.5 (49.7)	19.0 ± 3.9
$\chi_c^0 \to J/\psi\gamma$	130 (141)	226	128	90	212.5	51.7 (118)	95 ± 46
$\chi_c^1 \to J/\psi\gamma$	257 (289)	460	270	194	468.1	210 (232)	< 355
$\chi_c^2 \to J/\psi\gamma$	350 (398)	609	347	250	652.7	228 (380)	351^{+165}_{-125}

[a] Eichten *et al.* [Eic80]
[b] Moxhay & Rosner [Mox83]
[c] McClary & Byers [McC83]
[d] Godfrey & Isgur [God85]
[e] Gupta, Radford & Repko [Gup86]
The values in parentheses are the one-channel results for the multi-channel models.

Table 5.5: Comparison between the various models for charmonium.

	width (keV)						
transition	MR[a]	GI[b]	GRR[c]	KR[d]	Ful[e]	this work	experiment
$\Upsilon' \to \chi_b^0\gamma$	1.0	0.63	0.94	1.39	1.38	1.59 (1.64)	1.89 ± 0.59
$\Upsilon' \to \chi_b^1\gamma$	2.1	1.44	1.59	2.18	2.17	2.14 (2.66)	2.95 ± 0.72
$\Upsilon' \to \chi_b^2\gamma$	2.2	1.60	1.71	2.14	2.13	2.64 (2.73)	2.90 ± 0.71
$\chi_b^0 \to \Upsilon\gamma$	31	25.6	33.3	26.1	30.8	20.9 (19.8)	
$\chi_b^1 \to \Upsilon\gamma$	36	28.9	39.8	32.8	38.6	15.8 (25.4)	
$\chi_b^2 \to \Upsilon\gamma$	38	32.4	44.4	37.8	44.5	33.2 (31.7)	
$\Upsilon'' \to \chi_b^{0'}\gamma$	1.4	0.90	1.47	1.65	1.35	1.59 (1.69)	1.25 ± 0.46
$\Upsilon'' \to \chi_b^{1'}\gamma$	2.8	1.85	2.49	2.52	2.36	2.59 (3.02)	3.12 ± 1.06
$\Upsilon'' \to \chi_b^{2'}\gamma$	2.7	1.94	2.68	2.78	2.53	3.10 (3.30)	3.38 ± 1.10
$\chi_b^{0'} \to \Upsilon'\gamma$	12	10.0	14.2	11.3	13.0	5.45 (6.70)	
$\chi_b^{1'} \to \Upsilon'\gamma$	14	21.1	18.8	15.9	17.0	8.14 (8.63)	
$\chi_b^{2'} \to \Upsilon'\gamma$	16	14.4	22.2	18.7	20.1	8.53 (10.2)	

[a] Moxhay & Rosner [Mox83]
[b] Godfrey & Isgur [God85]
[c] Gupta, Radford & Repko [Gup86]
[d] Kwong & Rosner [Kwo88]
[e] Fulcher [Ful89]
The values of our work are the multi-channel results with in parentheses the one-channel results.

Table 5.6: Comparison between the various models for bottomonium.

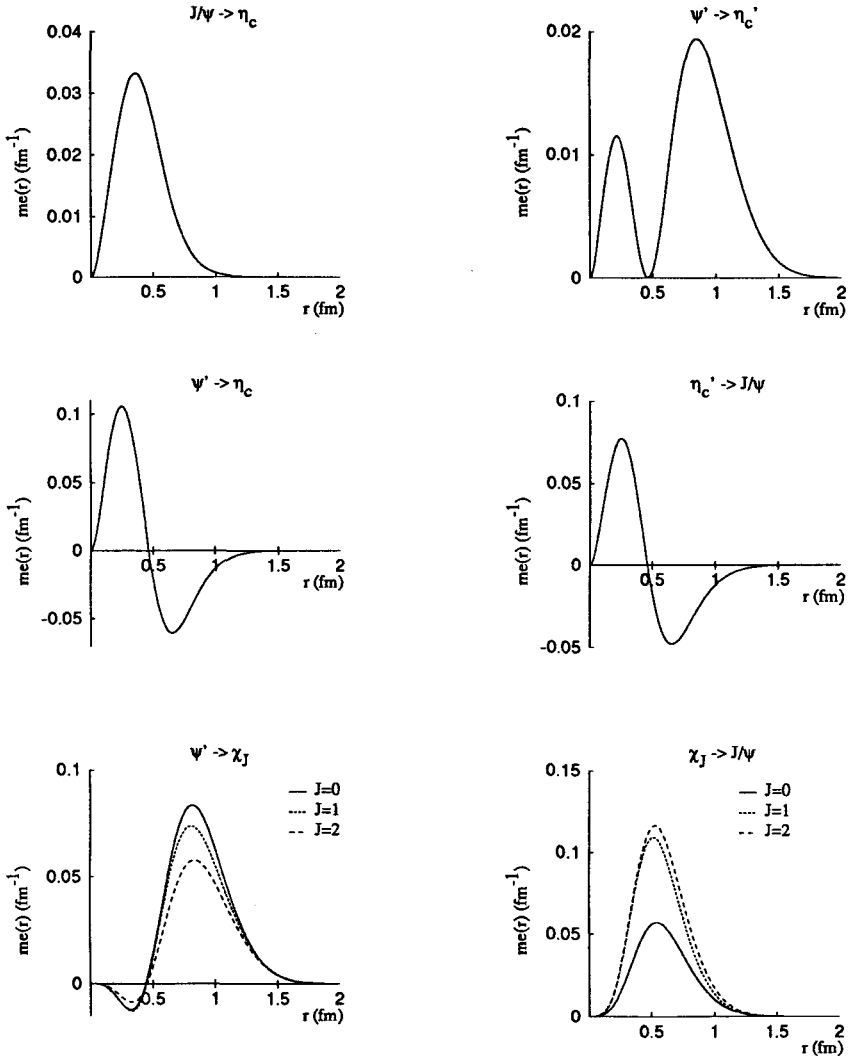

Figure 5.1: Integrands of matrix elements of radiative transitions in charmonium.

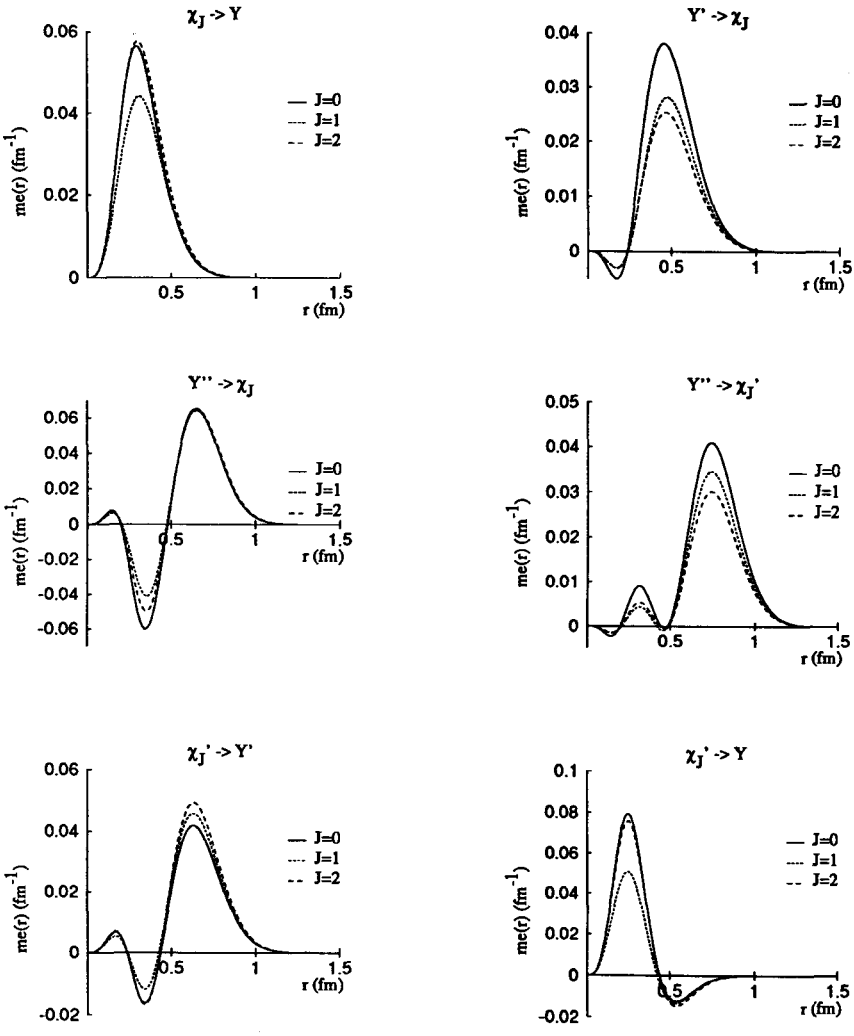

Figure 5.2: Integrands of matrix elements of radiative transitions in bottomonium.

Chapter 6

Conclusions

This final chapter states some conclusions that can be drawn from the work presented in the previous chapters. Furthermore, some thoughts concerning the future of the Unitarized Meson model are ventilated.

6.1 Findings

This section has two main parts: one deals with the spectra of charmonium and bottomonium and the information that can be extracted thereof. The other part deals with properties of quarkonium related to the wave function, such as leptonic and radiative widths.

The large number of potential models currently available to describe the charmonium and bottomonium spectra indicates that fitting a potential to the spectra is not very hard, provided one is satisfied with an accuracy of approximately 20 MeV, say. This holds for our model too as can be seen from Table 3.6. Note that the results for bottomonium are somewhat better than those for charmonium, especially for the P states. This is what was to be expected since our model is non-relativistic and relativistic corrections are more important in charmonium than in bottomonium. An important remark at this point is that—apart from the mass dependence of the harmonic-oscillator potential and the different values for the running coupling constant—our model describes both spectra[1] with one set of parameters. Most simple potential models are unable to do a fit with only one set and thereby in fact introduce a flavour-dependent potential, a feature for which our model is often criticized. Besides, the question is what such a fit is worth in case of a single-channel

[1] And even the spectra of the low lying mesons (refer to [Bev86a]).

model, because the coupling of the quark-antiquark channel to two-meson decay channels causes an appreciable shift in the mass of the $q\bar{q}$ bound state.

The reason why so many models give comparable results for the heavy quarkonia is the fact that their potentials are nearly the same in the region where these states reside (see also Fig. 1.6). And this phenomenon, in turn, is caused by the freedom one has to choose the parameters of the model (varying from one to about a dozen). The effects of all kinds of physical processes can be simulated by adjusting the parameters of the *effective potential* and by using the specific properties of the Schrödinger formalism (*e.g.* refer to Section 1.5.4 where was shown that the omission of a Coulomb term in the potential simulates a relativistic treatment for light quarks).

One of the effects that seems to be compensated by a specific choice of the parameters is the influence of hadronic decay. Although the mass shifts due to this unitarization effect are not the same for different particles—and much larger (up to several hundred MeV) than the accuracy of most models (about 20 MeV)—it proves to be possible to obtain a good fit to the data for a single-channel model. Apparently, the quarkonia spectra do not put enough constraints on the potential in order to determine it in a unique way, or to even give some indications about which ingredients are necessary and which are not. Therefore, a χ^2-fit for various single-channel potentials as was done in [Lic90] yields no relevant information.

How about the leptonic and radiative widths? Do these quantities put further constraints on the potential? The leptonic widths probe the wave function at the origin, whereas the radiative widths yield information on the full wave function. As far as the former are concerned, the incorporation of a colour-Coulomb interaction must have an important effect, both on the absolute value as on the ratio of the widths. In Table 6.1 the results without ([Rup82]) and with ([Met90], Chapter 3) a Coulomb term are given for the Unitarized Meson model. This table shows us that on one hand the absolute values of the widths have improved, but on the other hand the ratios have become worse. This is a consequence of the introduction of a Coulomb term in our model. Perhaps a new fit will improve this result somewhat, but I think we will have to live with it.

The leptonic widths are very sensitive to the precise form of the wave function. For example, a small change in the position of a node in the wave function may cause a large change of the overlap integral involving this wave function and hence in the leptonic width. Apart from the conclusion that the long-wavelength approximation is not a good approximation in the case of charmonium, it was shown in Chapter 5 that relativistic corrections are important in charmonium: only (pseudo) relativistic models are able to describe the E1 transitions in charmonium in agreement with

Γ (keV)	Rup82	Met90	experiment
J/ψ	1.83	5.45	4.72 $\pm$ 0.35
ψ'	0.88	3.35	2.15 $\pm$ 0.21
$\Gamma(2S)/\Gamma(1S)$	0.48	0.61	0.46 $\pm$ 0.06
Υ	0.28	1.62	1.34 $\pm$ 0.05
Υ'	0.16	1.14	0.60 $\pm$ 0.04
$\Gamma(2S)/\Gamma(1S)$	0.57	0.70	0.45 $\pm$ 0.03

Table 6.1: Leptonic widths in the Unitarized Meson model.

experiment. Other models are about a factor two higher than experiment. These relativistic corrections prove to be less important for bottomonium. Also, finite-size corrections are smaller as well as the influence of hadronic decay. Nevertheless, the fact that our model gives the best results for the experimentally known transitions in bottomonium is an indication for the correctness of our approach.

In my opinion most potential models give too much attention to the spectra of quarkonium, hoping to justify their specific choice of the potential. The calculation of radiative and leptonic widths provides another handle to confront these models with the—unfortunately sparse—data in order to learn more about the interquark interaction. To this end, also, new experimental data are urgently needed.

6.2 Future of the Unitarized Meson model

Now a colour-Coulomb interaction has been incorporated into the Unitarized Meson model and radiative transitions in heavy quarkonium have been calculated, the question arises in what direction future research should go. The most obvious way to proceed is to perform a new fit for both the light and heavy quark sector. (Remember that our model is already able to describe the light mesons [Bev86a]. It will be interesting, though, to see what influences the Coulomb term has on the old results; because the Coulomb interaction is strongly screened in our model and because light mesons lie farther away from the origin, the influence is expected to be smaller than for the heavy quarkonium states.) Perhaps a new set of parameters will improve the (ratio of) the leptonic widths. Also, the radiative transitions could be calculated for the light quark sector, where more experimental data are available.

When our model gives a satisfactory description of the light mesons, a connection

to popular subjects in this field could be made, such as $qq\bar{q}\bar{q}$-states, or $K\bar{K}$ molecules [Wei90].

In the—probably not so near—future our model could be applied to toponium, unless weak decay of the top quark ($t \to bW$) proceeds too fast to detect $t\bar{t}$ bound states. LEP will presumably be unable to find the top quark, but maybe LEP200 or the SSC (about to be built now) will.

Another obvious extension of our model is the inclusion of D states and the mixing of S and D states. Interesting will be the radiative transitions involving D states; these may be calculated using the formalism (and formulas) given in Chapter 4. These D-wave levels have not yet been discovered in bottomonium, but might be seen in near future experiments.

Quite a different line along which future research could proceed is to concentrate on the improvement of the model itself. Essential is our choice for the transition potential. A thorough investigation of the quark-pair-creation mechanism (with direct links to QCD calculations) might yield a better expression. Also, the phenomenological suppression of high thresholds might be substituted by a more fundamental mechanism.

As we saw in Chapter 5 there is a need for relativistic corrections in charmonium. This can be an interesting subject too.

Another possibility is to extend the formalism developed for the electromagnetic interactions. The addition of off-diagonal terms in the interaction Hamiltonian will enable us to describe processes like $M'M^* \to M'M\gamma$.

One of the problems one will encounter when one wants to improve essential features of the model (like the transition potential), is the complexity of the computer program. Moreover, the experts that know the ins and outs of the program have left the department and are difficult to reach and/or have lost their interest. So the computer program may be regarded as a black box and the number of changes that is easy to perform is very limited—probably only the D states and the extension for the radiative transitions. Major changes will require the program to be rewritten and this is—to my mind—too much for one person to do in the time available for PhD research. So I advise that a future research program will be very carefully thought over.

Appendix A

The vector potential

The vector potential in quantized form reads (see for example [Sak67], page 29)

$$\boldsymbol{A}(x) = \sqrt{4\pi}\hbar c \sum_{\lambda} \int \frac{d^3k}{(2\pi)^3} \frac{1}{2E} \left(e^{-ik\cdot x} \boldsymbol{\epsilon}_\lambda a^\lambda(\boldsymbol{k}) + h.c. \right) , \tag{A.1}$$

(where $E = \hbar\omega = \hbar ck$) with $\boldsymbol{\epsilon}_\lambda$ a polarization vector describing a certain helicity state and the operator a^λ satisfying

$$\left[a^\lambda(\boldsymbol{k}), a^{\lambda'\dagger}(\boldsymbol{k}') \right] = (2\pi)^3 2E \delta^{(3)}(\boldsymbol{k} - \boldsymbol{k}') \delta_{\lambda\lambda'} . \tag{A.2}$$

Using the Bauer expansion we rewrite equation (A.1)

$$\boldsymbol{A}(\boldsymbol{r}, t) = \frac{\sqrt{4\pi}\hbar c}{\pi} \sum_{\lambda,l,m} \int dk \sqrt{\frac{k}{2\hbar c}} \left(j_l(kr) Y_m^l(\hat{\boldsymbol{r}}) e^{-i\omega t} \boldsymbol{\epsilon}^\lambda a_{lm}^\lambda(k) + h.c. \right) , \tag{A.3}$$

where we defined the angle-independent operator $a_{lm}^\lambda(k)$ by

$$a_{lm}^\lambda(k) = \frac{1}{2\pi} \sqrt{\frac{k}{2\hbar c}} \int d\Omega_k i^l Y_m^{l*}(\hat{\boldsymbol{k}}) a^\lambda(\boldsymbol{k}) \tag{A.4}$$

satisfying

$$\left[a_{lm}^\lambda(k), a_{lm}^{\lambda'\dagger}(k') \right] = 2\pi\delta(k - k') \delta_{ll'} \delta_{mm'} \delta_{\lambda\lambda'} . \tag{A.5}$$

Transform the $(l, m) \otimes (1, \lambda)$ basis into a $(L, 1, J, M)$ basis using the vector spherical harmonics:

$$\sum_{\lambda,l,m} Y_m^l(\hat{\boldsymbol{r}}) \boldsymbol{\epsilon}_\lambda a_{lm}^\lambda(k) \rightarrow \sum_{J,L,M} \boldsymbol{Y}_{LM}^J(\hat{\boldsymbol{r}}) a_{LM}^J(k) , \tag{A.6}$$

where for the $a_{LM}^J(k)$ operators an analogue of equation (A.5) holds. Because we want our vector potential to satisfy $\boldsymbol{\nabla} \cdot \boldsymbol{A} = 0$, we make another transformation

with only the transverse combinations of the in Section 4.2 defined $\boldsymbol{f}$'s:

$$\sum_{J,L,M} 2kj_l(kr)\boldsymbol{Y}^J_{LM}(\hat{\boldsymbol{r}})a^J_{LM}(k) \rightarrow \sum_{L,M,i} \boldsymbol{f}^{(i)}_{kLM}(\boldsymbol{r})a^{(i)}_{LM}(k) \ , \tag{A.7}$$

with $i \in \{e, m\}$ and the multipole operators $a^{(i)}_{LM}(k)$ satisfying

$$\left[a^{(i)}_{LM}(k), a^{(i')\dagger}_{L'M'}(k')\right] = 2\pi\delta(k-k')\delta_{LL'}\delta_{MM'}\delta_{ii'} \ . \tag{A.8}$$

Finally we arrive at the desired expression for the vector potential

$$\boldsymbol{A}(\boldsymbol{r},t) = \sqrt{4\pi}\hbar c \sum_{l,m,i} \int \frac{dk}{2\pi}\sqrt{\frac{1}{2\hbar\omega}} \left(\boldsymbol{f}^{(i)}_{klm}(\boldsymbol{r})a^{(i)}_{lm}(k)e^{-i\omega t} + h.c.\right) \ . \tag{A.9}$$

Appendix B

The calculation of the matrix elements

Let us look at the form of the operators $H^{(i)}_{j,lm}$ ($i \in \{e,m\}$, $j \in \{o,s\}$). Essentially they can be written as

$$H^{(e)}_{o,lm} \sim \left[\sum_i q_i \nabla_i f(r_i) + \boldsymbol{r}_i g(r_i)\right] Y^l_{-m}(\hat{\boldsymbol{r}}) \cdot \nabla \tag{B.1}$$

$$H^{(m)}_{o,lm} \sim h(r) \boldsymbol{L} Y^l_{-m}(\hat{\boldsymbol{r}}) \cdot \nabla \tag{B.2}$$

$$H^{(e)}_{s,lm} \sim (p(r)\boldsymbol{S}_1 + q(r)\boldsymbol{S}_2) \cdot \boldsymbol{L} Y^l_{-m}(\hat{\boldsymbol{r}}) \tag{B.3}$$

$$H^{(m)}_{s,lm} \sim \left[\sum_i q_i \nabla_i f(r_i) + \boldsymbol{r}_i g(r_i)\right] \cdot \boldsymbol{S}_i Y^l_{-m}(\hat{\boldsymbol{r}}) \tag{B.4}$$

In the evaluation of (B.1), we use a consequence of the gauge invariance of the Hamiltonian [Sac51]: if the vector potential is a function of the gradient of an arbitrary scalar function $S(\boldsymbol{r})$, so

$$H_{int} = H_{int}(\varphi_\lambda, \nabla S) \,, \tag{B.5}$$

where φ_λ denotes the set of internal variables of H_{int}, and if we define

$$\Lambda = \frac{i}{\hbar c} \sum_i q_i S(\boldsymbol{r}_i) \,, \tag{B.6}$$

then the Hamiltonian is gauge invariant if

$$H_{int}(\varphi_\lambda, \nabla S) = e^{\Lambda} H_{int}(\varphi_\lambda) e^{-\Lambda} \,. \tag{B.7}$$

Assuming that we can expand the left-hand side in a power series of the coupling constant, and expanding the right-hand side in terms of commutators of Λ with H_0,

we see that the term linear in the vector potential equals

$$H_{int}(\varphi_\lambda, \nabla S) = [\Lambda, H_0] \ . \tag{B.8}$$

This means that the matrix element of an interaction Hamiltonian

$$H_{int} = -\frac{1}{\mu c}\boldsymbol{p} \cdot \sum_i q_i \nabla S(r_i)$$

becomes

$$\langle f | H_{int} | i \rangle = \hbar\omega \langle f | \Lambda | i \rangle \ , \tag{B.9}$$

where $\hbar\omega = E_i - E_f$.

The same result can be derived following a different approach, *viz.* via the Schrödinger equation [Bri62]:

$$\left[-\frac{\hbar^2}{2\mu}\nabla^2 + H_{int} - E_i\right] |i\rangle = 0 \tag{B.10}$$

with

$$H_{int} = -\frac{q}{2\mu c}(\boldsymbol{p} \cdot \nabla S + \nabla S \cdot \boldsymbol{p}) \ .$$

(In our case $H_{int} = -\frac{q}{\mu c}(\nabla S \cdot \boldsymbol{p} + \boldsymbol{A}' \cdot \boldsymbol{p})$, because $[\boldsymbol{p}, \boldsymbol{A}] = 0$.)
The matrix element becomes

$$\begin{aligned}
\langle f | H_{int} | i \rangle &= \frac{iq\hbar}{2\mu c}\{\langle f | \nabla S \cdot \nabla | i \rangle + \langle f | \nabla \cdot \nabla S | i \rangle\} \\
&= \frac{iq\hbar}{2\mu c}\{\langle f | \nabla S \cdot \nabla | i \rangle - \langle i | \nabla S \cdot \nabla | f \rangle^*\} \\
&= \frac{iq\hbar}{2\mu c}\left\{-\langle f \left| S\nabla^2 \right| i \rangle + \langle i \left| S\nabla^2 \right| f \rangle^*\right\} \\
&= \frac{iq\hbar}{2\mu c}(E_i - E_f)\frac{2\mu}{\hbar^2}\langle f | S | i \rangle \\
&= \frac{iq}{\hbar c}\hbar\omega \langle f | S | i \rangle \\
&= \hbar\omega \langle f | \Lambda | i \rangle \ .
\end{aligned} \tag{B.11}$$

Relation (B.9) is known as Siegert's theorem [Sie37], which states that the electric multipole emission operator is $\hbar\omega\Lambda$, independent of the nature of the interaction. This theorem is valid only in the long-wavelength approximation (see Appendix C), because then the expression for the vector potential (see equation (4.39)),

$$\boldsymbol{A} = \nabla S + \boldsymbol{A}'$$

reduces to $\boldsymbol{A} = \boldsymbol{\nabla} S$. In our case we will use this Siegert's theorem, but we will also account for the contribution due to $\boldsymbol{A}'$ and thus end up with a different expression for the electric multipole operator. For a discussion on Siegert's theorem see the clarifying paper of Mosconi and Ricci [Mos87].

Our expression for (B.1) has changed into

$$H^{(e)}_{o,lm} \sim \Lambda Y^l_{-m}(\hat{\boldsymbol{r}}) + g(r) Y^l_{-m}(\hat{\boldsymbol{r}})\, \boldsymbol{r} \cdot \boldsymbol{\nabla} \,. \tag{B.12}$$

The calculation of the matrix element is now straightforward. We will need the reduced matrix element $\langle L' \left\| Y^l \right\| L \rangle$, which is listed at the end of this Appendix.

For the calculation of the matrix elements of $H^{(m)}_{o,lm}$ and $H^{(e)}_{s,lm}$ we will use the following formula (this formula and others can be found in Ref. [Bri62]):

$$L_\mu Y^l_{-m}(\hat{\boldsymbol{r}}) = \sqrt{l(l+1)}\, C^{\,l\ \ 1\ \ l}_{-m\ \ \mu\ -m+\mu}\, Y^l_{-m+\mu}(\hat{\boldsymbol{r}}) \,. \tag{B.13}$$

So we end up with an expression for the matrix element of a tensor composed of two irreducible tensors. If

$$T^k_q = \sum_{q_1,q_2} C^{\,k_1\ \ k_2\ \ k}_{q_1\ \ q_2\ \ q}\, T^{k_1}_{q_1} T^{k_2}_{q_2} \,, \tag{B.14}$$

where $T^{k_1}_{q_1}$, $T^{k_2}_{q_2}$ are irreducible tensors of rank k_1, k_2 respectively, with respect to $\boldsymbol{L}$ or $\boldsymbol{S}$, then

$$\langle J'L'S'M' | T^k_q | JLSM \rangle = \frac{1}{\sqrt{2J'+1}} C^{\,J\ \ k\ \ J'}_{M\ \ q\ \ M'}\, \langle J'L'S' \| T^k \| JLS \rangle \tag{B.15}$$

according to the Wigner-Eckart theorem. The so called reduced matrix element can be evaluated as follows

$$\langle J'L'S' \| T^k_q \| JLS \rangle = \sqrt{(2J+1)(2k+1)(2J'+1)} \begin{bmatrix} L & k_1 & L' \\ S & k_2 & S' \\ J & k & J' \end{bmatrix} \langle L' \| T^{k_1} \| L \rangle \langle S' \| T^{k_2} \| S \rangle \tag{B.16}$$

if $T^{k_1}_{q_1}$, $T^{k_2}_{q_2}$ is irreducible with respect to $\boldsymbol{L}$ and $\boldsymbol{S}$ respectively. We will need this expression for $H^{(e)}_{s,lm}$ ($T^{k_1} \to Y^l$, $T^{k_2} \to S_i$).

$$\langle J'L'S' \| T^k_q \| JLS \rangle = \sum_{L''} (-1)^{J+S+L'} \delta_{SS'} \sqrt{(2J+1)(2k+1)(2J'+1)} \cdot \begin{bmatrix} L' & L & k \\ J & J' & S \end{bmatrix} \begin{bmatrix} L & L' & k \\ k_1 & k_2 & L'' \end{bmatrix} \langle L' \| T^{k_1} \| L'' \rangle \langle L'' \| T^{k_2} \| L \rangle \tag{B.17}$$

if $T^{k_1}_{q_1}$ and $T^{k_2}_{q_2}$ are both irreducible with respect to $\boldsymbol{L}$. We will need this expression for $H^{(m)}_{o,lm}$ ($T^{k_1} \to Y^l$, $T^{k_2} \to \nabla$). Here

$$\begin{bmatrix} a & b & c \\ d & e & f \\ g & h & i \end{bmatrix}$$

denotes the Wigner $9-J$ symbol and

$$\begin{bmatrix} a & b & e \\ d & c & f \end{bmatrix}$$

the Wigner $6-J$ symbol.

For the calculation of $H^{(m)}_{s,lm}$ we will need the following formula

$$\begin{aligned} \partial_\mu \left(1 + r\frac{\partial}{\partial r}\right) j_l(kr) Y^l_{-m}(\hat{\boldsymbol{r}}) = \\ \left(klj_{l+1}(kr) - k^2 r j_l(kr)\right) C^{\ l\ \ 1\ \ l+1}_{-m\ \ \mu\ -m+\mu} \sqrt{\frac{l+1}{2l+3}} Y^{l+1}_{-m+\mu}(\hat{\boldsymbol{r}}) - \\ \left(k(l+1)j_{l-1}(kr) - k^2 r j_l(kr)\right) C^{\ l\ \ 1\ \ l-1}_{-m\ \ \mu\ -m+\mu} \sqrt{\frac{l}{2l-1}} Y^{l-1}_{-m+\mu}(\hat{\boldsymbol{r}}) . \end{aligned} \tag{B.18}$$

Now we can apply formula (B.16) again.

The reduced matrix elements that we need are listed below.

$$\langle L' \| Y^l \| L \rangle = (-1)^{L'} \sqrt{\frac{(2L+1)(2l+1)(2L'+1)}{4\pi}} \begin{pmatrix} L & l & L' \\ 0 & 0 & 0 \end{pmatrix} \tag{B.19}$$

$$\langle L' \| \nabla \| L \rangle = \delta_{L',L+1} \sqrt{L+1} \left(\frac{\partial}{\partial r} - \frac{L}{r}\right) - \delta_{L',L-1} \sqrt{L} \left(\frac{\partial}{\partial r} + \frac{L+1}{r}\right) \tag{B.20}$$

$$\begin{aligned} \langle S' \| S_i \| S \rangle = \sqrt{(2S+1)(2S'+1)} (-1)^{S_1+S_2+1} \langle S_i \| S_i \| S_i \rangle \\ \cdot \begin{cases} (-1)^S \begin{bmatrix} S & 1 & S' \\ S_1 & S_2 & S_1 \end{bmatrix} (i=1) \\ (-1)^{S'} \begin{bmatrix} S & 1 & S' \\ S_2 & S_1 & S_2 \end{bmatrix} (i=2) \end{cases} \end{aligned} \tag{B.21}$$

$$\langle S_i \| S_i \| S_i \rangle = \sqrt{S_i(S_i+1)(2S_i+1)} \quad (i=1,2) . \tag{B.22}$$

Here $\begin{pmatrix} j_1 & j_2 & j_3 \\ m_1 & m_2 & -m_3 \end{pmatrix} = (-1)^{j_1-j_2+m_3}(2j_3+1)^{-1/2} C^{\ j_1\ \ j_2\ \ j_3}_{m_1\ \ m_2\ \ m_3}$ is the Wigner $3-J$ symbol.

Appendix C

The multi-channel transition coefficients and operators

In this section we will give expressions for the coefficients which follow from the evaluation of the various 3-J, 6-J, and 9-J symbols in the formulas for the decay widths (equations (4.54) and (4.58)). Furthermore will we define r-dependent operators which are going to be sandwiched between the wave functions and then integrated.

Let's start with the electric-dipole matrix elements. It proves to be convenient to define the diagonal 9x9-matrices $E^{(1)}(r)$ and $E^{(2)}(r)$ by

$$E_{ij}^{(k)} = E_i^{(k)} \delta_{ij} \ , \tag{C.1}$$

where

$$E_i^{(1)} = \begin{cases} 2\left((1+r\frac{\partial}{\partial r})j_1(\frac{1}{2}kr) + \frac{\hbar\omega}{2m_q c^2} j_1(\frac{1}{2}kr) r\frac{\partial}{\partial r}\right) & , \ i=1 \\ 2\left((1+r\frac{\partial}{\partial r})j_1(\frac{1}{2}kr) + \frac{\hbar\omega}{2m_M c^2} j_1(\frac{1}{2}kr) r\frac{\partial}{\partial r}\right) & , \ i=2 \\ (1+r\frac{\partial}{\partial r})\left(j_1(\frac{\mu_{M^*M}}{m_{M^*}}kr) + j_1(\frac{\mu_{M^*M}}{m_M}kr)\right) + & \\ \left(\frac{\hbar\omega\mu_{M^*M}}{m_{M^*}^2 c^2} j_1(\frac{\mu_{M^*M}}{m_{M^*}}kr) + \frac{\hbar\omega\mu_{M^*M}}{m_M^2 c^2} j_1(\frac{\mu_{M^*M}}{m_M}kr)\right) r\frac{\partial}{\partial r} & , \ i=3 \\ 2\left((1+r\frac{\partial}{\partial r})j_1(\frac{1}{2}kr) + \frac{\hbar\omega}{2m_{M^*} c^2} j_1(\frac{1}{2}kr) r\frac{\partial}{\partial r}\right) & , \ i=4,5 \\ 2\left((1+r\frac{\partial}{\partial r})j_1(\frac{1}{2}kr) + \frac{\hbar\omega}{2m_{M_s} c^2} j_1(\frac{1}{2}kr) r\frac{\partial}{\partial r}\right) & , \ i=6 \\ (1+r\frac{\partial}{\partial r})\left(j_1(\frac{\mu_{M_s^*M_s}}{m_{M_s^*}}kr) + j_1(\frac{\mu_{M_s^*M_s}}{m_{M_s}}kr)\right) + & \\ \left(\frac{\hbar\omega\mu_{M_s^*M_s}}{m_{M_s^*}^2 c^2} j_1(\frac{\mu_{M_s^*M_s}}{m_{M_s^*}}kr) + \frac{\hbar\omega\mu_{M_s^*M_s}}{m_{M_s}^2 c^2} j_1(\frac{\mu_{M_s^*M_s}}{m_{M_s}}kr)\right) r\frac{\partial}{\partial r} & , \ i=7 \\ 2\left((1+r\frac{\partial}{\partial r})j_1(\frac{1}{2}kr) + \frac{\hbar\omega}{2m_{M_s^*} c^2} j_1(\frac{1}{2}kr) r\frac{\partial}{\partial r}\right) & , \ i=8,9 \end{cases}$$

(C.2)

and

$$E_i^{(2)} = \begin{cases} 2g_q \frac{\hbar\omega}{m_q c^2} j_1(\frac{1}{2}kr) & , i=1 \\ 0 & , i=2 \\ g_{M^*} \frac{\hbar\omega}{m_{M^*}c^2} j_1(\frac{\mu_{M^*M}}{m_{M^*}}kr) & , i=3 \\ 2g_{M^*} \frac{\hbar\omega}{m_{M^*}c^2} j_1(\frac{1}{2}kr) & , i=4,5 \\ 0 & , i=6 \\ g_{M_s^*} \frac{\hbar\omega}{m_{M_s^*}c^2} j_1(\frac{\mu_{M_s^*M_s}}{m_{M_s^*}}kr) & , i=7 \\ 2g_{M_s^*} \frac{\hbar\omega}{m_{M_s^*}c^2} j_1(\frac{1}{2}kr) & , i=8,9 \end{cases} \quad \text{(C.3)}$$

In equation (C.2) we wrote $(1+r\frac{\partial}{\partial r})j_1(\beta kr)$ as a shorthand notation for $\beta kr j_0(\beta kr) - j_1(\beta kr)$.

Next we define the coefficient matrices $P_J^{(1)}$ and $P_J^{(2)}$. Remember that the channels with a M or M^* meson get an extra factor $\frac{1}{2}$, unlike the channels with a M_s or M_s^* meson. As the quantum numbers L and S are the same for the strange and non-strange channels, it is clear that their coefficients are equal too (apart from the already mentioned factor $\frac{1}{2}$). So we can write

$$P_J^{(i)} = \begin{pmatrix} P^{(i)}_{(q\bar{q})J} & & & & & & & & \\ & \frac{1}{2}P^{(i)}_{(M\bar{M})J} & & & & & & & \\ & & \frac{1}{2}P^{(i)}_{(M^*\bar{M})J} & & & & & & \\ & & & \frac{1}{2}P^{(i)}_{(M^*\bar{M}^*)J} & & & & & \\ & & & & P^{(i)}_{(M\bar{M})J} & & & & \\ & & & & & P^{(i)}_{(M^*\bar{M})J} & & & \\ & & & & & & P^{(i)}_{(M^*\bar{M}^*)J} & & \end{pmatrix} \quad \text{(C.4)}$$

with the elements on the diagonal square matrices, with numerical values

$$\begin{aligned} P^{(1)}_{(q\bar{q})0} &= q \;, & P^{(2)}_{(q\bar{q})0} &= -q \\ P^{(1)}_{(q\bar{q})1} &= -q \;, & P^{(2)}_{(q\bar{q})1} &= \tfrac{1}{2}q \\ P^{(1)}_{(q\bar{q})2} &= q \;, & P^{(2)}_{(q\bar{q})2} &= \tfrac{1}{2}q \\ P^{(1)}_{(M^*\bar{M})0} &= 0 \;, & P^{(2)}_{(M^*\bar{M})0} &= 0 \\ P^{(1)}_{(M^*\bar{M})1} &= -1 \;, & P^{(2)}_{(M^*\bar{M})1} &= -1 \\ P^{(1)}_{(M^*\bar{M})2} &= 0 \;, & P^{(2)}_{(M^*\bar{M})2} &= 0 \end{aligned}$$

$$
\begin{array}{llll}
P^{(1)}_{(M\bar{M})0} = -\sqrt{3}\,, & P^{(2)}_{(M\bar{M})0} = 0 \\
P^{(1)}_{(M\bar{M})1} = 0\,, & P^{(2)}_{(M\bar{M})1} = 0 \\
P^{(1)}_{(M\bar{M})2} = 0\,, & P^{(2)}_{(M\bar{M})2} = 0 \\
\left[P^{(1)}_{(M^*\bar{M}^*)0}\right]_{ij} = -\sqrt{3}\,\delta_{i1}\delta_{j1}\,, & P^{(2)}_{(M^*\bar{M}^*)0} = \emptyset \\
P^{(1)}_{(M^*\bar{M}^*)1} = \emptyset\,, & P^{(2)}_{(M^*\bar{M}^*)1} = \emptyset \\
\left[P^{(1)}_{(M^*\bar{M}^*)2}\right]_{ij} = -\frac{1}{5}\sqrt{15}\,\delta_{i1}\delta_{j2}\,, & \left[P^{(2)}_{(M^*\bar{M}^*)2}\right]_{ij} = -\frac{3}{10}\sqrt{15}\,\delta_{i1}\delta_{j2}
\end{array}
\tag{C.5}
$$

The charge of the quark is denoted by q. Note that the entries in Table 4.2 indicated by an x, *i.e.* empty channels, can be found back in the coefficients above: if a $q\bar{q}$ state cannot decay into a certain meson channel, the transition coefficients are zero.

The magnetic-dipole transition coefficients and operators follow in a similar way. Define

$$
M^{(k)}_{ij} = M^{(k)}_i \delta_{ij}\,, \tag{C.6}
$$

where for $n = 1, 2$

$$
M^{(n)}_i = \begin{cases}
2g_q \frac{\hbar\omega}{m_q c^2} j_{2\delta_{n2}}(\frac{1}{2}kr) & , \; i = 1 \\
0 & , \; i = 2 \\
g_{M^*} \frac{\hbar\omega}{m_{M^*}c^2} j_{2\delta_{n2}}(\frac{\mu_{M^*M}}{m_{M^*}}kr) & , \; i = 3 \\
2g_{M^*} \frac{\hbar\omega}{m_{M^*}c^2} j_{2\delta_{n2}}(\frac{1}{2}kr) & , \; i = 4, 5 \\
0 & , \; i = 6 \\
g_{M_s^*} \frac{\hbar\omega}{m_{M_s^*}c^2} j_{2\delta_{n2}}(\frac{\mu_{M_s^*M_s}}{m_{M_s^*}}kr) & , \; i = 7 \\
2g_{M_s^*} \frac{\hbar\omega}{m_{M_s^*}c^2} j_{2\delta_{n2}}(\frac{1}{2}kr) & , \; i = 8, 9
\end{cases}
\tag{C.7}
$$

The index $2\delta_{n2}$ indicates an index 0 for $n = 1$ and 2 for $n = 2$. The coefficient matrices $Q^{(i)}$ have the same form as the $P^{(i)}$ matrices:

$$
Q^{(i)} = \begin{pmatrix}
Q^{(i)}_{(q\bar{q})} & & & & & & \\
& \frac{1}{2}Q^{(i)}_{(M\bar{M})} & & \emptyset & & & \\
& & \frac{1}{2}Q^{(i)}_{(M^*\bar{M})} & & & & \\
& & & \frac{1}{2}Q^{(i)}_{(M^*\bar{M}^*)} & & & \\
& \emptyset & & & Q^{(i)}_{(M\bar{M})} & & \\
& & & & & Q^{(i)}_{(M^*\bar{M})} & \\
& & & & & & Q^{(i)}_{(M^*\bar{M}^*)}
\end{pmatrix}
\tag{C.8}
$$

with the following numerical values

$$Q^{(1)}_{(q\bar{q})}=-q\ ,\ Q^{(1)}_{(M\bar{M})}=0\ ,\ Q^{(1)}_{(M^*\bar{M})}=\tfrac{2}{3}\sqrt{6}\ \ ,\ Q^{(1)}_{(M^*\bar{M}^*)}=\begin{pmatrix}\frac{2}{3}\sqrt{2} & -\frac{1}{3}\sqrt{10}\\ 0 & 0\end{pmatrix}$$
$$Q^{(2)}_{(q\bar{q})}=0\ \ ,\ Q^{(2)}_{(M\bar{M})}=0\ ,\ Q^{(2)}_{(M^*\bar{M})}=-\tfrac{1}{3}\sqrt{6}\ ,\ Q^{(2)}_{(M^*\bar{M}^*)}=\begin{pmatrix}\frac{2}{3}\sqrt{2} & -\frac{1}{3}\sqrt{10}\\ 0 & 0\end{pmatrix} \qquad \text{(C.9)}$$

The same remarks hold for the Q matrices as did for the P matrices.

Finally it is noted that the wave function $u(r)$ can be written in this formalism as

$$u(r)=\begin{pmatrix} u_{(q\bar{q})}(r)\\ u_{(M\bar{M})}(r)\\ u_{(M^*\bar{M})}(r)\\ u_{(M^*\bar{M}^*)_1}(r)\\ u_{(M^*\bar{M}^*)_2}(r)\\ u_{(M_s\bar{M}_s)}(r)\\ u_{(M_s^*\bar{M}_s)}(r)\\ u_{(M_s^*\bar{M}_s^*)_1}(r)\\ u_{(M_s^*\bar{M}_s^*)_2}(r)\end{pmatrix}\ . \qquad \text{(C.10)}$$

The long-wavelength approximation

Usually, when dealing with electromagnetic transitions, it is assumed that that the size of the bound state emitting the photon is small compared to the wavelength of the photon. Then the following assumption is valid: instead of expanding the exponent in $\boldsymbol{A} \sim \boldsymbol{\epsilon} e^{i\boldsymbol{k}\cdot\boldsymbol{r}}$ according to the Bauer formula (see Appendix A), the exponent is replaced by unity. This approximation is called the long-wavelength approximation (often denoted by $kr \ll 1$). Corrections to this approximation are called finite-size or retardation effects.

In our derivation of the transition amplitudes the long-wavelength approximation was not made. To understand the results of other authors on this subject, however, we will calculate the widths in this approximation too. The following adjustments have to be made:

- $E^{(1)} \to \frac{4}{3}\beta kr$ (or $\to \frac{2}{3}\beta_1 kr + \frac{2}{3}\beta_2 kr$ for channels 3 and 7)
- $E^{(2)} \to 0$
- $M^{(1)} \to 2g_q \frac{\hbar\omega}{m_q c^2}$

- $M^{(2)} \to 0$.

This leads to the more familiar (one-channel) expressions (see Ref. [Nov78]):

$$\Gamma^{(e)}(n^3S_1 \to m^3P_J + \gamma) = \frac{4}{27}(2J+1)\alpha\hbar c\, q^2 k^3 \langle r \rangle^2 \tag{C.11}$$

$$\Gamma^{(e)}(n^3P_J \to m^3S_1 + \gamma) = \frac{4}{9}\alpha\hbar c\, q^2 k^3 \langle r \rangle^2 \tag{C.12}$$

$$\Gamma^{(m)}(n^3S_1 \to m^1S_0 + \gamma) = \frac{4}{3}\alpha\hbar c \left(\frac{\hbar c g_q}{m_q c^2}\right)^2 q^2 k^3\, \delta_{nm} \tag{C.13}$$

$$\Gamma^{(m)}(n^1S_0 \to m^3S_1 + \gamma) = 4\alpha\hbar c \left(\frac{\hbar c g_q}{m_q c^2}\right)^2 q^2 k^3\, \delta_{nm} \tag{C.14}$$

The δ_{nm} factor appears if we assume that the triplet and singlet wave functions are orthonormal, *i.e.* the hyperfine interaction does not affect the wave functions (as is the case in our model, where we calculate these effects in perturbation theory).

References

[Abr65] M. Abramowitz and I.A. Stegun (eds.). *Handbook of mathematical functions.* Dover Publications, Inc. New York (1965).

[Aer75] A. Aerts. *Charm below the threshold.* Master's thesis Institute for Theoretical Physics, University of Nijmegen, The Netherlands, 1975 (unpublished).

[Bag86] C. Baglin et al. *Search for the $^1P_1$ charmonium state in $\bar{p}p$ annihilations at the CERN ISR.* Phys. Lett. **171B**, 135–141 (1986).

[Bat53] Bateman Manuscript Project, A. Erdélyi et al. (eds.). *Higher transcendental functions,* Volume 2. McGraw-Hill, New York (1953).

[Ber82] R.J.B. Berens. *Electromagnetic transitions of charmonium.* Master's thesis Institute for Theoretical Physics, University of Nijmegen, The Netherlands, 1982 (unpublished).

[Bev80] E. van Beveren, C. Dullemond, and G. Rupp. *Spectra and strong decays of $c\bar{c}$ and $b\bar{b}$ states.* Phys. Rev. **D21**, 772–778, (E) D22, 787 (1980).

[Bev83a] E. van Beveren. *Recoupling matrix elements and decay.* Zeit. Phys. **C17**, 135–140 (1983).

[Bev83b] E. van Beveren, G. Rupp, T.A. Rijken, and C. Dullemond. *Radial spectra and hadronic decay widths of light and heavy mesons.* Phys. Rev. **D27**, 1527–1543 (1983).

[Bev83c] E. van Beveren, C. Dullemond, and T.A. Rijken. *On the influence of hadronic decay on the properties of hadrons.* Zeit. Phys. **C19**, 275–281 (1983).

[Bev83d] E. van Beveren. *The influence of strong decay on the spectra of hadrons.* PhD thesis Institute for Theoretical Physics, University of Nijmegen, The Netherlands, 1983 (unpublished).

[Bev84a] E. van Beveren, T.A. Rijken, C. Dullemond, and G. Rupp. *Geometric quark confinement and hadronic resonances.* In S. Albeverio, L.S. Ferreira, and L. Streit, editors, *Resonances - Models and Phenomena* Lecture Notes in Physics 211, pages 331–346, Bielefeld (1984).

[Bev84b] E. van Beveren, C. Dullemond, and T.A. Rijken. *The Dirac equation and its solutions for quarks confined by an SO(3,2)-invariant geometry.* Phys. Rev. **D30**, 1103–1106 (1984).

[Bev84c] E. van Beveren. *Coupling constants and transition potentials for hadronic decay modes of a meson.* Zeit. Phys. **C21**, 291–297 (1984).

[Bev84d] E. van Beveren, T.A. Rijken, and C. Dullemond. *Geometric quark confinement.* In J. Tran Thanh Van, editor, *Proceedings of the XIX Rencontre de Moriond*, pages 847–855, Moriond (1984).

[Bev86a] E. van Beveren et al. *A low lying scalar meson nonet.* Zeit. Phys. **C30**, 615 (1986).

[Bev86b] E. van Beveren, T.A. Rijken, and C. Dullemond. *Dielectric description of hadrons with anti-de Sitter symmetry.* J. Math. Phys. **27**, 1411–1418 (1986).

[Bic89] P.J. de A. Bicudo and J.E.F.T. Ribeiro. *Current quark model in a $^3P_0$ condensed vacuum.* Report IFM-13,14,15/89 Centro de Física da Matéria Condensada, Lisbon (1989).

[Bor88] F. Bormans, H. Janssen, and C. Dullemond. *Perturbation theory in models with geometrical confinement.* Il Nuovo Cim. **102A**, 1267–1283 (1989).

[Bow87] T. Bowcock et al. *Study of $\pi^+\pi^-$ transitions from the $\Upsilon(3S)$.* Phys. Rev. Lett. **58**, 307–310 (1987).

[Bow88] K.C. Bowler et al. *Quenched hadron mass calculations using staggered fermions at $\beta = 6.15$ and 6.3.* Nucl. Phys. **B296**, 732–756 (1988).

[Bra87] D.D. Brayshaw. *Relativistic description of quarkonia.* Phys. Rev. **D36**, 1465–1478 (1987).

[Bri62] D.M. Brink and G.R. Satchler. *Angular Momentum.* Clarendon Press, Oxford (1962).

[Buc81] W. Buchmüller and S.-H.H. Tye. *Quarkonia and quantum chromodynamics.* Phys. Rev. **D24**, 132–156 (1981).

[Car70] R. Carlitz and M. Kislinger. *Regge amplitude arising from $SU(6)_W$ vertices.* Phys. Rev. **D2**, 336–342 (1970).

[Din88] H.-Q. Ding. *A determination of the $q\bar{q}$ potential with very high statistics.* Phys. Lett. **B200**, 133–136 (1988).

[Din90] H.-Q. Ding, C.F. Baillie, and G.C. Fox. *Calculation of the heavy-quark potential at large separation on a hypercube parallel computer.* Phys. Rev. **D41**, 2912–2916 (1990).

[Dul77] C. Dullemond and E. van Beveren. *Confining Potentials and Regge Poles.* Ann. of Phys. **105**, 318–349 (1977).

[Dul82] C. Dullemond, G. Rupp, T.A. Rijken, and E. van Beveren. *A numerical method for solving a coupled channel Schrödinger equation.* Comp. Phys. Comm. **27**, 377–384 (1982).

[Dul84a] C. Dullemond, T.A. Rijken, and E. van Beveren. *Quark-gluon model with conformal symmetry.* Il Nuovo Cim. **80A**, 401–428 (1984).

[Dul84b] C. Dullemond. *On the center-of-mass motion of geometrically confined classical particles.* J. Math. Phys. **25**, 2638–2647 (1984).

[Dul88a] C. Dullemond. *Induced geometry and confinement.* Gen. Relativ. and Grav. **20**, 139–170 (1988).

[Dul88b] C. Dullemond. *Quarks and gluons in a model with induced geometry.* Gen. Relativ. and Grav. **20**, 989–1005 (1988).

[Dul88c] C. Dullemond. *Electrodynamics in a model with induced geometry.* Gen. Relativ. and Grav. **20**, 1099–1113 (1988).

[Eic75] E. Eichten et al. *Spectrum of Charmed Quark-Antiquark Bound States.* Phys. Rev. Lett. **34**, 369–372 (1975).

[Eic78] E. Eichten et al. *Charmonium: The model.* Phys. Rev. **D17**, 3090–3717 (1978).

[Eic80] E. Eichten et al. *Charmonium: Comparison with experiment.* Phys. Rev. **D21**, 203–233, 313 (E) (1980).

[Fog79] G. Fogleman, D.B. Lichtenberg, and J.G. Wills. *Heavy meson spectra calculated with a one parameter potential.* Lett. Nuovo Cim. **26**, 369 (1979).

[For86] Ph. de Forcrand. *QCD from Chippewa Falls.* J. Stat. Phys. **43**, 1077–1094 (1986).

[Ful89] L.P. Fulcher. *Issues in QCD and properties of the* Υ *system.* Phys. Rev. **D39**, 295 (1989).

[God85] S. Godfrey and N. Isgur. *Mesons in a relativized quark-model with chromodynamics.* Phys. Rev. **D32**, 189–231 (1985).

[Gro77] D. Gromes. *Effective Hamiltonian for Charmonium and similar two-fermion systems.* Nucl. Phys. **B131**, 80–92 (1977).

[Gup86] S.N. Gupta, S.F. Radford, and W.W. Repko. *Semirelativistic potential for heavy quarkonia.* Phys. Rev. **D34**, 20 (1986).

[Gup87] R. Gupta et al. *Hadron mass spectrum on an* $18^3 \times 42$ *lattice.* Phys. Rev. **D36**, 2813–2827 (1987).

[Hei84] K. Heikkila, N.A. Tornqvist, and S. Ono. *Heavy* $c\bar{c}$ *and* $b\bar{b}$ *quarkonium states and unitarity effects.* Phys. Rev. **D29**, 110–120 (1984).

[Ken89] R.D. Kenway. *Non-perturbative calculations in the Standard Model.* Rep. Prog. Phys. **52**, 1475–1518 (1989).

[Kon86] K. Königsmann. *Radiative decays in the* ψ *family.* Phys. Rep. **139**, 243 (1986).

[Kwo88] W. Kwong and J.L. Rosner. *D-wave quarkonium levels of the* Υ *family.* Phys. Rev. **D38**, 279 (1988).

[Lic89] D.B. Lichtenberg et al. *Testing static quark-antiquark potentials with bottomonium.* Zeit. Phys. **C41**, 615–622 (1989).

[Lic90] D.B. Lichtenberg et al. *Flavor dependence of the static quark-antiquark potential.* Zeit. Phys. **C46**, 75–85 (1990).

[Luc89] W. Lucha and F.F. Schöberl. *Phenomenological aspects of nonrelativistic potential models.* Report HEPHY/PUB-527, Institut für Theoretische Physik, Universität Wien (1989).

[Luc90] W. Lucha and F.F. Schöberl. *The relativistic virial theorem.* Phys. Rev. Lett. **64**, 2733 (1990).

[Mar80] A. Martin. *A fit of* Υ *and charmonium spectra.* Phys. Lett. **93B**, 338–342 (1980).

[Mar81] A. Martin. *A simultaneous fit of* $b\bar{b}$, $c\bar{c}$, $s\bar{s}$ *(bcs pairs) and* $c\bar{s}$ *spectra.* Phys. Lett. **100B**, 511–514 (1981).

[McC83] R. McClary and N. Byers. *Relativistic effects in heavy-quarkonium spectroscopy.* Phys. Rep. **139**, 243 (1983).

[Met90] K. Metzger. *A unitarized meson model including color Coulomb interaction.* PhD thesis Institute for Theoretical Physics, University of Nijmegen, The Netherlands, 1990 (unpublished).

[Mic69] L. Micu. *Decay rates of meson resonances in a quark model.* Nucl. Phys. **B10**, 521–526 (1969).

[Mos87] B. Mosconi and P. Ricci. *Center-of-mass motion and Siegert's theorem.* Phys. Rev. **C36**, 60 (1987).

[Mox83] P. Moxhay and J.L. Rosner. *Relativistic corrections in quarkonium.* Phys. Rev. **D28**, 1132 (1983).

[Nov78] V.A. Novikov et al. *Charmonium and gluons.* Phys. Rep. **41**, 1–133 (1978).

[PDG88] Particle Data Group. *Review of particle properties.* Phys. Lett. **204B**, 1 (1988).

[Qui77] C. Quigg and J.L. Rosner. *Quarkonium level spacings.* Phys. Lett. **71B**, 153–157 (1977).

[Qui79] C. Quigg and J.L. Rosner. *Quantum mechanics with applications to quarkonium.* Phys. Rep. **56**, 167–235 (1979).

[Ric79] J.L. Richardson. *Heavy quark potential and the* Υ, J/ψ *systems.* Phys. Lett. **82B**, 272–274 (1979).

[Ros55] M.E. Rose. *Multipole Fields.* Wiley, New York (1955).

[Roy67] R. Van Royen and V.F. Weisskopf. *Hadron decay processes and quark model.* Il Nuovo Cim. **50A**, 617 (1967).

[Rup82] G. Rupp. *Spectra and decay properties of pseudo-scalar and vector mesons in a multichannel quark model.* PhD thesis Institute for Theoretical Physics, University of Nijmegen, The Netherlands, 1982 (unpublished).

[Sac51] R.G. Sachs and N. Austern. *Consequences of Gauge Invariance for Radiative Transitions.* Phys. Rev. **81**, 705 (1951).

[Sak67] J.J. Sakurai. *Advanced Quantum Mechanics.* Addison-Wesley, Reading, MA (1967).

[Sie37] A.J.F. Siegert. *Note on the Interaction Between Nuclei and Electromagnetic Radiation.* Phys. Rev. **52**, 787 (1937).

[Son87] X.T. Song and H. Lin. *A new phenomenological potential for heavy quarkonium.* Zeit. Phys. **C34**, 223–231 (1987).

[Wei90] J. Weinstein and N. Isgur. $K\bar{K}$ *molecules.* Phys. Rev. **D41**, 2236 (1990).

Samenvatting

Stralingsovergangen in quarkonium

Dit proefschrift heeft als onderwerp stralingsovergangen in quarkonium, in het bijzonder die in charmonium en bottomonium. De eigenschappen van deze twee families van mesonen worden uitgerekend in het geünitariseerde mesonmodel, dat de afgelopen tien jaar in Nijmegen is ontwikkeld. Dit model is een zogenaamd meerkanaalspotentiaalmodel. Wat potentiaalmodellen zijn en wat hun betekenis is in de hoge-energiefysika wordt besproken in Hoofdstuk 1. Daar wordt ook kort aandacht besteed aan andere modellen (de "echte" theorie quantumchromodynamika en de benadering daarvan op een rooster). Het blijkt dat potentiaalmodellen de grootste beschrijvende en voorspellende kracht hebben als het gaat om eigenschapppen als massa, leptonische vervalbreedte en stralingsovergangen van quarkonium.

In Hoofdstuk 2 wordt een vereenvoudigd "speelmodel" besproken, dat alle essentiële ingrediënten van het volledige model bevat en daarnaast een aantal benaderingen, waardoor alles volledig analytisch is uit te rekenen—dit is in het volledige model niet mogelijk: daar moet er een komputer aan te pas komen. Een korte beschrijving van het volledige model wordt aan het eind van het hoofdstuk gegeven.

In Hoofdstuk 3 wordt het model uitgebreid om naast de S-toestanden ook de P-toestanden van charmonium en bottomonium te kunnen beschrijven, essentiëel om straks stralingsovergangen te kunnen uitrekenen. Dit hoofdstuk is (met een enkele kleine wijziging) als THEF-NYM Rapport no. 90.12 geschreven met Kees Metzger, Eef van Beveren en Kees Dullemond en wordt als zodanig gepubliceerd.

Hoofdstuk 4 behandelt de theorie van de stralingsovergangen, eerst voor een éénkanaalsmodel en daarna voor het geünitariseerde Nijmegenmodel, dat meerdere kanalen bevat.

In Hoofdstuk 5 worden de resulaten van het gereken in het vorige hoofdstuk gepresenteerd en daarna vergeleken met de experimentele waarden en met de resultaten van konkurrerende modellen. Ook wordt een uitgebreide analyse gemaakt van de

resultaten: welke effekten spelen een rol en hoe belangrijk zijn ze. Hieruit blijkt dat een veelgemaakte benadering (de zogenaamde lange-golflengtebenadering) helemaal niet zo'n goede benadering is als vaak wordt beweerd, zeker niet voor charmonium. Ook blijkt dat de invloed van de aangehechte kanalen niet te verwaarlozen is en dat de aanhechting van deze kanalen de resultaten verbetert. Na de vergelijking met andere modellen kan de konklusie getrokken worden, dat er voor de beschrijving van stralingsovergangen in charmonium een relativistisch model nodig is, of op zijn minst relativistische korrekties op de golffunkties nodig zijn. Voor bottomonium blijkt dat niet zo nodig te zijn.

Tot slot worden in Hoofdstuk 6 bovenstaande resultaten en konklusies geformuleerd en worden ideeën gegeven voor de voortzetting van het onderzoek aan quarkonium met het geünitariseerde mesonmodel.

Curriculum Vitae

Geboren op 5 april 1964 in Eindhoven.

Opleiding:

Gymnasium-β aan het Augustinianum te Eindhoven van 1976–1982.
Natuurkunde aan de K.U. Nijmegen van 1982–1986; afstudeer richting Theoretische Hoge-energiefysica.
Wetenschappelijk medewerker van de K.U.N. op de onderwijsstimuleringsplaats "Computeralgebra en symbolisch rekenen" van 16-10-1986 tot 1-8-1987.
Assistent-in-opleiding aan de afdeling Theoretische Natuurkunde II van de K.U.N. van 1-8-1987 tot 15-10-1990.

KOLOFON

Omslag ontwerp	Hanneke Stevens
Lettertype omslag	New Century Schoolbook 20pt (1.5x verbreed)
Papier omslag	300 grams houtvrij Stresa met marmerdessin
Tekstprogramma omslag	PostScript V2.0 (Adobe Systems Inc.)
Printer omslag	Apple LaserWriter Plus (Apple Computers Inc.)
Lettertype binnenwerk	Times en Symbol
Papier binnenwerk	opdikkend opaak 90 grams houtvrij offset
Tekstverwerker binnenwerk	LaTeX V2.09, TeX V3.0 (American Mathematical Society)
Printer binnenwerk	Océ 6750 Laserprinter
Druk	Febodruk, Enschede

Stellingen

I.

Het doen van een χ^2-fit aan charmonium en bottomonium voor éénkanaalspotentialen levert geen relevante informatie op.

D.B. Lichtenberg *et al.* Zeit. Phys. **C46**, 75–85 (1990).

II.

De theoretische waarden voor stralingsovergangen van mesonen, waarvan de golffunktie meerdere knopen bevat, zijn dermate onnauwkeurig te berekenen in de meeste potentiaalmodellen, dat de publikatie ervan zinloos is.

Hoofdstuk 5 van dit proefschrift.

III.

Voor vele modellen binnen de hoge-energiefysika geldt dat ze niet zozeer gevormd worden door een stelsel veronderstellingen en vergelijkingen, maar veeleer door het komputerprogramma waarin dat stelsel vertaald is.

IV.

In het licht van de vorige stelling kan beweerd worden, dat de uitbreiding van een model onbetrouwbare resultaten kan opleveren, doordat de numerieke methoden in het overeenkomstige komputerprogramma niet op zo'n uitbreiding berekend zijn.

V.

De grote verscheidenheid aan potentialen voor charmonium en bottomonium levert slechts minieme verschillen op in eigenschappen als spektra en leptonische en stralingsbreedtes. Hieruit volgt dat de vorm van de interaktie tussen (anti)quarks vooralsnog niet uit potentiaalmodellen is af te leiden.
Dit betekent echter niet dat de QCD-"voorspelling" (Coulomb- plus lineaire potentiaal) de enige juiste is.

VI.

Een opvallende, opzettelijke fout op een van de eerste pagina's van een proefschrift vergemakkelijkt de verdediging van dat proefschrift.

VII.

Relativistics zijn niet lekker.

VIII.

Het doel van de hoge-energiefysika is: één formule op een T-shirt.

IX.

Het autogebruik moet worden teruggedrongen door

(a) het verbeteren van het openbaar vervoer, en

(b) door bij de aankoop van een auto te toetsen op—door de overheid vastgestelde—normen betreffende de noodzaak van het gebruik van een auto.

Nijmegen, 25 januari 1991,
Ton Verschuren.